



POLITECNICO
MILANO 1863

SCUOLA DI INGEGNERIA INDUSTRIALE
E DELL'INFORMAZIONE

Acetic Acid Production from Biogas: An Economic and Feasibility Assessment

TESI DI LAUREA MAGISTRALE IN
CHEMICAL ENGINEERING
INGEGNERIA CHIMICA

Author: **Giorgio Garancini**

Student ID: 10490616
Advisor: Flavio Manenti
Co-advisor: Matteo Fedeli
Academic Year: 2021-2022

Abstract

The proposed M.Sc. thesis work deals with the economic assessment of a biogas based acetic acid synthesis plant. The economic analysis is referred to steady-state simulations implemented on Aspen HYSYS® V11 suite. This study was carried out in collaboration with the SUPER (SUstainable Process Engineering Research) group of the Department of Chemical, Material, and Chemical Engineering “Giulio Natta” of Politecnico di Milano. The simulated plant can be divided in three sections. In the first one syngas is produced through reforming of biogas produced from maize crop. In the second section the produced syngas is converted into methanol. In the third one acetic acid is synthesized through methanol carbonylation and is then separated and collected. The plant capacity is of 8064 ton/year of glacial acetic acid (sold for 14.515 Mln€/year) starting from 1052 m³/h of biogas. The economic assessment of the plant is carried out by calculating the fixed capital investment needed to purchase and install the plant units (19.277 Mln€) and the manufacturing costs related to operating the plant (12.140 Mln€/year). The plant profitability is evaluated after 10 years of operations for three different cases of depreciation (straight-line, sum of the years digit, double declining line) through different profitability indicators (payback period, cumulative cash flow position, net present value etc.) and a cash flow diagram is produced for every case. For all the three cases analyzed the plant presents positive profitability indicators with the best results provided by the sum of the years digit depreciation case (payback period of 5.33 years, discounted payback period of 7.51 years, cumulative cash position of 13.156 Mln€ after 10 years, and net present value of 3.715 Mln€). A risk analysis for the plant investment through Monte Carlo method, involving 1000 generated scenarios taking into account possible revenues and manufacturing costs variation during the plant operations, reveals that the project is subject to high risk. In 17% of the generated scenarios the plant does not reach the break-even point after 10 years and only 31.3% of the scenarios present cumulative cash positions higher than 5 Mln€ after 10 years. Moreover only 9.9% of the scenarios present a positive net present value.

Key-words: biogas, acetic acid, process simulation, economic evaluation, circular economy.

Abstract

La seguente tesi si occupa della valutazione economica di un impianto di produzione di acido acetico che sfrutta biogas come materia prima. L'analisi economica è riferita a una simulazione in stato stazionario sviluppata tramite il software Aspen HYSYS® V11. Questo studio è stato condotto in collaborazione con il gruppo SUPER (Sustainable Process Engineering Research) del Dipartimento di Ingegneria Chimica, dei Materiali e Chimica "Giulio Natta" del Politecnico di Milano. L'impianto simulato può essere suddiviso in tre differenti sezioni. Nella prima, il biogas prodotto da mais tramite digestione viene convertito in gas di sintesi tramite reforming. Nella seconda sezione il gas di sintesi prodotto viene convertito in metanolo. Nella terza avviene la sintesi dell'acido acetico tramite carbonilazione del metanolo, a cui segue la separazione del prodotto finito. L'impianto progettato ha una capacità produttiva pari a 8064 ton/anno di acido acetico glaciale (che viene venduto per un totale di 14.515 Mln€/anno) partendo da 1052 m³/h di biogas. La valutazione economica del progetto è effettuata calcolando gli investimenti di capitale fisso necessari ad acquistare e installare le unità e i macchinari dell'impianto (19.277 Mln€) e i costi di produzione relativi alle operazioni produttive (12.140 Mln€/anno). La redditività è valutata dopo dieci anni di operazioni per tre casi differenti di deprezzamento (straight-line, sum of the years digit, double declining line) attraverso diversi indici di profittabilità (tempo per rientrare dall'investimento, cumulative cash flow position, valore attuale netto ecc.). Inoltre, per ogni caso analizzato viene prodotto un diagramma dei flussi di cassa. Gli indicatori di profittabilità analizzati si presentano positivi per ogni caso considerato, e i risultati migliori sono relativi al caso di deprezzamento "sum of the years digit" (tempo per rientrare dell'investimento di 5.33 anni e di 7.51 anni se i flussi di cassa vengono scontati al primo anno, cumulative cash position di 13.156 Mln€ dopo dieci anni e valore attuale netto di 3.715 Mln€). È stata condotta un'analisi di rischio relativa all'investimento economico nell'impianto utilizzando il metodo Monte Carlo. In questa analisi sono stati generati mille scenari che tengono conto di possibili variazioni nelle entrate e nei costi di produzione durante i dieci anni di operazione dell'impianto. I risultati dell'analisi rivelano che il rischio connesso all'investimento è elevato. Nel 17% dei casi, dopo 10 anni, non viene raggiunto il pareggio di bilancio e solo nel 31.3% dei casi viene prodotto un utile maggiore di 5 Mln€, inoltre solo nel 9.9% dei casi si raggiunge un valore attuale netto positivo.

Parole chiave: biogas, acido acetico, simulazione di processo, valutazione economica, economia circolare.

Contents

Abstract	i
Abstract	iii
Contents	v
Introduction	1
1 Technologies	5
1.1. Biogas	5
1.1.1. Biogas production.....	6
1.1.2. Biogas utilization and prospects	12
1.2. Syngas	17
1.2.1. Steam reforming	18
1.2.2. Autothermal catalytic reforming.....	21
1.2.3. Hydrocarbons partial oxidation	23
1.2.4. Dry reforming	25
1.2.5. Biogas reforming	26
1.3. Methanol.....	29
1.3.1. Methanol production	30
1.3.2. Methanol synthesis prospects.....	35
1.4. Acetic acid	37
1.4.1. Acetaldehyde process	37
1.4.2. Methanol carbonylation.....	38
1.4.3. Other production technologies.....	42
2 Tools and instruments	47
2.1. Aspen HYSYS®	47
2.2. Microsoft Excel®	47
2.3. MATLAB®	47
3 Process simulation	49
3.1. Syngas production section	49
3.1.1. Reforming thermodynamic and kinetics	53
3.2. Syngas refining section.....	56
3.2.1. Reverse water-gas shift reactor thermodynamic and kinetics.....	60

3.3.	Methanol production section.....	62
3.3.1.	Methanol synthesis thermodynamic and kinetics.....	68
3.4.	Acetic acid production section.....	71
3.4.1.	Acetic acid synthesis thermodynamic and kinetics.....	75
3.5.	Separation section.....	76
3.6.	Plant furnace and utilities.....	82
4	Economic analysis.....	85
4.1.	Capital costs.....	85
4.1.1.	Compressors capital costs estimation.....	89
4.1.2.	Pumps capital costs estimation.....	90
4.1.3.	Heat exchangers capital costs estimation.....	91
4.1.4.	Reactors and furnace capital cost estimation.....	97
4.1.5.	Flash separators capital cost estimation.....	98
4.1.6.	Columns capital cost estimation.....	99
4.1.7.	Tank separator capital cost estimation.....	102
4.1.8.	Cooling towers capital cost estimation.....	102
4.2.	Operating costs.....	106
4.2.1.	Cost of operating labor.....	107
4.2.2.	Utility costs.....	108
4.2.3.	Raw material costs.....	110
4.2.4.	Waste treatment costs.....	111
4.2.5.	Cost of manufacture estimation.....	111
4.3.	Cash flow diagram and economic assessment.....	112
4.3.1.	Straight line depreciation.....	113
4.3.2.	Sum of the years digit depreciation.....	116
4.3.3.	Double declining balance depreciation.....	118
4.3.4.	Case comparison.....	120
4.3.5.	Risk analysis.....	121
5	Conclusions.....	127
	Bibliography.....	129
	List of tables.....	136
	List of acronyms.....	140

Introduction

Acetic acid (chemical formula CH_3COOH) is the most important organic acid produced worldwide. Commonly found in nature in aqueous solutions (mainly in animal and plant systems), acetic acid has been produced as vinegar for more than 5000 years through fermentation [1].

Vinegar production from ethanol solutions occurs spontaneously in the presence of air as acetic acid-producing bacteria are naturally present in the environment.

The first evidence of the production of vinegar made from beer is from Babylonians around 3000 BC. Traces of acetic acid found in ancient Egypt urns confirm its utilization for culinary purposes. Ancient romans used vinegar as reported by many writings, in particular Lucius Junius Moderatus Columella (4-70 AD) wrote about vinegar making from figs in "De re rustica"[2].

The pure compound was first extracted from vinegar by distillation in the 17th century by the German chemist Georg Ernst Stahl [3].

At ambient condition acetic acid is a clear, colorless liquid with a pungent odor. It is soluble in water, alcohol, acetone, benzene, and other organic solvents. It has a pKa of 4.5 and its corrosiveness justifies caution in handling. It is a vesicant, and it can cause irritation to skin eyes and mucous membranes when in solution and severe damage when in concentrated forms. It has a low flash point of 39°C and it is readily combustible with autoignition point of 516°C [1], [3].

Industrial production of acetic acid started in the early 20th century mainly by acetaldehyde oxidation. This process has been progressively abandoned starting from the 1960s when BASF and later Monsanto developed a catalyzed methanol carbonylation process with great advantages over other processes. At present carbonylation of methanol is still the most relevant production path for acetic acid [1], [3].

Acetic acid has various industrial applications. The most important is the production of vinyl acetate monomer that is then used in the production of latex emulsion resins for paint applications, paper coatings, textile treatments and adhesive production like polyvinyl acetate.

Another application of acetic acid is related to the productions of acetic anhydride, an important acetylating and dehydrating agent used in the production of plastic materials, explosives, brake and drilling fluids, detergents, dyes, pharmaceuticals and

flavors and fragrances. It is also used to produce cellulose acetate, an important polymer used in the textile and manufacturing industry.

An important application of acetic acid is linked to the production of purified terephthalic acid used in the synthesis of PTA (polyethylene terephthalate) one of the most important plastic materials.

Lastly acetic acid is used in the production of other acetates (as butyl acetate and ethyl acetate) and as a solvent for esters [1], [4], [5].

Figure 0.1 summarizes the different applications of acetic acid and Figure 0.2 shows the market distribution for its different applications in 2020.

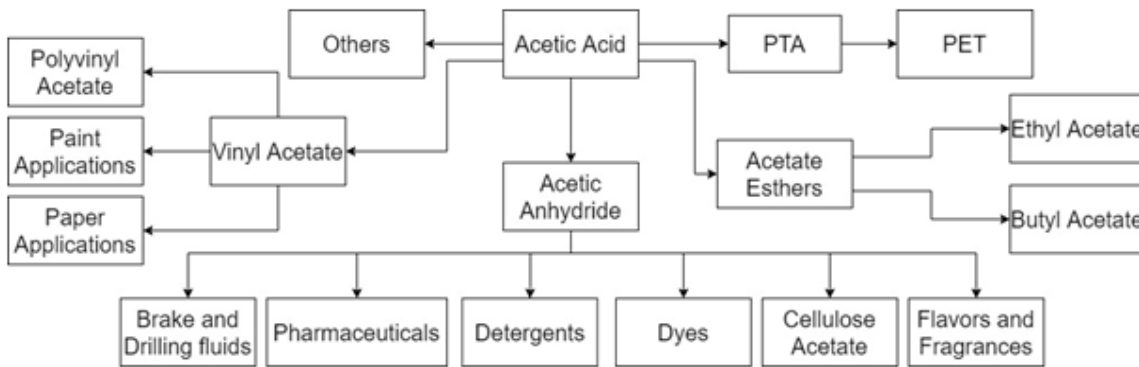


Figure 0.1 Acetic acid different applications

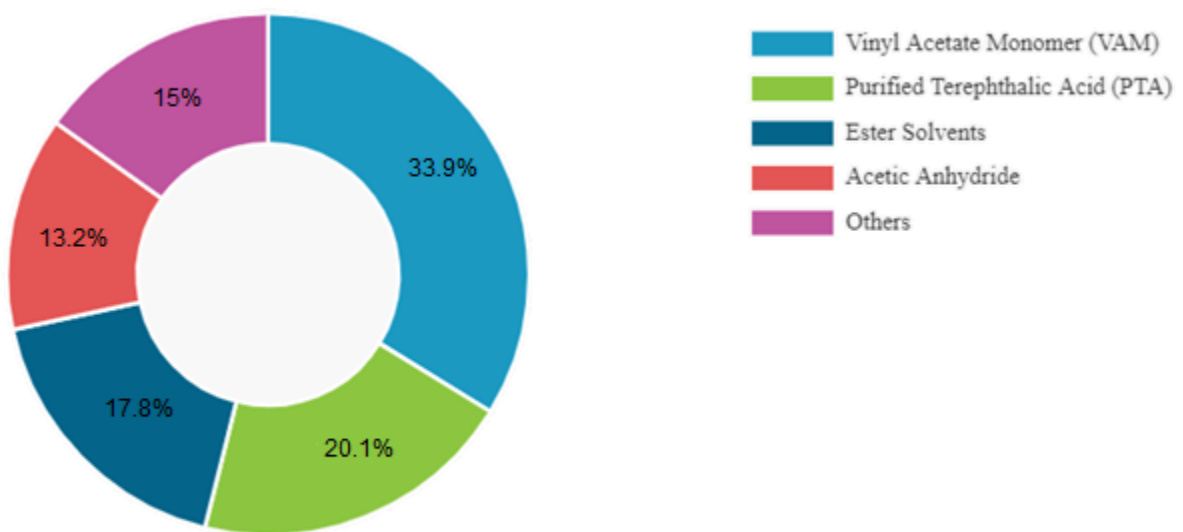


Figure 0.2 Global acetic acid market share, by application (2020) [5]

The global production of acetic acid has increased constantly passing from 7 million metric tons per year in 2005 [1] to more than 14 million metric tons per year in 2014 [6].

After a growth stop in 2020 caused by Covid-19 pandemic, the total acetic acid market reached a value of USD 7.29 billion in 2021 and of USD 8.48 billion in 2022. It is expected that the market will constantly grow for the forthcoming years at a compound annual growth rate (CAGR) between 2.62% and 5.4% [5], [7].

Various companies and joint ventures share the market. The key competitors are BP Plc, Shanghai Huayi Company, LyondellBasell Industries, Celanese, Daicel Corporation and many others [4], [5].

The biggest producer worldwide is China followed at distance by U.S.A.

As already mentioned, the principal production route for acetic acid is the carbonylation of methanol. Both methanol and carbon monoxide are produced starting from fossil fuels (usually natural gas and naphtha) via syngas production.

This process is environmentally heavy impacting, as a great amount of greenhouse gases is emitted when fossil fuels are burned in the furnace that supplements the heat necessary for the reforming reactions that lead to syngas. A more detailed description of syngas production, methanol production and acetic acid production will be provided in the next chapter.

A more environmentally friendly approach to the production of acetic acid is to use renewable feedstocks as starting materials for syngas production.

Biogas can fulfill this role, as it is a renewable source of methane that can be used as a reactant in the syngas reformer as well as a fuel to aliment the reformer furnace.

This thesis aim is to model a chemical plant that produces acetic acid starting from biogas and to provide an economic feasibility study to evaluate the plant's potential.

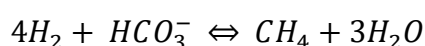
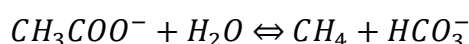
1 Technologies

1.1. Biogas

The term biogas refers to a mixture of methane and carbon dioxide (the concentration of methane may vary from 50% to 70%) generated via anaerobic digestion by microorganisms called methanogens. Usually, biogas is saturated in water, and it contains traces of other compounds like hydrogen sulfide. All organic matter can be transformed by methanogens under anaerobiosis, and biogas has been produced naturally by microorganisms since the origin of life on earth [1]. Even though not all the methane produced by methanogenesis is released in the atmosphere, as 60% of it is consumed by other aerobic or anaerobic methane-oxidizing bacteria, methanogenesis is responsible for approximately 70% of global methane emissions every year [8]. This represents a potential problem as methane is a greenhouse gas several times stronger than carbon dioxide.

All the methanogens belong to the archaea kingdom and can be found in a wide variety of environments. Methanogens are classified into three groups: hydrogenotrophic, acetotrophic and methylotrophic. Hydrogenotrophic methanogens oxidize hydrogen, formate and simple alcohols and reduce carbon dioxide to methane. Acetotrophic methanogens split acetate into methane and carbon dioxide and methylotrophic methanogens use methylated compounds [8].

Anaerobic methanation comprehends a set of complex metabolic pathways. A schematic simplification of the chemical reactions involved can be provided by the following reactions [1]:



Methanogenesis was discovered in 1776 by the Italian physicist and chemist Alessandro Volta (1745-1827) when he conducted experiments in Maggiore Lake. In 1868 Antoine Béchamp (1816-1908) demonstrated that methane was derived by a

microbiological process [9]. At the end of the 19th century methanogenesis was applied for the first time to reduce organic matter content of sewage sludge [1]. In the 1970s the rise of oil price greatly increased interest in the production of biogas and in the 1990s the awareness of climate change and renewable energy sources led biogas production to be an established technology.

1.1.1. Biogas production

Anaerobic degradation of organic matter leading to biogas can be divided into four steps (as schematized in Figure 1.1): hydrolysis, acidogenesis, acetogenesis/dehydrogenation, and methanation [10].

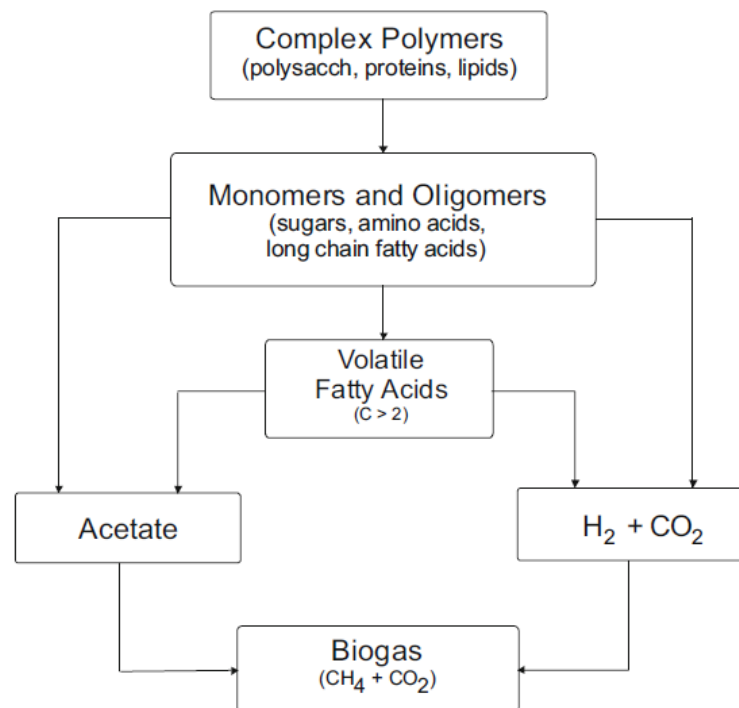


Figure 1.1 The stages of the methane fermentation process [10]

Each step is carried out by different microorganisms that live in syntrophic relationship based on the different environment.

The first step is usually carried out by fermentative bacteria (species of *Butyrivibrio*, *Propionibacterium*, *Clostridium*, *Bacteroides*, *Ruminococcus*, *Acetivibrio*, *Bifidobacterium*, *Eubacterium*, *Peptostreptococcus*, *Peptococcus*, *Selenomonas*, *Lactobacillus*, *Streptococcus*) that are able to hydrolyze organic polymers (like polysaccharides and proteins) in oligomers and monomers through extracellular enzymes. The products of hydrolysis are then utilized by other bacterial species to

form short-chain fatty acids, acetate, alcohol, hydrogen, and carbon dioxide (acidogenesis). In the third step (acetogenesis/dehydrogenation), short-chain fatty acids are oxidized by acetogenic bacteria (*Acetobacterium*, *Acetoanaerobium*, *Acetogenium*, *Butyrivacterium*, *Clostridium*, *Eubacterium*, and *Pelobacter*) to acetate, formate, hydrogen, and carbon dioxide. Acetates, carbon dioxide and hydrogen can be converted to methane by archaea methanogens (species of *Methanobacterium*, *Methanobrevibacter*, *Methanothermus*, *Methanococcus*, *Methanomicrobium*, *Methanogenium*, *Methanospirillum*, *Methanoplanus*, *Methanosarcina*, *Methanotherix*) during the methanation step [9]–[11].

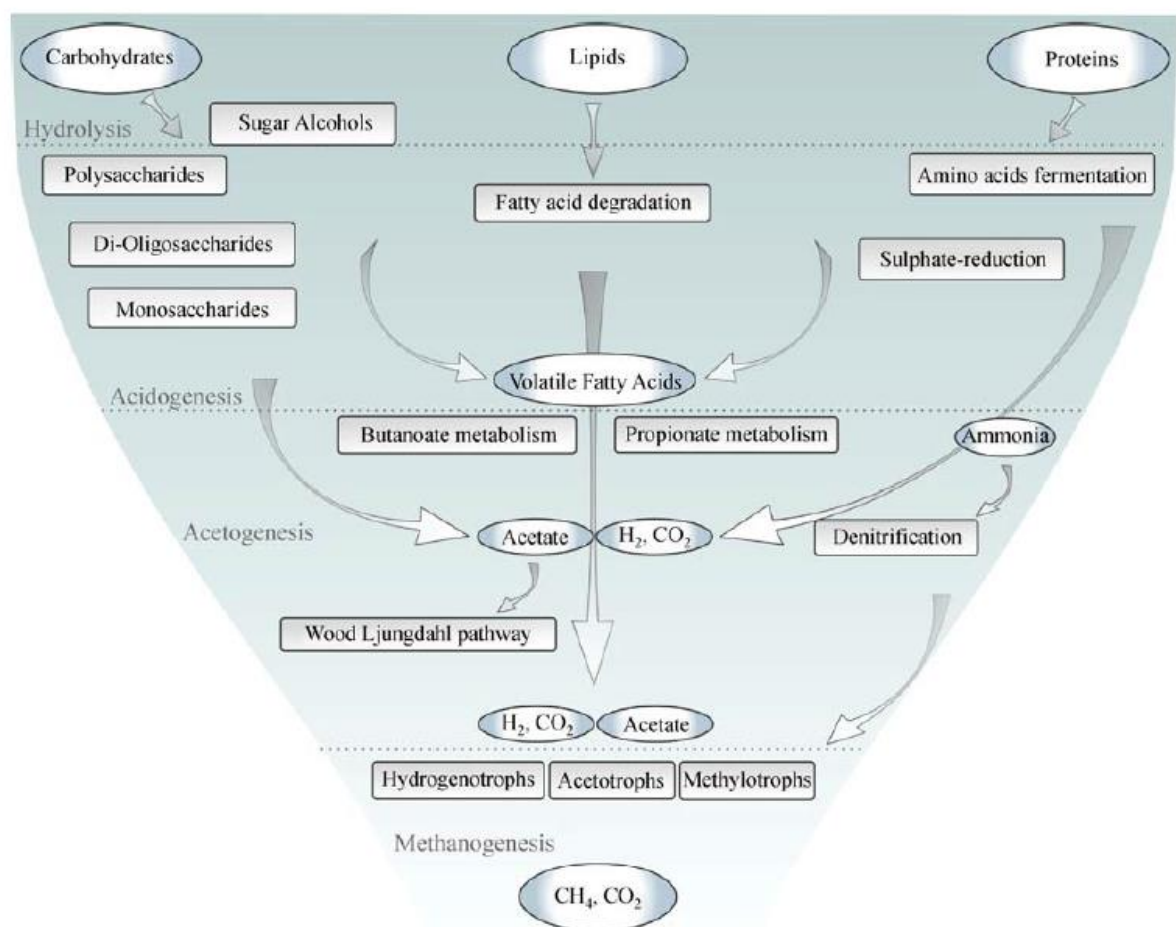


Figure 1.2 Representation of the functional roles of the microbial species involved in biogas production [9]

Landfills can be considered the first generation of anaerobic reactors built. Domestic solid waste is buried and disposed of in landfills, this generates an isolated environment with lack of oxygen. This condition is suitable for anaerobic digestion

and landfills act like batch reactors (Figure 1.3 C). In normal conditions the biogas generated escapes into the atmosphere presenting fire and explosions hazard and contributing to greenhouse gases emission. Starting from the 1970s biogas generated from landfills started to be utilized all over the world [1].

The first reactors intentionally designed for anaerobic digestion were stirred reactors (Figure 1.3 A-B). They were operated in batch mode for more solid feedstock and in continuous mode for more fluid ones, but their performances were limited [1].

The second generation of biogas reactors started to be implemented in the 1970s and its aim was to optimize the biogas generation conditions. The new main feature was the recycle of active biomass. The main limitation of first-generation reactors was the loss of active biomass during the discharge operations. Microorganisms are taken out of the reactor when the effluent is removed, and this limits the biological conversion of the substrate. Recycling the active biomass allows to maintain a constant concentration of microorganisms in the reactor thus increasing its performance. The active biomass sedimentation occurs in a separate sedimentation tank followed by a recycle (Figure 1.3 D) or in a built-in decanter (Figure 1.3 E) or through membrane filtration. These types of reactors are called contact reactors [1], [11].

With the third generation of reactors various methods to maintain the active biomass inside the reactors were applied. The first one was to immobilize the active biomass on a support medium inside a plug-flow reactor. Initially gravel was used as carrier, and it was later substituted by plastic packaging, polymeric foams, and ceramic rings. This design is known as anaerobic filter (Figure 1.3 G). A variation of this configuration is the fluidized bed reactor, where the dimension of the carrier particles is sufficiently small to allow them to be fluidized by the effluent stream, granting a constant mixing. The second method was to flocculate the microorganisms inside the reactor. Under certain conditions the active biomass organizes itself into heavy granules and can be retained. The reactor consists of a sludge bed, a sludge blanket and a clarifier zone supplemented with a system of baffles that acts as a three-phase separator. This reactor configuration is known as upflow anaerobic sludge blanket reactor (UASB reactor Figure 1.3 F) and is currently one of the most common configurations for anaerobic digestors [1], [11].

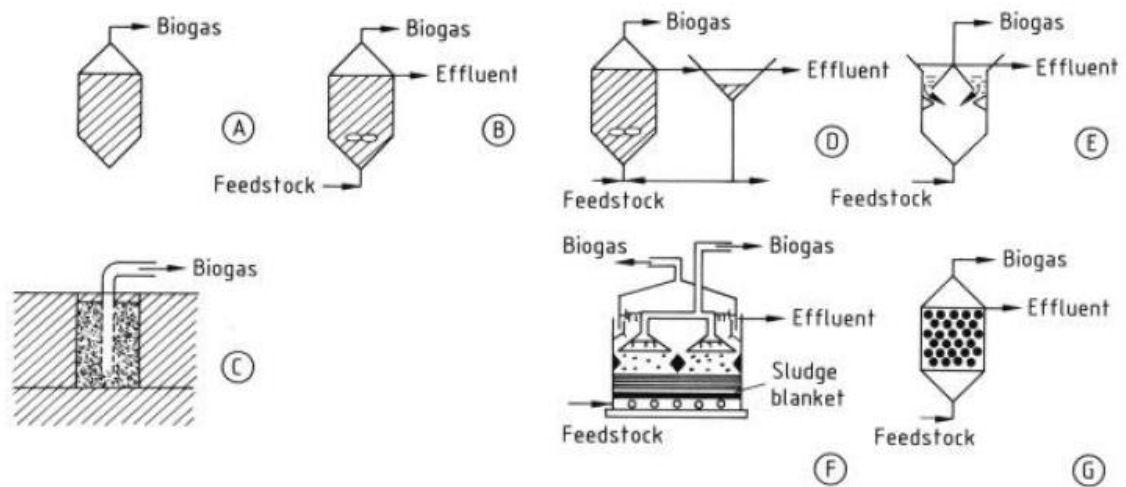


Figure 1.3 Different reactor configurations for anaerobic digestion [1]

The last improvement made was the application of reactors in series. Each stage of anaerobic digestion can be optimized controlling the reaction conditions (like pH and temperature) in each reactor. The most common configuration is a two-stage reactor where hydrolysis and acetogenesis are decoupled from methanogenesis [1], [11]. Figure 1.4 shows a two-stage reactor configuration plant.

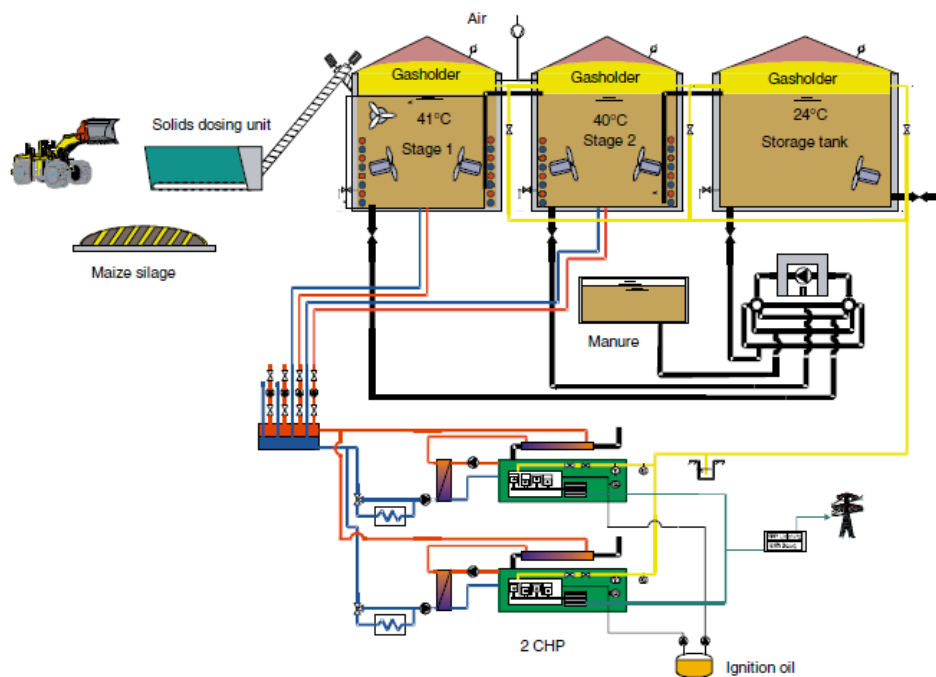


Figure 1.4 Typical two-stage agricultural biogas plant [10]

Many factors influence biogas production operations, the most important are temperature, pH, concentration of volatile fatty acids and concentration of inhibitors.

The digestion process is operated at mesophilic (35-42°C) or thermophilic (45-60°C) temperatures depending on the characteristic of the microorganisms present. Thermophilic conditions present advantages over mesophilic ones such as higher organic load due to higher reaction rates, shorter retention times, better degradation of long chain fatty acids, better quality of the effluent digestate, smaller reactor size and better sanitation of the effluent. It is important to maintain a constant temperature during the operations as temperature fluctuations lead to imbalances in the digestion process like ammonia accumulation and high concentration of volatile fatty acids (especially at thermophilic conditions) [9]–[11].

Biogas production occurs in a narrow pH range ranging from 6 to 8.5. Out of these limits the process deteriorates and methane production decreases. pH variations are usually generated by changes in other parameters like temperature. As mentioned before temperature variations can lead to ammonia accumulation thus increasing pH, or high concentration of fatty acids thus lowering pH [9]–[11].

The concentration of volatile fatty acids is one of the most popular monitoring parameters during biogas production operations. Volatile fatty acids concentration directly reflects the kinetic coupling between acid-former and acid-consumer microorganisms (as VFA are a key intermediate in the process), and its variation can be related to organic overloading, temperature variations and presence of toxic or inhibitory compounds. High concentrations of VFA have inhibitory effect on methanogenesis, it has also been demonstrated that the inhibition is related to the undissociated form of the VFA, and thus low pH levels favors it [9]–[11].

Some compounds, when they exceed certain concentrations, can reduce biogas production or fatally compromise the process. One common inhibitor is ammonia. When present in high concentration, ammonia greatly reduces biogas production. Ammonia inhibition increases at higher temperature therefore is common when operating at thermophilic conditions. Ammonia is a common compound in many organic residues like manure, and it can also originate during the digestion process due to protein degradation [9]–[11].

Another common inhibitor are long chain fatty acids (LCFA) present in various agro-industrial residues. LCFA can be oxidized to stable compounds and therefore any subsequent oxidation is thermodynamically unfavored leading to a process inhibition [9]–[11].

A wide range of biomass can be used as substrate as long as its main components are carbohydrates, proteins and lipids. However, strong lignified substances like

wood are not suitable for anaerobic digestion as their decomposition is very slow. The complex structure of lignin (a polymer of p-coumaryl, coniferyl and sinapyl alcohol) and its low solubility in water provides low degradability and high resistance to microbial attack. Energy crops (like grass and miscanthus) and agricultural residues (sugar beet, maize, wheat, rye, sorghum, sunflower) are the main substrates utilized in biogas production together with animal manure (pigs, cows, chickens). Energy crops and agricultural residues are easily harvested and can be stored by ensiling. This process consists in the comminution of the biomass and the subsequent partial conversion of the soluble carbohydrates into lactic acid, acetate, propionate and butyrate. The low pH value reached during this biochemical process inhibits the growth of detrimental microorganisms. Ensiling gives also benefits to the biogas production process as the chemical structures of the plant materials are partially degraded and thus easily digestible [10], [12].

Other substrates utilized in biogas production are sewage sludge, municipal solid waste and food waste [12].

An interesting feeding procedure for biogas plants is co-digestion. Different organic residues can be treated simultaneously in the same anaerobic digester leading to different advantages:

- Increased loading of readily digestible matter.
- Based on the chemical composition of the substrates used, an optimal balance of micro and macronutrients for the microorganisms can be reached.
- Possibility to dilute inhibitory compounds.
- The buffer capacity of the influent mixture can be increased (manure is known for its buffer capacity) maintaining optimal pH values.
- Optimization of the substrate rheology.
- Better hygienic stabilization

When correctly applied, co-digestion ensures higher volumetric biogas production and improved economics of the plant [9]. In Table 1.1 various substrates with their respective methane yields are reported.

Depending on the content of dry matter present inside the reactor two fermentation typologies can be defined: dry and wet fermentation.

With the term dry fermentation, it is described the digestion process in which the total content of solid matter ranges between 15% and 35%. Usually for these operating conditions CSTR, contact reactors and batch reactors are preferred [9], [10].

Wet fermentation describes digestion processes in which the total content of solid matter is below 10%. The large amount of liquid allows the usage of UASB reactors and anaerobic filters [9], [10].

Table 1.1: Methane yields of various substrates [9]

Category	Substrate	Methane yield (ml/g)
Livestock manure	Cattle	242-399
	Mink	239-248
	Pig	313-322
	Poultry	107-438
Agricultural wastes	Barley	322-335
	Corn silage	270-298
	Fruit and vegetables	153-342
	Meadow grass	282-388
	Palm oil mill effluent	378-503
	Rice straw	279-280
	Ryegrass	140-360
	Switchgrass wheat	122-246 245-319
Oil	Rapeseed oil	704 \pm 16
	Oleic acid	837 \pm 0.3
Household/ Municipal/ Industrial wastes	Kitchen waste	541-683
	Organic fraction of municipal solid waste	300-570
	Slaughterhouse waste	561-657
	Sewage sludge	249-274

1.1.2. Biogas utilization and prospects

The majority of biogas produced nowadays in biodigesters is utilized to produce electric energy and heat mainly in CHP (combined heat and power) applications. Biogas can be easily burned inside internal combustion engines and gas turbines to produce energy with good power efficiencies (up to 40%) and heat [9]–[11], [13].

The produced biogas needs to be treated and purified before entering the energetic production cycle as it contains other substances other than methane and carbon

dioxide (mainly H_2S and H_2O) that can lead to corrosion problems or emission of dangerous compound.

H_2S can be removed via biological desulfurization. Some microorganisms (like sulfobacter oxidans) can oxidize H_2S into elemental sulfur in the presence of oxygen. This process may be carried out inside the reactor (by adding a small amount of air to the raw biogas) or in a separate section using trickling beds. The addition of air, however, may lead to a lower methane concentration in the biogas. In order to avoid this problem, the biogas stream may be washed with water to absorb H_2S . The water stream is then treated separately in a trickle bed where biological desulfurization happens. H_2S can also be removed by water scrubbing and chemical washing [10], [11].

Water removal is usually carried out by refrigeration or cooling after compression in order to condensate the vapor [11].

Biogas may also be fully upgraded to biomethane if the methane content is greater than 95% and the contaminants are removed. There are different methods to remove CO_2 , the most used are water scrubbing and pressure swing adsorption on activated carbons or molecular sieves. Chemical washing (with amines or CaOH solutions) is effective but less common. Finally cryogenic separation and membrane separation are also possible but costly [10], [11].

Lastly biomethane needs to be sterile. The use of filters allows to separate the microorganism from the gaseous stream guaranteeing sterility [10].

The main use of biomethane is to be injected in the gas grid or to be used as a fuel by gas vehicles. Figure 1.5 shows the different end use of biogas in 2018.

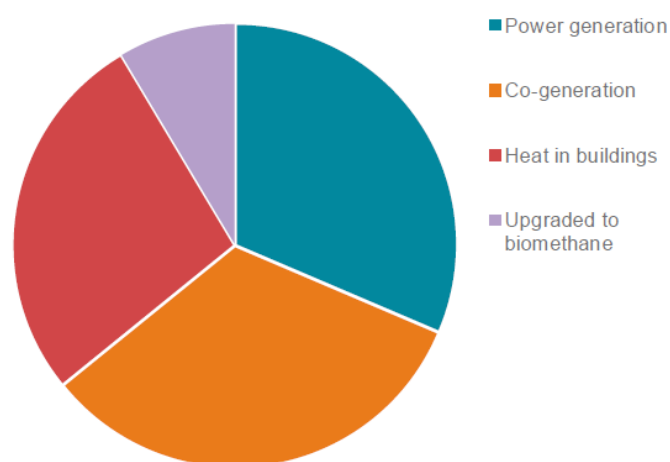


Figure 1.5 Biogas consumption by end use (2018) [13]

Purified biogas has also attracted attention for its possible utilization in fuel cells. In hot fuel cells the presence of carbon dioxide does not inhibit the electrochemical process and favors the transfer of heat acting as a heat carrier [10], [11]. Fuel cells are characterized by greater electrical efficiencies compared to internal combustion engines, but their investment and maintenance costs are higher [10].

Biogas can be easily converted to syngas (a more detailed description of this process is given in the following section) thus opening new routes in the chemical industry. Important chemicals like hydrogen, methanol and their derivatives could be produced starting from renewable sources, reducing their environmental impact.

Lastly, biogas can be used as a clean fuel for cooking, thus representing a valuable resource for people living in rural areas and developing countries [13].

It is also important to note that the digestate, the principal byproduct of biogas production, has a high content of nutrients and can be used as a fertilizer. The anaerobic digestion process enhances the fertilizing properties of the digestate increasing the mineralization of organically bounded nutrients and lowering the carbon to nitrogen ratio. The digestate has improved flow properties, allowing it to penetrate faster in the soil reducing nitrogen losses. The anaerobic digestion process leads also to a reduction in the odor of the feedstock up to 80% [10].

Possibilities to produce biogas are widely distributed around the world and the availability of sustainable feedstocks for these purposes is set to grow by 40% over the period to 2040. In 2018 the production of biogas was 35 million tons of oil equivalent; this represents only a fraction of the biogas overall potential. It is believed that full utilization of biogas potential could cover up to 20% of today world gas demand [13].

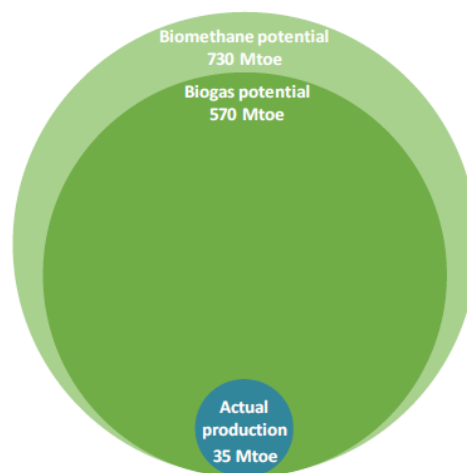


Figure 1.6 Biogas and biomethane production in 2018 against the sustainable potential today [13]

Biogas is a strategic resource in the European bio-based economy. EU renewable energy directives and governmental incentives have allowed a constant growth of the biogas sector in the recent years [14].

Germany is the leading country in biogas production, promoting anaerobic digestion since the 1990s. With the renewable energy act (EEG), Germany promoted electricity generation from renewable sources with high feed-in tariffs. In 2013 a total of 9035 biogas plants were operating with new plants opened every year despite the reduction of incentives [15].

Italy is the second leading country in Europe in biogas production. Following Germany example, Italy promoted biogas production with high feed-in tariffs. In 2014, 1391 plants were operating, and Italy was one of the countries with the highest growth rate in biogas production [15].

The majority of biogas produced in Europe utilizes agricultural substrate as a feedstock (approximately 80%) however other sources like manure and municipal wastes show interesting potential. The potential of biogas production from manure in Italy is estimated to be 2.2 Gm³/year representing 8% of electricity production and 21% of thermal energy production derived from renewable sources [16].

Nowadays biogas upgrading to biomethane is not cost efficient without incentives, as the average price for biomethane is higher than natural gas. The cost gap however is projected to narrow over time as biogas technologies improve and natural gas becomes more expensive. Carbon pricing will play an important role in the cost competitiveness of biomethane.

1.2. Syngas

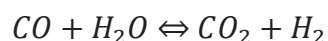
Syngas is the name given to a gas mixture of carbon monoxide and hydrogen generated from a carbon containing fuel. Syngas is a fundamental intermediate in the production of various important chemicals such as ammonia and methanol and it is used in Fischer-Tropsch synthesis to produce synthetic fuels and lubricants. It also finds application in oil refining and other industrial processes like iron ore reduction and hydrogenation of fats. Syngas can be produced by different processes and starting from different raw materials (mainly hydrocarbons like coal, natural gas and naphtha) leading to different hydrogen to carbon monoxide ratios [1], [17].

Production of syngas started in the middle of 1800s when coal was gasified to produce town gas for illumination purposes. In the 1900s syngas started to be produced as an intermediate for the synthesis of chemical compounds. Methanol synthesis is carried out starting from syngas while Haber-Bosch ammonia synthesis process utilizes hydrogen derived from syngas as a reagent. With the production of these two chemicals and all of their derivatives, syngas has played a key role in the industrial organic chemistry since the 20th century [1].

Nowadays natural gas is the primary source for syngas production for its cost effectiveness and relatively high purity. LPG, fractions of crude oil like light naphtha and crude-oil high boiling residue can be used in syngas production, but they have disadvantages compared to natural gas, in particular higher concentrations of impurities and contaminants. Coke is the least desirable raw material for syngas production as it is expensive to treat and has the highest content of impurities. In recent years interests in biomasses as raw material has increased. Wood in particular represents a renewable source for the production of clean fuel gas (low sulfur content) [1].

Syngas production usually relies on catalysts, and to avoid their deactivation raw materials need to be treated in order to remove contaminants, mainly sulfur.

After the synthesis the syngas produced is usually conditioned balancing the carbon monoxide to hydrogen ratio needed for subsequent applications. This process is carried out through water-gas shift equilibrium (as reported in the following reaction) in dedicated reactors [1].



Based on the feedstock and the technology used, gasification processes generate different impurities, the most common are:

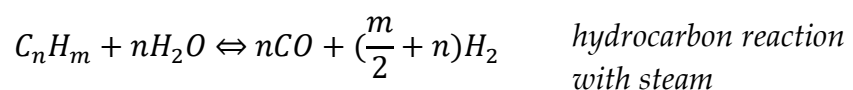
- Dust
- Tar and gas liquor
- Carbon
- Oxygen
- Cyanic compounds
- Nitrogen oxides
- Carbon dioxide
- Hydrogen sulfide, carbonyl sulfide and organic sulfur
- Ammonia

All these impurities are generally removed through adsorption (using activated carbons, molecular sieves and other adsorbents) or absorption processes (washing with different solvents) [1].

1.2.1. Steam reforming

Steam reforming is the most common method for producing hydrogen and syngas, and natural gas is the most common feedstock for this process followed by naphtha. The process was developed by BASF in the 1930s and was commercialized to produce hydrogen for hydrogenation purposes and for ammonia synthesis [1].

In steam reforming hydrocarbons are catalytically converted into hydrogen and carbon monoxide by reacting with steam. The process is governed by the thermodynamic equilibrium of the following reactions:



The overall process is highly endothermic therefore a great amount of energy needs to be provided to the reactants to be converted. After being preheated at 500°C, usually in the convective section of a furnace or a firebox, the steam-hydrocarbon mixture reaches the reactor section (usually multiple fire-heated tubes) where it enters in contact with a nickel-based catalyst at the desired reaction temperature (normally between 800°C and 900°C). The product composition reflects equilibria of the aforementioned equations and can be easily calculated for the specific reaction condition and reactants composition [1], [18]. In Figure 1.7 equilibrium compositions for different reaction conditions of a definite methane steam reforming feed are presented.

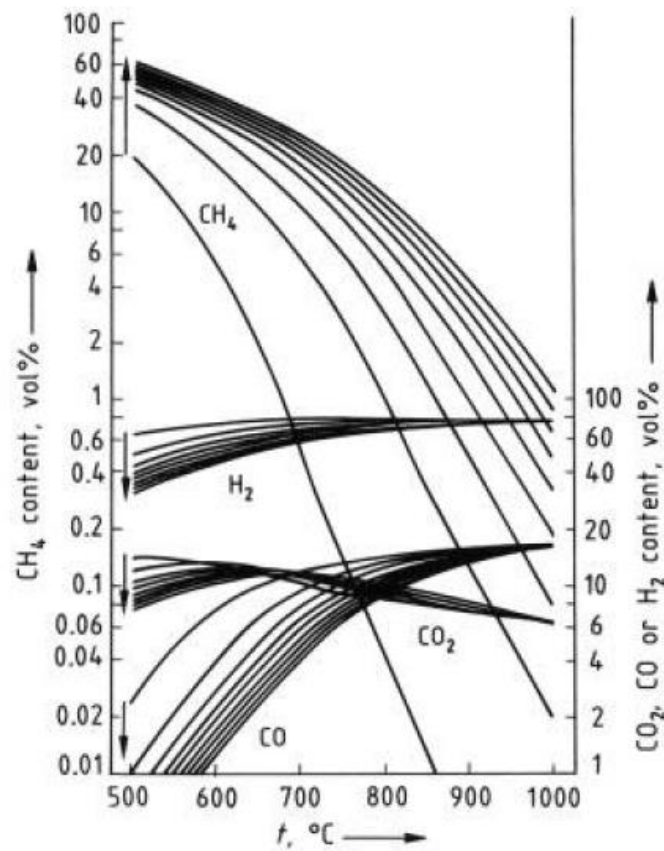


Figure 1.7 Equilibrium composition for methane reforming at 500 – 1000 °C and pressures (in the direction of the arrows) of 0.1, 0.5, 1, 1.5, 2, 2.5, 3, 3.5, 4 MPa. Molar steam/methane ratio 3.333 corresponding to 5 kg H₂O per kilogram of carbon [1]

Two configurations of tubular reformers are commonly used. Top or bottom fired reformers consist of parallel rows of tubes heated by the radiation of the burner flame and the flue gases, while wall-fired reformers present a singular row of tubes heated by the radiant side wall. Reformer tubes are made of special alloys able to withstand high temperatures and have wall thicknesses of 10-20 mm that allow working pressures up to 4 MPa. The fired length of the tube is between 9 and 15 m. The flue gases heat is recovered and used to preheat the reagents. The reformer tubes are positioned in a firebox consisting of several layers of insulating and refractory materials that must resist high temperature (greater than 1200°C). An exterior metal skin contains the refractory materials [1]. Figure 1.8 reports different reformer types.

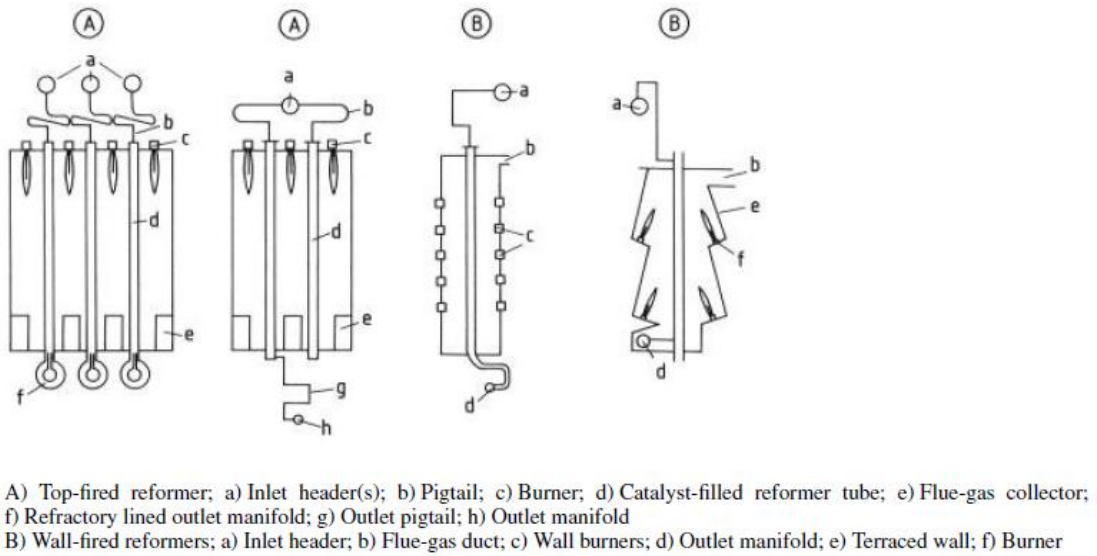
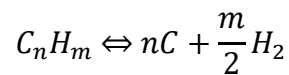


Figure 1.8 Reformer types [1]

A commonly experienced phenomenon in steam reforming is carbon deposition inside the reformer tubes. Carbon deposition arises from decomposition of hydrocarbons in the first half of the reformer's tubes when the concentration of hydrocarbons is higher. The following reaction expresses the decomposition of hydrocarbons and governs the carbon formation in steam reforming [1].



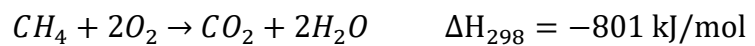
Carbon formation is more pronounced in the reforming of heavier hydrocarbons and for low steam/hydrocarbon ratios. To ensure low carbon deposition steam/hydrocarbons ratio is maintained between 3 and 5.

Carbon deposition has a detrimental effect on the reforming reaction as the generated carbon deposits cover the nickel catalyst reducing its activity. Another cause of catalyst deactivation is the presence of poisons like sulfur, arsenic, copper, vanadium, lead and halogens. Sulfur is particularly dangerous as it is found in every hydrocarbon feedstock and needs to be removed by adsorption using zinc oxides as adsorbents [1].

1.2.2. Autothermal catalytic reforming

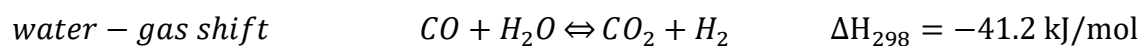
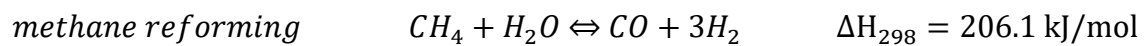
Autothermal catalytic reforming is a variation of steam reforming where part of the hydrocarbons is combusted with air or oxygen in order to supply the needed energy to the reforming reactions. This process is carried out in dedicated reactors where three different sections can be identified [1], [19], [20].

In the first section, known as combustion zone, hydrocarbons and oxygen are mixed and combusted using a burner. The reaction proceeds as a sub-stoichiometric process (oxygen/hydrocarbon ratio is usually 0.55-0.60) and oxygen is completely consumed [19]. If methane is taken as an example for the various hydrocarbons, the following reaction applies



The second section is known as thermal zone and is the final part of the combustion chamber. The main reactions are thermal methane reforming, water-gas shift reactions and pyrolysis of higher hydrocarbons [19].

The combustion chamber is followed by the catalytic zone. In this third zone a fixed bed of catalyst allows catalytic reforming to happen. For methane the following reactions apply



The heat necessary to the reforming reactions is supplied by the combustion of hydrocarbons in the combustion zone. The catalyst (usually nickel supported by magnesia-alumina) is designed to withstand the high temperature reached in the reactor (up to 1400°C at the inlet of the catalytic bed) [19]. Figure 1.9 shows the design of an autothermal reforming reactor.

An advantage of autothermal catalytic reforming is the flexibility in the composition of the syngas produced. With this process a carbon monoxide over hydrogen ratio suitable for chemical synthesis of methanol can be directly achieved. However, the high cost of pure oxygen generation limits the use of autothermal catalytic reforming only to large scale plants [19], [20].

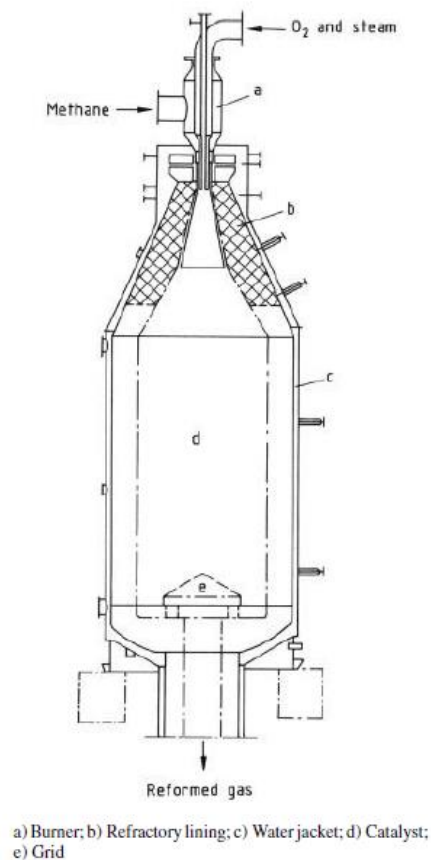


Figure 1.9 Autothermal reformer [1]

Autothermal catalytic reforming is very popular in the production of synthesis gas for ammonia production. For this specific process air can be used instead of pure oxygen, as nitrogen will be used in the following ammonia reactor.

In modern ammonia plants autothermal catalytic reforming is combined with steam reforming to produce the perfect syngas composition. Part of the hydrocarbons are reacted with steam in the primary reformer (where steam reforming is carried out), then the products and unreacted hydrocarbons and steam are mixed with air and reacted in the secondary reformer (where autothermal catalytic reforming happens) [19], [20].

In Figure 1.10 the reforming section of an ammonia synthesis plant is reported.

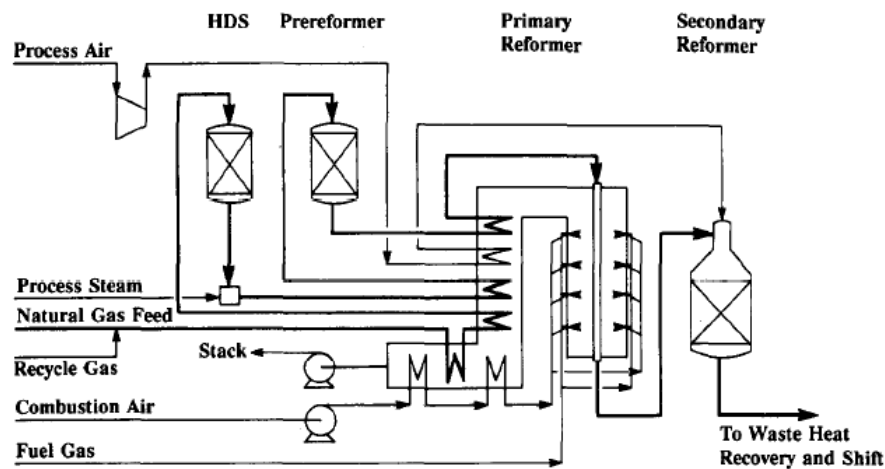
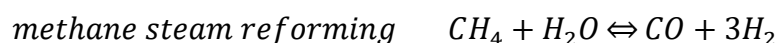
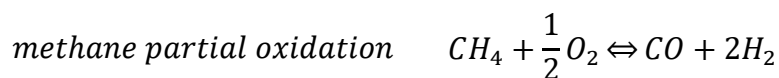


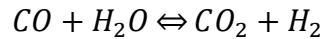
Figure 1.10 Reforming section for production of ammonia synthesis gas [19]

1.2.3. Hydrocarbons partial oxidation

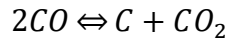
Partial oxidation is a reaction that occurs when a sub-stoichiometric fuel-air mixture is combusted in a high temperature (1350-1600 °C) reformer. Partial oxidation does not require a catalyst and therefore has the advantage of not being particularly sensitive to contaminants. This explains the use of cheaper feedstocks like heavy oil, liquid products from coal gasification and tar oil that are of lower quality compared to other hydrocarbons. Another interesting feature of partial oxidation is that the syngas's hydrogen/carbon dioxide ratio tends to 2, a value suitable for methanol synthesis and Fischer-Tropsch processes. Like autothermal catalytic reforming, partial oxidation needs pure oxygen as a reactant, reducing greatly the economics of the overall process. Several reactions take place inside the partial oxidation reformer and the composition of the products is defined by thermodynamic equilibrium. The principal reactions for methane are reported below, other hydrocarbons follow similar behavior [1], [20], [21].



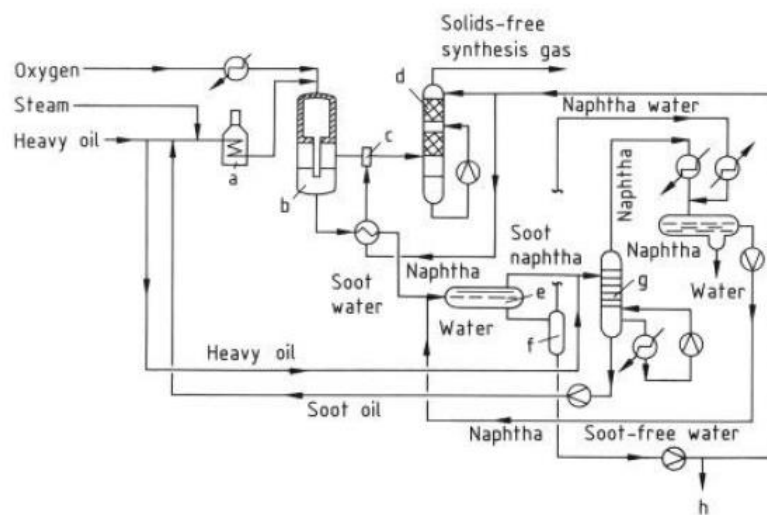
water – gas shift



Boudouard equilibrium



Partial oxidation reactors present a rather simple design that consists of a burner and an insulated chamber. The exothermicity of oxidation reactions maintains high temperatures inside the reactor limiting carbon formation. There are three commercially established processes (Shell, Texaco, Lurgi) for partial oxidation and all of them share a similar configuration [1]. A schematic representation of the Texaco process is shown in Figure 1.11.



a) Preheater; b) Reactor; c) Venturi scrubbing section; d) Soot scrubber; e) Decanter; f) Flash distillation; g) Naphtha column; h) Water clarification

Figure 1.11 Texaco gasification process [1]

The possibility to perform partial oxidation using a catalyst is of great interest and it is subject of intensive study. The use of a catalyst allows lower reaction temperatures (900-1000°C) and faster kinetics leading to residence times in the order of milliseconds, opening the possibility of using compact reactors. Catalytic partial oxidation (CPO) reaction mechanism is not yet completely clarified. Two possibilities have been proposed. The first one is the “direct mechanism” in which hydrocarbons and oxygen in the adsorbed phase directly react to produce CO and H₂. The second one is the “indirect mechanism” in which hydrocarbons are completely oxidized by oxygen to form CO₂ and H₂O, then the unreacted

hydrocarbons undergo steam reforming and dry reforming with the H₂O and CO₂ previously formed [20], [22], [23].

Many efforts have been put into finding the ideal catalyst to sustain partial oxidation but to date no industrial process has been developed. Two families of catalyst have been identified and are subject to research, noble metals and nickel based.

Noble metals, although very expensive, show high activity towards catalytic partial oxidation. Platinum catalysts (promoted with CeZr or non-promoted) achieve high conversion of methane and have high selectivity towards CO and H₂ however they are quickly deactivated either because of carbon deposition or metal sintering. Rhodium base catalysts show excellent performances in CPO with high activity, selectivity and stability. The downside of rhodium is its high cost (rhodium is the most expensive noble metal) and the need to precisely design the catalyst in order to minimize metal loading. Ruthenium catalysts are interesting because they are the cheapest noble metal catalysts, however ruthenium stability is low when it is supported on alumina and silica. Other supports (like titania and zirconia) have been investigated to improve the stability of ruthenium although lower selectivities are achieved. Palladium catalysts are highly active for methane combustion however their limited stability makes them unsuitable for CPO [22].

Nickel has the advantage of being inexpensive and it is widely studied for CPO. The disadvantages of nickel catalysts are carbon deposition, sintering, solid state reactions and volatilization of metal carbonyls that lead to fast deactivation. Various supports have been investigated, in particular MgO, ZrO₂, TiO₂ and Al₂O₃. Promoters like alkaline and alkaline earth metals, lanthana and ceria have been used to improve CPO performances of nickel catalysts [22].

1.2.4. Dry reforming

The name dry reforming defines a catalyzed process that utilizes carbon dioxide instead of steam to reform hydrocarbons. The dry reforming reaction for methane is reported below



Dry reforming's most appealing features are the possibility to generate syngas with a composition suitable for various chemical processes like oxo synthesis and Fischer-Tropsch (hydrogen/carbon dioxide ratios that tend to 1), and the fact that during dry reforming two greenhouse gases are consumed. The main disadvantage of dry reforming is that the absence of steam and the high concentration of CO₂ lead to intensive carbon deposition and subsequent catalyst deactivation. In the recent

years a lot of work has been done in order to develop catalysts that are able to limit coke formation, however industrial application of dry reforming remains limited [20], [24].

It is believed that dry reforming proceeds via a bi-functional mechanism, hydrocarbon dehydrogenation happening on nonvalent metal sites and carbon dioxide dissociation on basic sites. Noble metals (Pt, Pd, Rh, Ir, Ru) are very active in dehydrogenation reactions and have been intensely studied but their relatively high cost hinders possible scale-up applications. Transition metals, mainly Ni and Co, have been investigated as cheap alternatives to noble metals even though their stability and coke resistance are lower [24].

To improve CO₂ dissociation and to limit coke formation different promoters have been investigated. Alkali and alkaline-earth metals supply basic sites to carbon dioxide dissociation and favor the distribution of the active metal phase. Rare earth metals can also improve CO₂ dissociation as they introduce active surface oxygen species in the catalyst increasing oxygen storage and transfer capacity. Lastly transition metal oxides (ZrO₂, TiO₂, MnO₂, MnO₃) have been selected as promoters as they show high oxygen mobility properties [24].

1.2.5. Biogas reforming

Biogas is a suitable raw material for syngas production, offering the advantage of being a renewable and sustainable source. The high content of carbon dioxide in biogas (30-50%) does not represent an obstacle for the conversion into syngas as CO₂ can act as a reactant in the reforming reactions. Carbon dioxide removal in biogas is therefore not needed, avoiding substantial costs in gas purification. These features combined with the fact that biogas reforming directly converts two green-house gases into a valuable product, have raised the interest in this technology [25].

Three possible routes can be followed to convert biogas to syngas: dry reforming, bi-reforming and tri-reforming.

Dry reforming, which has already been discussed in the previous subsection, is the direct reaction between methane and carbon dioxide producing hydrogen and carbon monoxide. The main advantage of this reaction is that it does not require additional reactants aside from biogas and it produces a syngas with hydrogen over carbon monoxide ratio that tends to 1 suitable for further chemical synthesis. However, as already mentioned, dry reforming presents various disadvantages. The first one is that it is a highly endothermic reaction requiring very high temperatures (900 °C), secondly the thermodynamic equilibrium limits the complete conversion of reactants (in order to increase methane conversion an excess of carbon dioxide is needed and vice versa). Lastly the reaction conditions allow the

formation of carbon and its deposition on the catalyst thus limiting its activity. The problems related to dry reforming of biogas prevent the development of the technology at commercial scale [26], [27].

Bi-reforming refers to the combination of carbon dioxide and steam to reform biogas. Steam reforming is less energy demanding than dry reforming and the presence of steam inhibits deposition of carbon on the catalyst. High steam and carbon dioxide over methane ratios allow the complete consumption of methane. Carbon dioxide conversion increases at high temperatures due to dry reforming and reverse water gas shift reaction, however carbon dioxide is never completely converted as steam is a more efficient reforming agent. Syngas produced via bi-reforming presents hydrogen over carbon monoxide ratio greater than 1 with the ratio greatly influenced by inlet composition (CO_2 and steam concentrations with respect to methane) and reaction conditions [26], [28].

Tri-reforming of methane is the combination of dry reforming, steam reforming and partial oxidation of methane. The main advantages of tri-reforming are the higher energy efficiency (derived by the fact that methane partial oxidation is an exothermic process that counterbalances the endothermicity of dry and steam reforming), inhibition of carbon formation due to the presence of steam and oxygen, high methane conversion and desirable syngas composition. Tri-reforming present similar disadvantages to bi-reforming as carbon dioxide is never completely converted, moreover tri-reforming requires the presence of pure oxygen and consequently costly air separation units [26].

1.3. Methanol

Methanol (CH_3OH) is the simplest alcohol and is one of the most important chemicals produced worldwide. Methanol as raw material is utilized in the production of various molecules, the most important are formaldehyde, MTBE, dimethyl ether and acetic acid. Industrially, methanol is also employed in the manufacture of paints, resins, silicones, adhesives, antifreeze and plastics. Thanks to its characteristics (high octane number), it is also used as a transportation fluid in addition to gasoline and in some dedicated engines it can be used in pure form. The molecular structure of methanol allows it to burn in a cleaner way when compared to other fuels, moreover its high solubility in water and fast degradability in both aerobic and anaerobic conditions minimize the hazardousness of its release in the environment. Methanol is also studied as hydrogen carrier in fuel cells applications and as fuel in direct methanol fuel cells (DMFCs) [1], [29].

Liquid methanol can serve as an efficient energy storage medium as it is easily transportable, it can be used as fuel, and it is a building block to produce intermediates and synthetic hydrocarbons. These properties lead to the idea that methanol will be a key compound in the future, with the possible development of a methanol-based economy [1], [29].

Global methanol demand reached 75 million metric tons in 2015 and the worldwide methanol capacity is nowadays 110 million metric tons according to IHS [30].

Methanol was obtained for the first time in 1600s by Sir Robert Boyle (1627-1691) through wood distillation, and this process remained the most important source of "wood alcohol" for more than two centuries. At the beginning of the 20th century BASF researched a method for synthetic production of methanol starting from syngas, and in 1923 opened the first methanol plant where syngas was supplied via coal gasification. The operating conditions for the BASF process were very intensive (300-400°C and 250-300 atm) and the reaction needed a zinc/chromium oxide catalyst. In the following years, research was aimed at reducing process economics mainly lowering the operating pressure and temperatures of the process. In the 1960s, thanks to the use of a cleaner syngas produced via steam reforming of methane, a new and more active copper/zinc oxide catalyst was employed by ICI allowing less strict operating conditions (300°C and 100atm). A few years later Lurgi developed a process with even more favorable operating condition reaching nowadays standard of 200-250°C and 40-50 atm [1], [29].

1.3.1. Methanol production

Nowadays methanol industrial production is still based on syngas, although a lot of work has been done to optimize process conditions and developing new reactor designs and new catalytic systems.

Methanol synthesis can be divided into three steps: syngas production, conversion of syngas into methanol, distillation of the reactor products. Syngas production has already been discussed in the previous chapter and only small details will be discussed in this paragraph.

The vast majority of methanol produced worldwide is derived from syngas produced from natural gas. The main advantage of natural gas is that is relatively cheap when compared to liquid hydrocarbons and usually contains smaller concentrations of contaminants. This last feature is extremely important in methanol synthesis, as the copper/zinc oxide catalyst used are extremely sensitive to sulfur. Using natural gas allows cheaper purification steps greatly improving process economics [1], [29], [31].

An important characteristic of the syngas produced for methanol synthesis is its composition. Two key parameters are used to determine optimal syngas composition and can be calculated from the following Equation 1.1 and Equation 1.2:

$$SN = \frac{Y_{H_2} - Y_{CO_2}}{Y_{CO} + Y_{CO_2}} \quad \text{Equation 1.1}$$

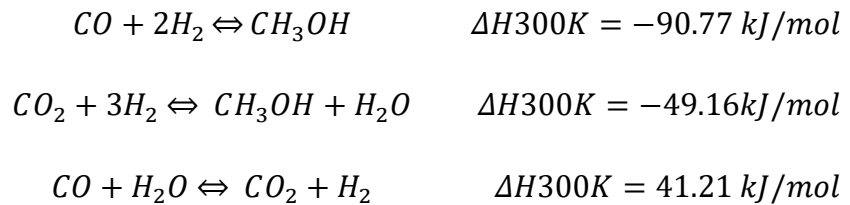
$$COR = \frac{Y_{CO_2}}{Y_{CO} + Y_{CO_2}} \quad \text{Equation 1.2}$$

Stoichiometric number (SN) defines hydrogen over carbon oxides ratio. SN equal to 2 defines a stoichiometric mixture for methanol production, however for optimal industrial operation values slightly larger (excess of hydrogen) are used [29], [32].

COR, or carbon oxides ratio, defines the ratio between carbon monoxide and carbon dioxide and is usually kept around 0.6. For higher values (higher concentration of CO₂) slower kinetics and lower equilibrium conversions are obtained, with the advantage of lower selectivity to side products [32].

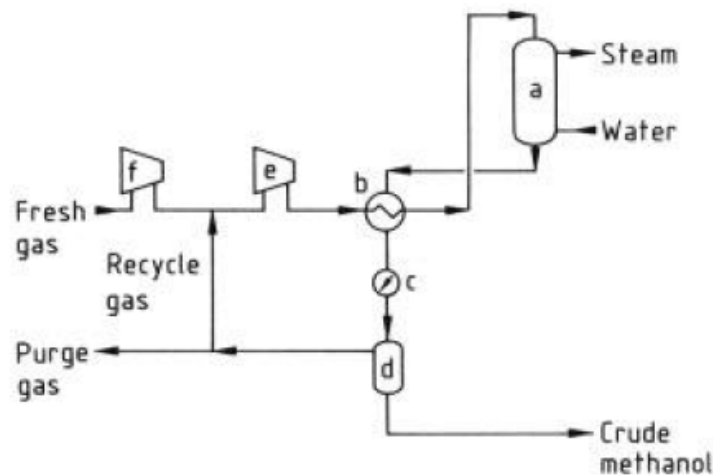
The synthesis process of methanol can be classified in two classes based on the pressure used. High pressure processes (200-300 atm) are now obsolete and have been substituted by low pressure processes (50-100 atm), with numerous advantages such as lower investment and operating cost and improved operation reliability.

Methanol production from syngas can be described by the following equilibrium reactions:



Where the second equilibrium reaction can be seen as the sum of the first and the third one. The overall reaction is exothermic and proceeds with a reduction of moles, therefore it is favored at low temperatures and high pressure. Nowadays temperature is kept in the range of 200-300°C, the minimum temperature at which modern catalysts are active. The pressure levels used (50-100 atm) allow a maximum conversion of synthesis gas to methanol in the range of 10-15%, therefore the unreacted gas needs to be recycled to guarantee sufficient yield [33].

Figure 1.12 gives a schematic representation of the synthesis section of a methanol plant.



a) Reactor; b) Heat exchanger; c) Cooler; d) Separator;
e) Recycle compressor; f) Fresh gas compressor

Figure 1.12 Methanol synthesis [1]

All the methanol plants built worldwide share the same basic configuration represented in Figure 1.12 Methanol synthesis [1]. Syngas is compressed to the desired pressure and is preheated in a heat exchanger with the effluent of the

reactor, taking advantage of the overall exothermicity of the reaction involved. Syngas is then introduced in the reactor where it contacts the catalyst and is converted to methanol. The effluent is cooled and separated in a separator (usually a flash drum). Crude methanol is then sent to the rectification section of the plant while the unreacted syngas is recycled back with the fresh syngas feed. Part of the recycled syngas is purged to respect stoichiometric number and avoid inert accumulation [1].

The main differences of methanol synthesis section at industrial level are related to the reactor design. Two families of reactors are commonly adopted: adiabatic reactors and isothermal reactors.

The most adopted solution is ICI adiabatic reactor. In this configuration the reactor is composed of a single bed of catalyst. Cold syngas is introduced at various points in the reactor bed in order to quench the reaction. The temperature profile assumes a sawtooth shape along the reactor's axis.

A similar approach is followed in the Kellogg's and Haldor Topsoe processes, with the difference that these processes use multiple catalyst beds with intermediate coolers.

Lurgi's methanol reactor belongs to the isothermal reactor family. This reactor is built similarly to a shell and tube heat exchanger, where the catalyst is loaded tube side while shell side boiling water is used to maintain isothermal conditions.

Similar approaches to Lurgi are adopted by Mitsubishi and Linde.

Fluidized bed reactors and liquid phase technologies have also been proposed in order to optimize reaction conditions and temperature controllability.

Other researched technologies comprehend membrane reactors (with the advantage of direct separation of synthesis products from unreacted syngas) and one-step technologies, where multiple in series reactions are conducted in the same reactor. The advantage of membrane reactors and one-step technologies is that the thermodynamic equilibrium is shifted towards the products when methanol is removed from the reacting environment (either through the membrane or through its consumption in a subsequent reaction) [1], [29], [34].

In Figure 1.13 different kind of methanol reactors are represented.

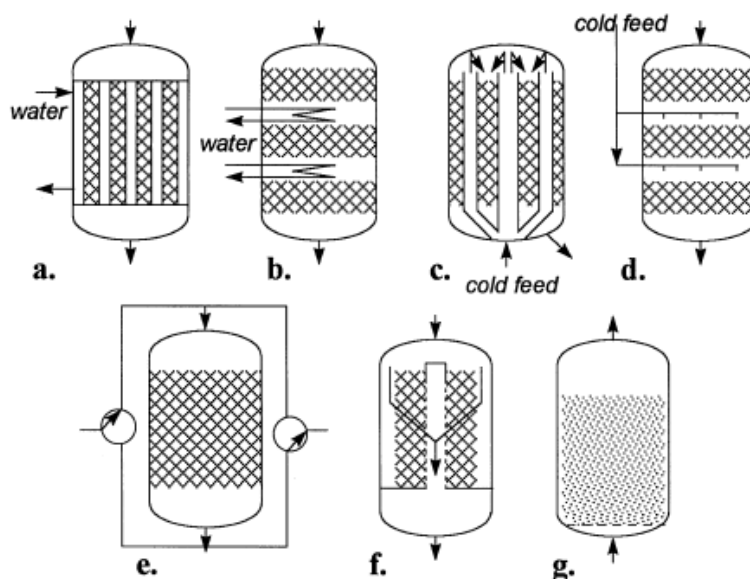


Figure 1.13 Different methanol synthesis reactors. (a) isothermal reactor with external cooling bath; (b) adiabatic reactor with intermediate coolers; (c) adiabatic reactor with cold feed cooling; (d) adiabatic reactor with intermediate feed gas quench; (e) feed-effluent heat exchange by periodic flow reversal; (f) radial flow reactor; (g) fluidized bed reactor [34].

It is important to note that methanol synthesis kinetic mechanism is still debated, and through the years many kinetic pathways have been proposed. The most discussed issue regards the molecule from which methanol originates. Until the 1980s kinetic mechanisms were exclusively based on the hydrogenation of carbon monoxide to methanol and the role of carbon dioxide was to increase the yield displacing reverse water gas shift equilibrium. Afterwards the role of carbon dioxide started to gain importance and different studies claimed that methanol originates only from carbon dioxide, while carbon monoxide is consumed via water gas shift to generate carbon dioxide. Lately the most common belief is that both mechanisms may happen with a predominant conversion of carbon dioxide to methanol at industrial reaction conditions [1], [29], [31], [32], [35], [36].

Methanol purification is usually carried out in distillation columns. First light ends (like dissolved gases) are removed from crude methanol in a light end column, then methanol is separated from heavier compounds (water and higher alcohols) in one or more distillation columns.

In Figure 1.14 and Figure 1.15 the two most common methanol synthesis processes plant diagrams are reported.

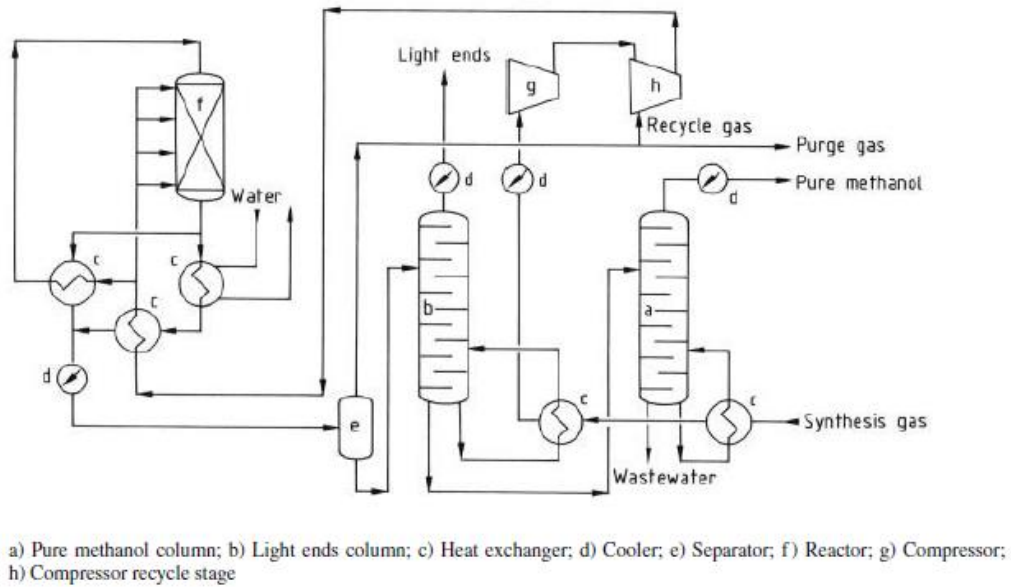


Figure 1.14 ICI low-pressure methanol process [1]

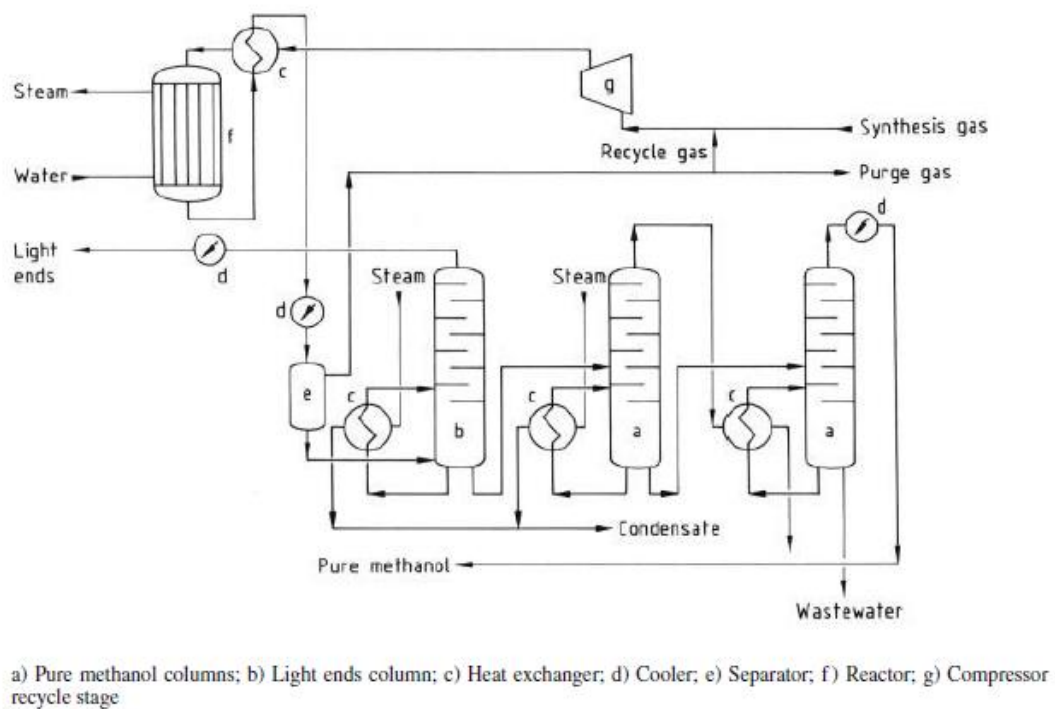


Figure 1.15 Lurgi low-pressure methanol process [1]

1.3.2. Methanol synthesis prospects

Methanol synthesis' future relies on the utilization of renewable sources and is part of the broader vision of green economy. Methanol can be produced starting from carbon dioxide and hydrogen [37], [38]. The consumption of a greenhouse gas in combination with the use of hydrogen generated from renewable sources could represent a way to possible zero emission chemical production. While carbon dioxide sources are easy to exploit (industry off gases, combustion gases), hydrogen is mainly produced from hydrocarbons and its production from water via electrolysis is not economically attractive.

Biomasses (wood, agricultural crops, municipal solid waste, animal waste) can be gasified through partial oxidation and pyrolysis, producing mixtures of H₂, CO, CO₂ and H₂O that can be converted to methanol using already available technologies. Although high quantities of biomass would be needed (producing issues related to land usage, crop cultivation competing with food, transportation problems) this could represent a carbon neutral way to produce methanol not relying on fossil fuels [29].

Alternatively, methanol can be produced starting from biogas. As already mentioned, biogas is a suitable renewable source of syngas as it is generated via anaerobic digestion from biomasses and waste. Biogas can be converted into syngas as mentioned in the previous section and subsequently to methanol using conventional technologies. Excess hydrogen generated in steam reforming of biogas is also a renewable source of hydrogen that can be used with carbon dioxide from different sources to produce methanol [29], [39], [40]–[44].

Direct conversion of carbon dioxide into methanol through hydrogenation is the most promising route for future green methanol production as technologies are already available.

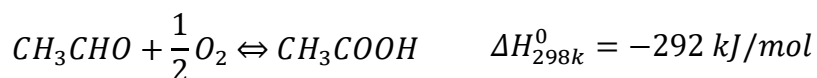
In 2012 Carbon Recycling International (CRI) was the first company to ever built a methanol pilot plant which utilizes carbon dioxide generated in a geothermal powerplant and hydrogen generated through electrolysis of water to produce methanol. In 2016 the production capacity of George Olah renewable methanol plant was scaled from 1300 to 4000 tons per year. In 2022 Carbon Recycling International is commissioning a new CO₂-to-methanol production facility located adjacent to a coke oven gas production (COG) in Anyang city, Henan Province, China. The plant is the world's largest production of fuel from captured CO₂ emissions with a capacity of 110.000 tons low-carbon intensity methanol per year [45].

1.4. Acetic acid

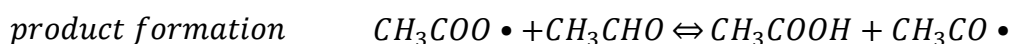
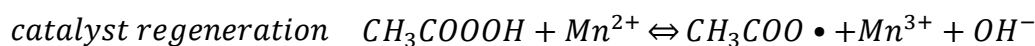
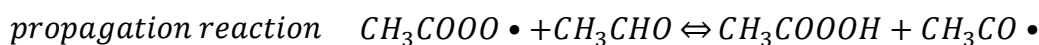
The most important characteristics of acetic acid and its utilization have already been discussed in the introduction of this thesis work. In this section the main industrial production routes of acetic acid will be discussed.

1.4.1. Acetaldehyde process

Acetaldehyde oxidation represented the main route for acetic acid production until the 1960s. This process has gradually been abandoned in favor of methanol carbonylation and is now rarely used only in eastern developing countries. Oxidation of acetaldehyde is an exothermic process with a reduction in the number of moles and is therefore favored at low temperatures and low pressures. The typical values for these parameters are 60-80 °C and 3-10 atm. Air or enriched air is used as an oxidizing agent. Uncatalyzed reactions are accompanied by production of unwanted byproducts (formic acid, ethanol, methanol, acetone, formaldehyde, CO, CO₂, methane), therefore the use of a catalyst is necessary to increase selectivity towards acetic acid. Mn, Cu, Co based redox catalysts have been utilized [1].



The oxidation of acetaldehyde proceeds through a rather complex free-radical chain mechanism, which produces peracetic acid as intermediate. A simplified reaction scheme is provided with the following reactions.



Secondary reactions are responsible for side product production.

A schematic representation of acetaldehyde oxidation plant is reported in Figure 1.16 Oxidation of acetaldehyde to acetic acid [1]Figure 1.16.

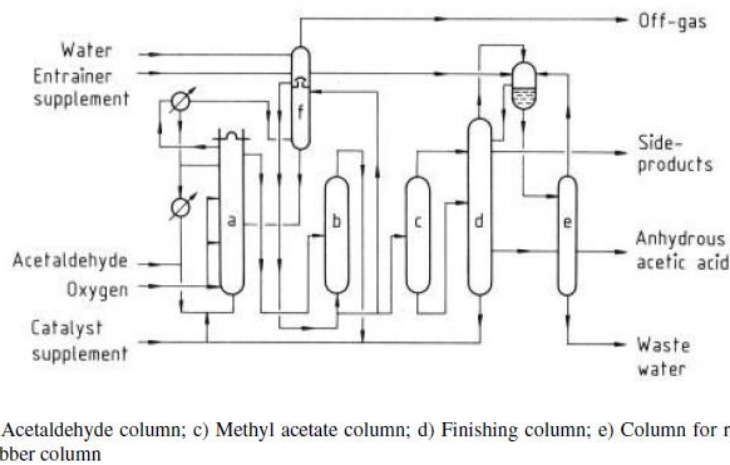
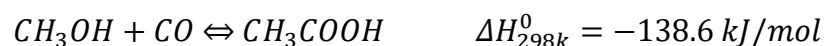


Figure 1.16 Oxidation of acetaldehyde to acetic acid [1]

Acetaldehyde, air, and the catalyst are fed to the reactor. The off gases are scrubbed with crude product and water in two different scrubbers to recover the reactants. The reactor mixture is continuously recirculated after being cooled down in an external heat exchanger to remove the reaction heat. The products and unreacted acetaldehyde are sent to a distillation train. In the first column acetaldehyde is separated and recirculated to the reactor, in the second column methyl acetate is removed from the top and the bottoms are sent to the third column where acetic acid is separated from water through azeotropic distillation using ethyl acetate. The last column separates water from ethyl acetate that is recovered and sent back to the third column [1].

1.4.2. Methanol carbonylation

Carbonylation of methanol is the principal industrial route to acetic acid production.



This reaction was described by BASF in 1913 in their studies on acetic acid formation at high temperatures and pressures, however the commercialization of the first industrial process based on methanol carbonylation happened in 1960, when BASF opened the first plant in Germany. The BASF process was characterized by high pressures (up to 700 bar) and temperatures of about 250°C. A cobalt iodide catalyst was needed to ensure high conversion of reactant and the harsh pressure conditions were needed to achieve commercially acceptable reaction rates. Figure 1.17 shows

the proposed reaction mechanism for the BASF cobalt process. It is important to note that this mechanism is characterized by two catalytic cycles, one that involves the metal carbonyl catalyst and one that involves the iodide promoter. All the carbonylation processes share this feature [1].

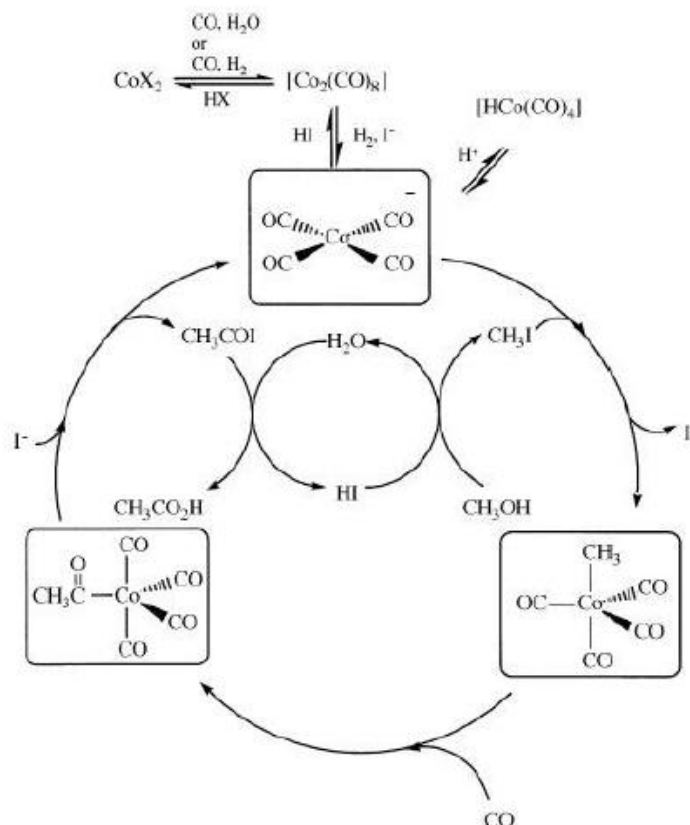


Figure 1.17 Reaction cycle proposed for the cobalt-catalyzed methanol carbonylation reaction (BASF process) [1]

Figure 1.18 shows a representation of BASF acetic acid plant. The reactants (carbon monoxide and methanol), catalyst, water and dimethyl ether are sent to the high-pressure reactor. The products are cooled down and sent to a train of separators at decreasing pressure levels. The gaseous streams are washed and scrubbed with fresh methanol in two separate columns to recover iodine containing compounds before being discarded as off-gases. The methanol solution is recirculated to the reactor. The liquid products are sent to a distillation train. In the first column the catalyst is recovered and recirculated to the reactor, in the second one compounds lighter than acetic acid are separated through azeotropic distillation, in the third one acetic acid is separated from heavier compounds (mainly propionic acid) and in the

last one side products are recovered from the bottom while the top products are recirculated to the second column.

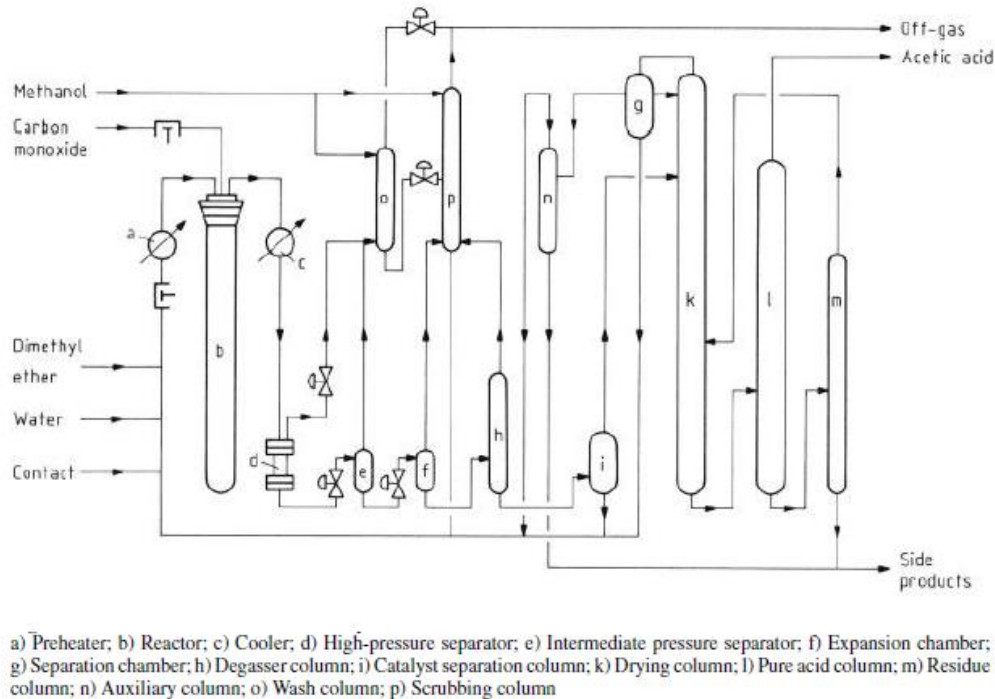


Figure 1.18 BASF acetic acid production process [1]

In 1970 Monsanto commercialized a methanol carbonylation process based on a rhodium iodide catalyst system. This catalyst proved to be several times more active compared to BASF cobalt catalyst. A direct consequence of the catalyst improved activity was the less severe reaction conditions. The Monsanto process is conducted at 180°C and 30-50 atm, making it easier to manage and economically more attractive. In 1980 Celanese improved the rhodium catalyzed system of the Monsanto process, adding catalyst co promoters that allowed lower reaction-water concentrations. Another improvement made by using rhodium catalyzed systems is the reduction of biproduct formation such as methane, acetaldehyde, and propionic acid [1].

Figure 1.19 shows the reaction cycle for the Monsanto process. As already mentioned, two cycles can be identified, the metal carbonyl catalyst one and the iodide promoter one.

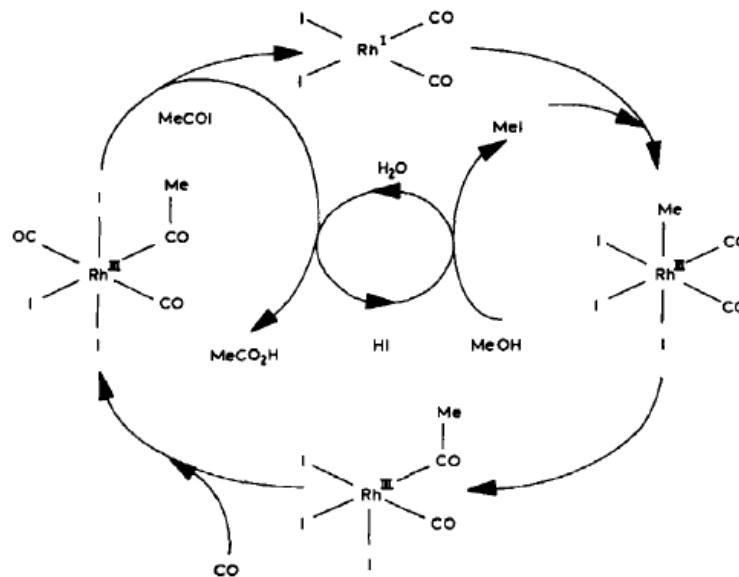


Figure 1.19 Monsanto rhodium catalyzed carbonylation of methanol reaction cycle [46]

The plant configuration of Monsanto process (reported in Figure 1.20) is similar to the BASF one, the biggest difference is represented by the reactor. In Monsanto process a CSTR reactor with external cooling jacket is utilized as the pressure requirements are less strict.

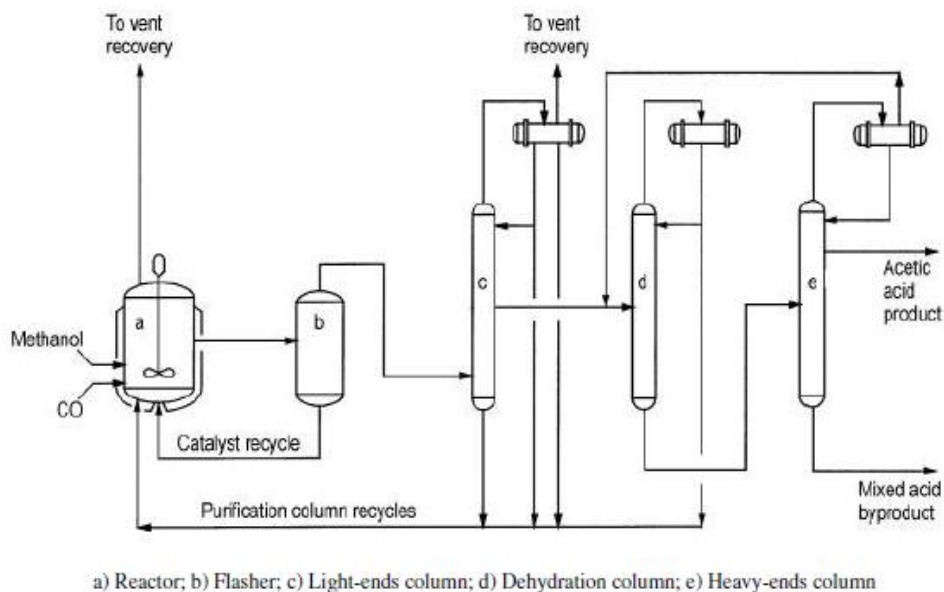


Figure 1.20 Monsanto acetic acid production process [1]

The most recent development in acetic acid production via methanol carbonylation has been made in 1996 when BP chemicals announced the Cativa™ process. The principal innovation of this process is that it utilizes an iridium-based catalyst. The main advantages of Cativa™ process are the lower price of iridium with respect to rhodium and the extreme robustness of the iridium catalyst even at low water concentrations [46], [47], [48], [49].

The reaction cycle of this process is similar to the Monsanto one, the main difference is the rate determining step. Methyl iodide addition to the iridium center is about 150 times faster with respect to the equivalent step in the rhodium process, while the subsequent CO insertion to form the iridium-acyl species is the slowest step of the cycle [1], [46], [47].

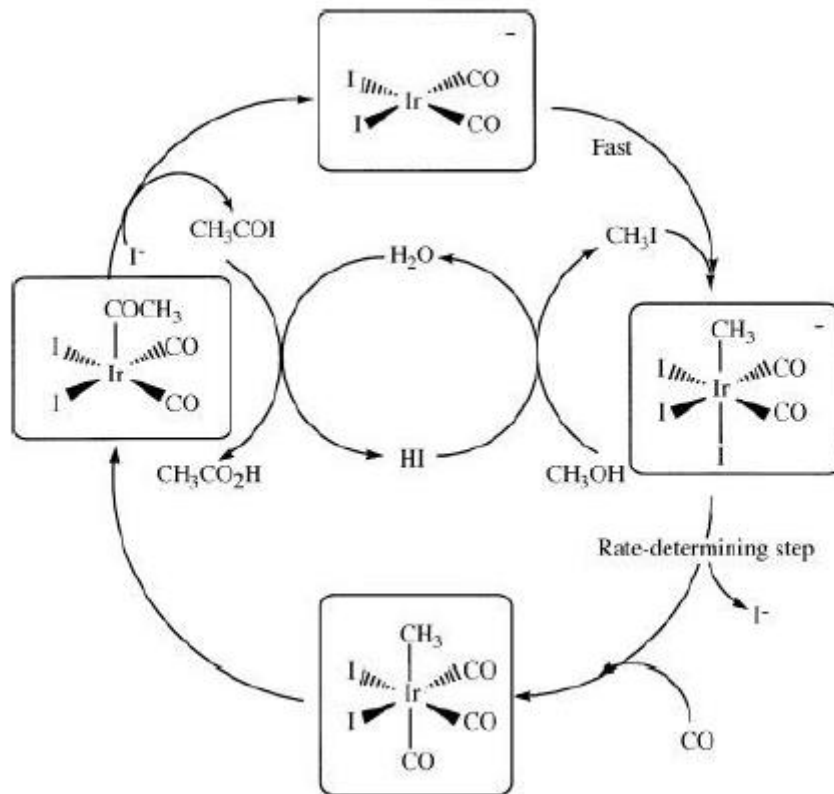


Figure 1.21 Reaction cycle proposed for the iridium-catalyzed methanol carbonylation reaction (Cativa process) [1]

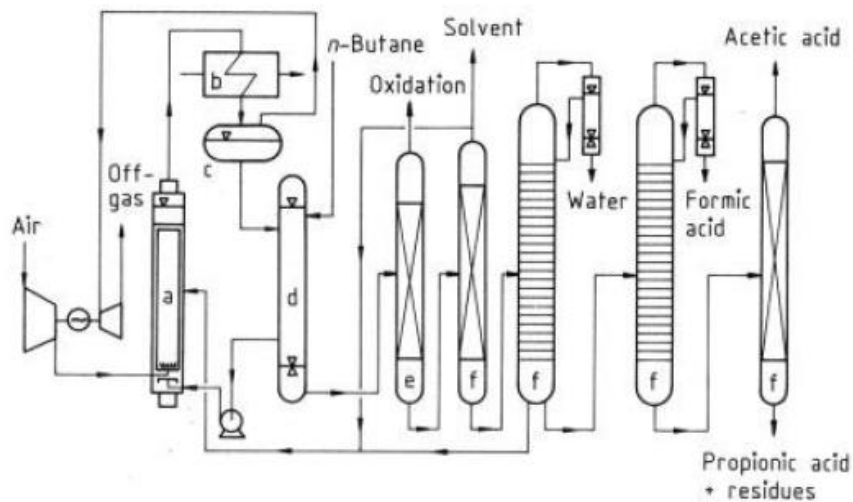
1.4.3. Other production technologies

Other acetic acid manufacturing technologies are based on oxidation of hydrocarbons. Due to the competitiveness of methanol carbonylation these

technologies are less common and already existing plants have reduced their production significantly.

Liquid-phase oxidation of hydrocarbons (LPO) is a process that converts butane and light naphtha to a variety of products, including acetic acid. The reaction between hydrocarbons and oxygen proceeds through a radical chain mechanism. The use of a catalyst is not necessary in LPO but using one can maximize product selectivity towards a specific compound. Mn, Co, Ni and Cr are commonly used during LPO operations [1].

Industrial operations are characterized by a wide range of parameters, usually temperatures are between 150°C and 200°C and pressure up to 50 atm. The hydrocarbons are oxidized by oxygen or air in a sparged tubular reactor, the products are then sent to phase separators where the unreacted hydrocarbons are separated from an aqueous layer. The hydrocarbons are recycled to the reactor, while the water rich phase is sent to distillation. Remaining less soluble hydrocarbons are separated and recycled to the reactor, while the residual hydrocarbon-free product (composed of aldehydes, ketones, esters, alcohols, water and volatile monocarboxylic acids) is sent to further distillation columns. Water removal is the most difficult purification step and it's usually done through azeotropic distillation. Figure 1.22 shows a *n*-butane LPO process [1].



a) Reactor; b) Air cooler; c) Collector; d) Separation vessel; e) Pressure column; f) Distillation column

Figure 1.22 Oxidation of *n*-butane in the liquid phase (Chemische Werke Hüls process) [1]

In 1997 Showa Denko K.K. constructed the first commercial acetic acid plant based on ethylene oxidation. In this process, acetic acid is manufactured with high selectivity from a mixture of ethylene and oxygen in the vapor-phase at 160–210 °C over a solid catalyst. In Figure 1.23 the process flowsheet of ethylene oxidation plant is reported [50].

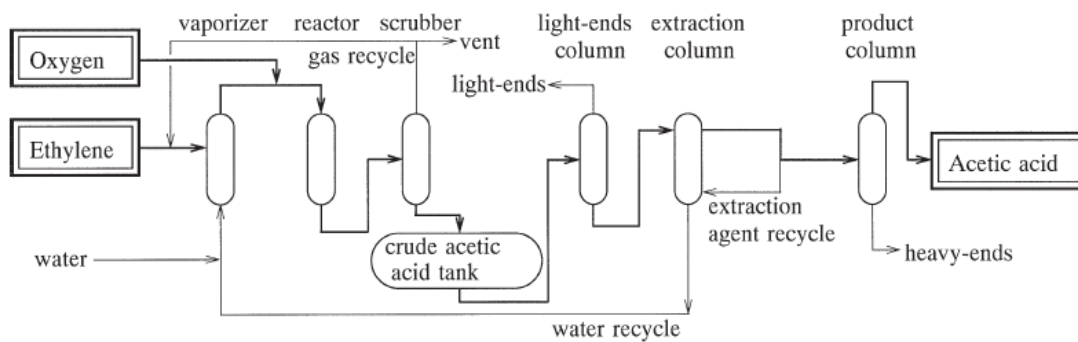


Figure 1.23 Process flowsheet of direct oxidation to ethylene into acetic acid [50]

An important mention needs to be made with regards to biological acetic acid production. Today the biological route of acetic acid production accounts for about 10% of world production. It remains important because many of the world food purity laws stipulate that vinegar used in foods must be of biological origin [1], [51].

Two distinct groups of acetic acid producing microorganisms can be identified: aerobes acetic acid bacteria and anaerobes acetogens ones.

Acetic acid bacteria have the ability to oxidize ethanol to acetic acid under aerobic conditions. *Acetobacter*, *Gluconacetobacter* and *Gluconobacter* are the main genera of acetic acid bacteria for aerobic fermentation [1], [51].

Acetogens are facultative autotrophs that can grow by the oxidation of a large variety of organic substrates, including hexoses, pentoses, alcohols, methyl groups and formic acid, or by the oxidation of inorganic substrates such as hydrogen or carbon monoxide, which is usually coupled with the reduction of CO₂ into acetate via the Wood–Ljungdahl pathway [51].

Three methods are used to produce biological acetic acid: Orleans method, generator method and submerged method.

The Orleans method is the oldest of the three. It is a slow continuous process in which vinegar is fermented in a large barrel (200 liters) and about 10-15 liters can be

withdrawn every week as wine is added to replace the vinegar removed. The overall process is carried out for 8-14 weeks [51].

The generator method (also called trickling method or German method) uses a trickle bed tank filled with wood shavings that act like support material for bacterial growth. The alcoholic solution is trickled down to the shavings and recirculated to the top of the tank with a pump. The advantage of this method is the increased surface area provided by the supporting material. Oxygen exchanges are therefore maximized, increasing vinegar production [51].

The submerged method was introduced in the 1950s. The system consists of a stainless-steel fermentation tank equipped with a cooling system, air supply system and agitation system. The alcoholic solution is loaded in the tank and fermented for 24-48 h. Air is bubbled from the bottom of the tank through all the process and the fermentation broth is maintained agitated and at constant temperature by the cooling system. Different reactor configurations can be used (bubble column, cavitator, Frings acetator) [51].

2 Tools and instruments

This thesis process simulation work has been carried out using the software Aspen HYSYS® V11. Other software utilized to carry out the economic assessment of the simulated chemical plant are Microsoft Excel® and MATLAB® R2017b.

2.1. Aspen HYSYS®

Aspen HYSYS® is a chemical process simulator developed by AspenTech®. This software is used to mathematically model chemical processes, from unit operations to full chemical plants and refineries. HYSYS can perform the principal calculations of chemical engineering, including mass balance, energy balance, vapor-liquid equilibrium, heat transfer, mass transfer, chemical kinetics, fractionation, and pressure drops. Other features of this software are the simple graphic interface, complete databases of chemical species with their physical and thermodynamical properties, reliable thermodynamic models and robust solving algorithms. HYSYS is used extensively in industry and academia for steady-state and dynamic simulation, process design, performance modelling, and optimization.

2.2. Microsoft Excel®

Microsoft Excel® is a software developed by Microsoft and it is one of the most used spreadsheets worldwide. It features calculation or computation capabilities, graphing tools, pivot tables, and a macro programming language called Visual Basic for Applications (VBA).

2.3. MATLAB®

MATLAB® is a proprietary multi-paradigm programming language and numeric computing environment developed by MathWorks®. MATLAB® allows matrix manipulations, plotting of functions and data, implementation of algorithms, creation of user interfaces, and interfacing with programs written in other languages.

3 Process simulation

A conceptual design of the biogas to acetic acid plant has been carried out through Aspen HYSYS®. For the sake of simplicity, the plant has been divided into five main sections:

- Syngas production
- Syngas refining
- Methanol production
- Acetic acid production
- Separation section

A combination of SRK (Soave-Readlich-Kwong) and NRTL-SRK (non-random two-liquid model for the liquid phase combined with SRK model for vapor phase) fluid packages has been chosen to model the thermodynamic properties of the components used in the simulation.

3.1. Syngas production section

The first section of the plant is dedicated to syngas production. In Figure 3.3 Syngas synthesis section an overview of this section is provided.

Syngas is produced starting from biogas with a molar composition of 60% methane and 40% carbon dioxide. The plant has been designed to convert 1052 m³/h (44.61 kmol/h) of biogas available at 25°C and atmospheric pressure (stream 1). Biogas is compressed in two separate compressors (referred as K-105 and K-106) with intermediate cooling in order to reach pressure compatible with syngas synthesis. The compressors have an adiabatic efficiency of 0.75 and compression ratio of 4.94 and 4.14 respectively, the pressure of biogas after the first compressor is 500 kPa and after the second compressor is 2030 kPa. Intermediate cooling is provided by cooling water in a heat exchanger (E-100) and the gas is cooled to 35°C. In every heat exchanger of the plant a pressure drop of 10 kPa is taken into consideration. After the second compressor biogas (stream 7) is heated in a heat exchanger (E-107) from 177.9°C to 230°C using high pressure steam. The heated stream (stream 16) is then mixed with steam at 215°C (stream 138). The composition of the mixed stream

(stream 6) and its physical properties are reported in Table 3.1. In Figure 3.1 the subsection described above is reported.

CH₄ molar flow	26.7690 kmol/h
CO₂ molar flow	17.8638 kmol/h
H₂O molar flow	49.2140 kmol/h
H₂ molar flow	0.0001 kmol/h
Temperature	219.2°C
Pressure	2020 kPa

Table 3.1 Composition and Physical properties of stream 6

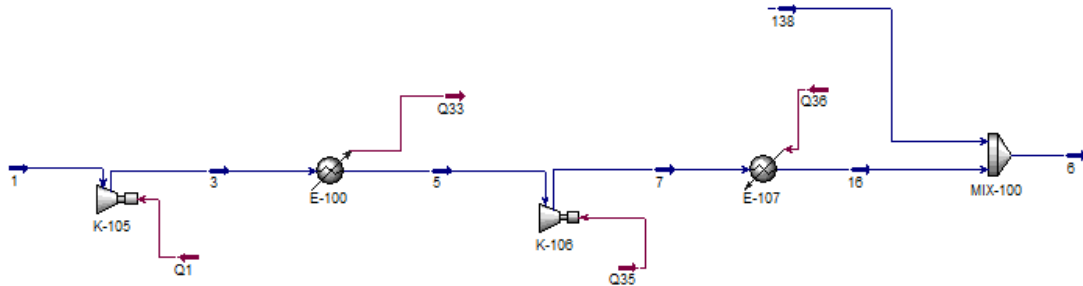


Figure 3.1 Biogas compression train

The mixed stream is heated to 650°C in a process-to-process heat exchanger (E-115) before entering the reforming reactor (PFR-101). In the reformer bi-reforming of biogas is carried out at 900°C and 2010 kPa in accordance with information found in literature. The reformer has been modeled as a multiple-pipes reactor of total volume 2.5 m³, each pipe is 10 m in length and 1.5 inches in diameter with wall thickness of 1 cm. A total number of 219 pipes compose the reactor. A void fraction of 0.4 has been considered as the reactor is loaded with reforming catalyst (standard nickel catalyst) with density of 2500 kg/m³. A total pressure drop of 200 kPa is considered through the reactor. An overview of the thermodynamic and kinetics involved in the reactor will be discussed in the following subsection. The product composition (stream 60) is reported in Table 3.2.

CH₄ molar flow	3.0610 kmol/h
CO₂ molar flow	11.7418 kmol/h
CO molar flow	29.8287 kmol/h
H₂O molar flow	31.6280 kmol/h
H₂ molar flow	65.0049 kmol/h

Table 3.2 Composition of stream 60

Stream 60 is cooled down to 533.5°C in the process-to-process heat exchanger used to heat the reactants (stream 6) and is then sent to a series of two process-to-process heat exchangers (E-120 and E-117) where the heat recovered is used to produce the steam necessary to the reformer. In the first heat exchanger (E-120) syngas (stream 135) is cooled from 533.4°C to 239.7°C while steam at 215°C and 2020 kPa is produced. In the second heat exchanger (E-117) syngas (stream 136) is cooled from 239.7°C to 126.5°C while water is heated up from 31.43°C to 213.8°C. Syngas (stream 134) is further cooled down with cooling water in a fourth heat exchanger (E-103) to 35°C before entering a flash separator (V-100). In the separator syngas (stream 10) is separated from water (stream 11) at 35°C and 1770 kPa. The separated water is pumped at 2030 kPa and recirculated to the steam generating units (E-117 and E-120) through a pump (P-102). Make-up fresh water available at 25°C and atmospheric pressure (stream 61) is added to the recirculated water through a second pump (P-101). Both pumps have adiabatic efficiencies of 0.75. Figure 3.2 reports the subsection described above. In Table 3.3 the composition and physical properties of the syngas stream exiting the separator (stream 10) are reported.

CH₄ molar flow	3.0610 kmol/h
CO₂ molar flow	11.7241 kmol/h
CO molar flow	29.8283 kmol/h
H₂O molar flow	0.3823 kmol/h
H₂ molar flow	65.0049 kmol/h
Temperature	35°C
Pressure	1770 kPa

Table 3.3 Composition and physical properties of stream 10 **Error! Reference source not found.**

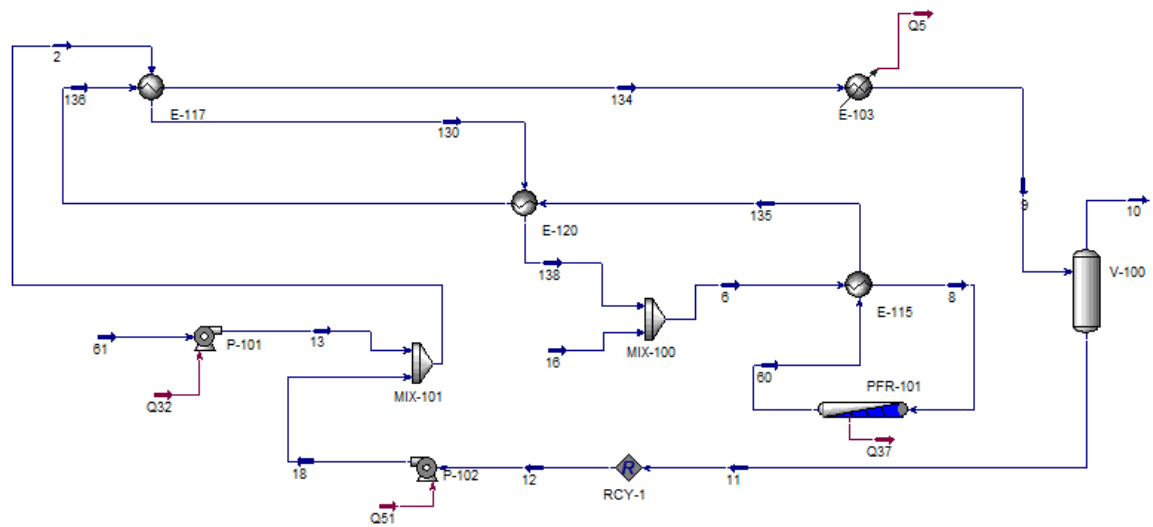


Figure 3.2 Reforming reactor, water separation and steam generation subsection

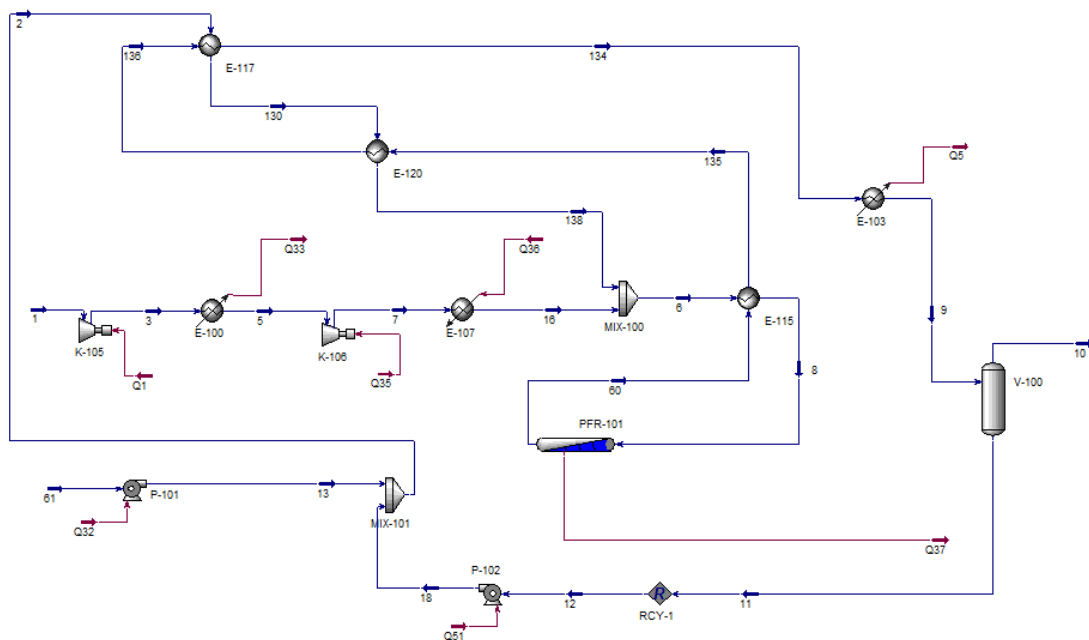


Figure 3.3 Syngas synthesis section

3.1.1. Reforming thermodynamic and kinetics

A thermodynamic analysis on the equilibrium composition of the reforming process can be carried out with the Gibbs free energy minimization technique. A system is thermodynamically favorable when its Gibbs free energy is at a minimum, this condition corresponds to a differential of Gibbs free energy equal to 0. Equation 3.1 express the total Gibbs free energy of a system containing N compounds of i species.

$$G^t = \sum_{i=1}^N n_i \mu_i = \sum_{i=1}^N n_i \left(G_i^0 + RT \ln \left(\frac{f_i}{f_i^0} \right) \right) \quad \text{Equation 3.1}$$

Where n is the number of moles and μ is the chemical potential that it can be expressed as a function standard Gibbs free energy (G^0), temperature (T), gas constant (R), fugacity at the operating condition (f_i) and fugacity at the standard state (f_i^0).

The Gibbs free energy minimum of the system can be found using the Lagrange multiplier method. The lagrangian function is expressed in Equation 3.2.

$$\sum_{i=1}^N n_i \left(G_i^0 + RT \ln \left(\frac{f_i}{f_i^0} \right) + \sum_k \lambda_k \alpha_{ik} \right) = 0 \quad \text{Equation 3.2}$$

Where λ_k is the Lagrange multiplier and α_{ik} is the number of atoms of the kth element present in each molecule of species i.

Hysys can automatically perform these calculations when a Gibbs reactor is implemented in the simulation. After defining the chemical species that can be formed, the equilibrium composition is calculated once the reactant stream and system conditions (temperature and pressure) are defined.

Six chemical species have been taken into account for the equilibrium composition in the reforming reactor: methane, carbon dioxide, carbon monoxide, water, hydrogen and carbon. The inlet stream (stream 8) enters the reactor at 650°C and 2010 bar, the outlet stream exits at 900°C and 1810 bar. The composition of the inlet stream can be seen from Table 3.1 as it is equal to stream 6. The composition of the outlet stream of the Gibbs reactor is reported in Table 3.4 and compared with the composition of the outlet stream of the simulation multiple pipe reformer. The results obtained in the multiple pipe reformer are in line with the thermodynamic evaluation of the Gibbs reactor. It is important to note that the steam to methane ratio used in the reformer (steam/methane ratio of 1.84) guarantees high methane conversion and no carbon formation, results that are in line with data found in literature.

Chemical species	Gibbs reactor	Multiple pipe reformer
CH ₄	0.0234	0.0217
CO ₂	0.0820	0.0831
CO	0.2116	0.2112
H ₂ O	0.2277	0.2239
H ₂	0.4553	0.4602
C	0	0

Table 3.4 Gibbs reactor outlet stream composition and multiple pipe reformer outlet stream composition (molar fractions)

The reformer reaction set is based on three reactions: steam reforming of methane, water gas shift, and carbon dioxide methanation. These reactions with their respective heat of reaction are reported below



For steam reforming reaction rate, Equation 3.3 has been used

$$R_{MSR} = \frac{K \frac{P_{CH_4} P_{H_2O}}{P_{H_2}^{2.5}} - K' P_{H_2}^{0.5}}{\left(1 + K_1 P_{CO} + K_2 P_{CH_4} + K_3 P_{H_2} + K_4 \frac{P_{H_2O}}{P_{H_2}}\right)^2} \quad \text{Equation 3.3}$$

Where the rate is expressed in kmol/m³/h and the base unit for the pressure of the components (P_x) is expressed in bar.

The terms K, K', K₁, K₂ and K₃ have been calculated with the following equation:

$$K_x = A_x \exp\left(-\frac{E_x}{RT}\right) \quad \text{Equation 3.4}$$

Where R is the gas constant, T is the temperature expressed in K, E_x is the activation energy expressed in kJ/kmol, and A_x is the frequency factor. The values of activation energy and frequency factor for every term are reported in the following table.

K_x	A_x	E_x (kJ/kmol)
K	2.96e ¹⁸	2.4010e ⁵
K'	2.47e ⁵	17035
K1	8.23e ⁻⁵	-70650
K2	6.65e ⁻⁴	-38280
K3	6.12e ⁻⁹	-82900
K4	1.77e ⁵	88680

Table 3.5 activation energies and frequency factors for steam reforming reaction

For water gas shift reaction rate, Equation 3.5 has been used

$$R_{wgs} = \frac{K \frac{P_{CO}P_{H2O}}{P_{H2}} - K' P_{CO2}}{\left(1 + K1P_{CO} + K2P_{CH4} + K3P_{H2} + K4 \frac{P_{H2O}}{P_{H2}}\right)^2} \quad \text{Equation 3.5}$$

Where the rate is expressed in kmol/m³/h and the base unit for the pressure of the components (P_x) is expressed in bar.

The terms K, K', K1, K2 and K3 have been calculated with Equation 3.4.

The values of activation energy and frequency factor for every term are reported in the following table.

K_x	A_x	E_x (kJ/kmol)
K	1.37e ⁹	67130
K'	7.75e ¹⁰	1.0443e ⁵
K1	8.23e ⁻⁵	-70650
K2	6.65e ⁻⁴	-38280
K3	6.12e ⁻⁹	-82900
K4	1.77e ⁵	88680

Table 3.6 activation energies and frequency factors for water-gas shift

For methanation reaction rate, Equation 3.6 has been used

$$R_{CH_4} = \frac{K \frac{P_{CH_4} P_{H_2O}^2}{P_{H_2}^{3,5}} - K' P_{CO_2}}{\left(1 + K_1 P_{CO} + K_2 P_{CH_4} + K_3 P_{H_2} + K_4 \frac{P_{H_2O}}{P_{H_2}}\right)^2} \quad \text{Equation 3.6}$$

Where the rate is expressed in kmol/m³/h and the base unit for the pressure of the components (P_x) is expressed in bar.

The terms K, K', K₁, K₂ and K₃ have been calculated using Equation 3.4.

The values of activation energy and frequency factor for every term are reported in the following table.

K_x	A_x	E_x (kJ/kmol)
K	7.14e ¹⁷	2.4390e ⁵
K'	3.37e ⁶	57417
K₁	8.23e ⁻⁵	-70650
K₂	6.65e ⁻⁴	-38280
K₃	6.12e ⁻⁹	-82900
K₄	1.77e ⁵	88680

Table 3.7 activation energies and frequency factors for methanation

3.2. Syngas refining section

The second section of the plant is dedicated to syngas refining. Syngas composition needs to be modified to meet process specifications. Figure 3.4 provides an overview of this plant section.

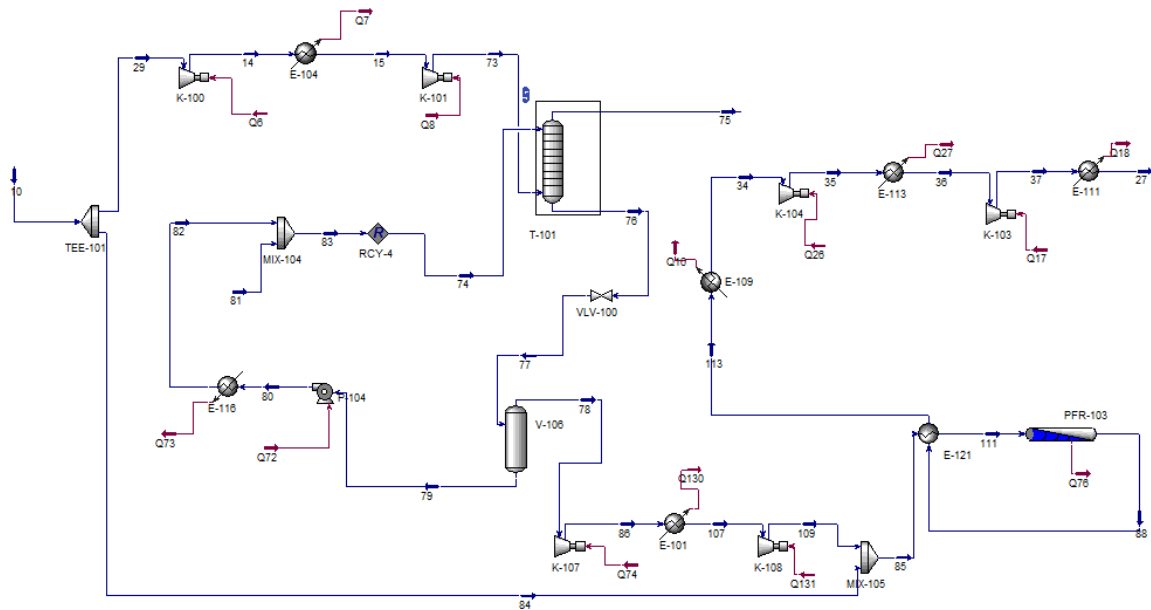


Figure 3.4 syngas refining section

The syngas stream (stream 10) is divided into two separate streams (in TEE-101). The first one (stream 29, equal to 59% of total syngas) is the syngas stream destined for methanol synthesis, the second one (stream 84) is the syngas stream that contains the carbon monoxide necessary to acetic acid production.

Stream 29 is sent to a series of two compressors (K-100 and K-101) with intermediate cooling provided by cooling water (heat exchanger E-104). In the first compressor syngas at 35°C and 1770 kPa is compressed to 4000 kPa. The intermediate heat exchanger cools the compressed syngas from 138.3 °C to 50°C. In the second compressor syngas is compressed from 3990 kPa to 8000 kPa. The adiabatic efficiency of the two compressors is 0.75 and the compression ratios are respectively 2.26 and 2.01. After compression syngas (stream 73) is sent to an absorber (column T-101) where is contacted countercurrent with water (stream 74) to reduce the concentration of carbon dioxide. 2500 kmol/h of water at 35°C (corresponding to 45.15 m³/h) are necessary to reduce the carbon dioxide content of syngas to levels acceptable for methanol synthesis. The absorber has been modeled as a 10 stages column with perfect efficiency and no pressure drops. In Table 3.8 the composition (molar fraction) of the syngas at the outlet of the column (stream 75) is compared with the composition of the inlet stream (stream 73).

Chemical species	Stream 73	Stream 75
CH ₄	0.0278	0.0302
CO ₂	0.1066	0.0349
CO	0.2712	0.2923
H ₂ O	0.0035	0.0010
H ₂	0.5909	0.6416

Table 3.8 Absorber inlet and outlet streams composition comparison (molar fractions)

The absorber water outlet stream (stream 76) is sent to a flash separator (V-106) operating at atmospheric pressure where water is degassed. The recovered water (stream 79) is pumped at 8000kPa (P-104) and cooled down to 35°C with cooling water in a heat exchanger (E-116) before it is recycled to the absorber. In Figure 3.5 the subsection described above is showed.

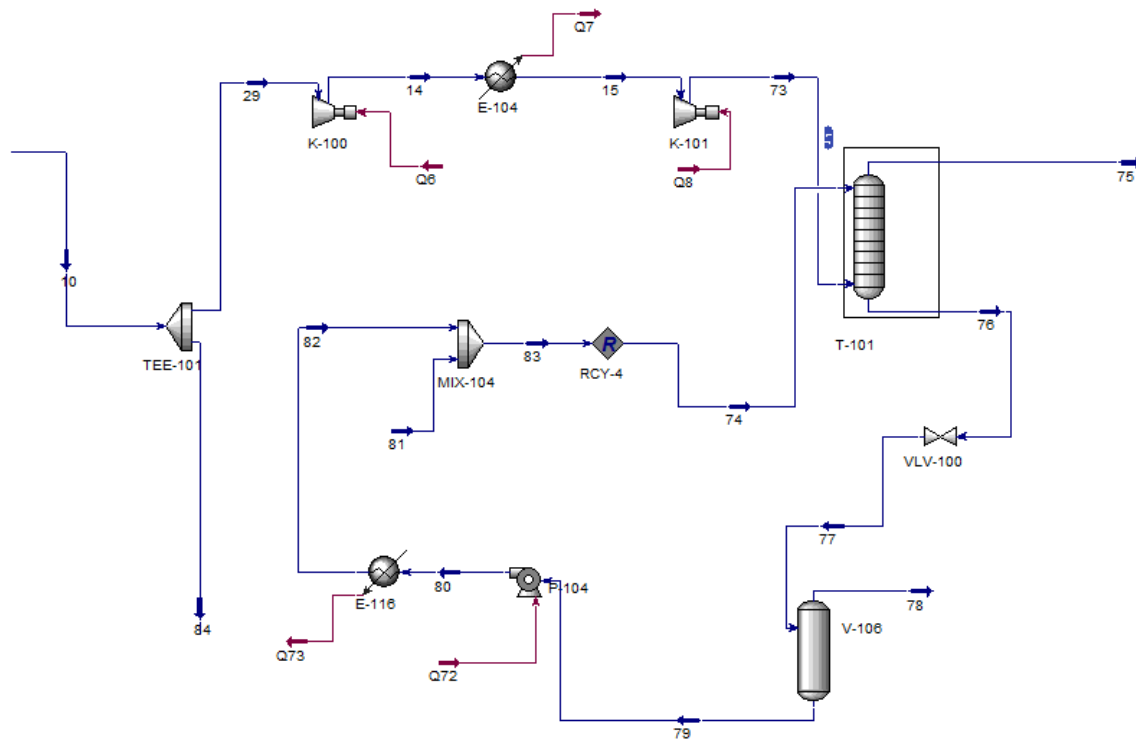


Figure 3.5 Carbon dioxide removal subsection

The gaseous stream exiting the flash separator (stream 78) is rich in carbon dioxide and is recovered to improve the composition of the second stream of syngas (stream 84). Stream 78 is compressed in a first compressor (K-107) from atmospheric pressure to 500 kPa, then it is cooled down from 200.9°C to 70°C in a heat exchanger

using cooling water (this stream is not cooled below 70°C to avoid water condensation). A second compressor (K-108) is used to bring the pressure to 1770 kPa. The carbon dioxide rich stream (stream 109) is mixed with syngas (stream 84) in MIX-105. The mixed stream (stream 85) is sent to a process-process heat exchanger (E-121) where it is heated from 58.75°C to 690°C before entering a fire-heated multi-tubular reactor. In this reactor (PFR-103) reverse water-gas shift is carried out at 900°C to maximize the content of carbon monoxide. The reactor has been modeled as the steam reformer seen previously (PFR-101). The total volume of the reactor is 2.5 m³, each pipe is 10 m in length and 1.5 inches in diameter with wall thickness of 1 cm. A total number of 219 pipes compose the reactor. A void fraction of 0.4 has been considered as the reactor is loaded with reforming catalyst (standard nickel catalyst) with density of 2500 kg/m³. A total pressure drop of 200 kPa is considered through the reactor. The reactor outlet stream is cooled down from 900°C to 279.8°C in the process-process heat exchanger used to preheat the inlet stream of the reactor. In Table 3.9 the composition of the reactor inlet and outlet streams (expressed in kmol/h) is compared.

Chemical species	Stream 111	Stream 88
CH ₄	1.2551	1.6304
CO ₂	9.6325	4.3012
CO	12.3693	17.3240
H ₂ O	0.5019	6.2085
H ₂	26.6782	20.2262

Table 3.9 water-gas shift reactor inlet and outlet streams compositions (kmol/h)

The quenched stream (stream 113) is further cooled down with cooling water in a heat exchanger (E-109) from 279.8°C to 130°C. A series of two compressors with intermediate cooling is used to compress the gaseous stream from 1750 kPa to 4010 kPa, a pressure level compatible with acetic acid synthesis. The first compressor (K-104) increases the pressure from 1750 kPa to 2700 kPa (adiabatic efficiency of 0.75 and compression ratio of 1.54). The second compressor (K-103) increases the pressure from 2690 kPa to 4010 kPa (adiabatic efficiency of 0.75 and compression ratio of 1.49). Intermediate cooling is provided by cooling water in heat exchanger E-113 and the gaseous stream temperature is lowered from 195.7 °C to 135 °C. The relatively high temperature at the outlet of heat exchanger E-109 and heat exchanger E-113 is needed to avoid water condensation in the compressors.

The compressed stream (stream 37) is cooled down in a third heat exchanger (E-111) from 195.9 °C to 180°C in order to meet the temperature requirement for acetic acid synthesis. In Figure 3.6 the subsection described above is showed.

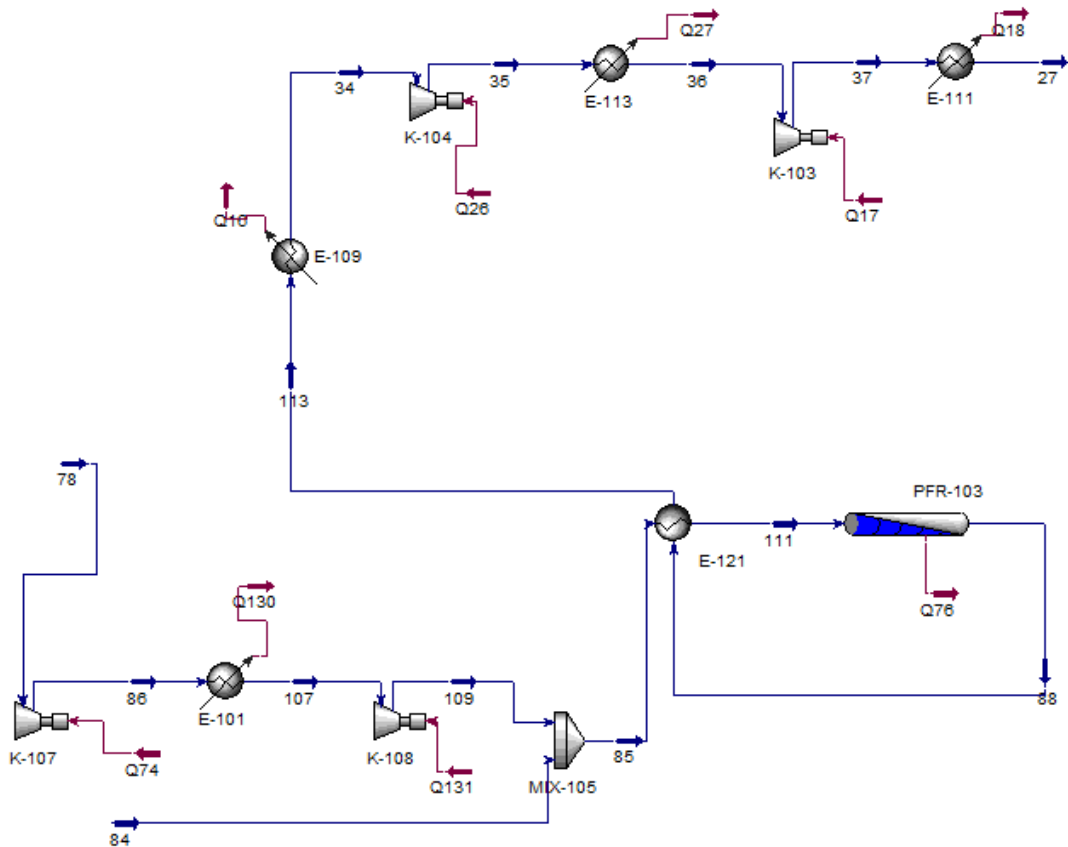


Figure 3.6 Carbon dioxide recovery and reverse water-gas shift reactor section

3.2.1. Reverse water-gas shift reactor thermodynamic and kinetics

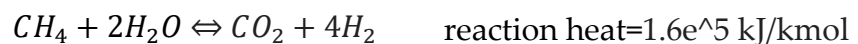
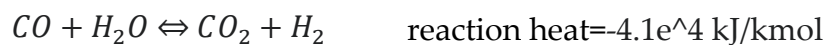
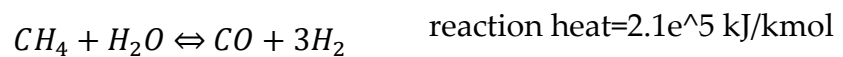
A Gibbs reactor has been modeled in Hysys to evaluate equilibrium composition at the reaction conditions. The chemical species considered are methane, carbon monoxide, carbon dioxide, water, hydrogen and carbon. The inlet stream to the Gibbs reactor has the same composition of stream 111 (as shown in Table 3.9 water-gas shift reactor inlet and outlet streams compositions Table 3.9), it enters at 690°C and 1760 kPa. The outlet stream is at 900°C and 1560 kPa. The stream composition is reported in Table 3.10 and compared to the simulated multi-tubular reactor outlet stream composition.

Chemical species	Gibbs reactor	Multi-tubular reactor
CH ₄	1.7320	1.6304
CO ₂	4.2703	4.3012
CO	17.2546	17.3240
H ₂ O	6.3410	6.2085
H ₂	19.8853	20.2262
C	0	0

Table 3.10 Comparison between Gibbs reactor outlet composition and multi-tubular reverse water-gas shift reactor outlet composition (kmol/h)

The results obtained for the multi-tubular reactor are compatible with the thermodynamic evaluation of the Gibbs reactor. Comparing the inlet and outlet composition of the Gibbs reactor, it is possible to notice that the reaction proceeds with a major consumption of carbon dioxide and hydrogen and production of water and carbon monoxide, a result compatible with reverse water-gas shift. A minor production of methane can also be identified. Lastly it is important to note that carbon formation is thermodynamically unfavored at the reaction conditions.

The reverse water-gas shift multi-tubular reactor reaction set is based on the same reactions used for the reformer: steam reforming of methane, water gas shift, and carbon dioxide methanation. These reactions with their respective heat of reaction are reported below



Since the reactions that characterize the system are the same, the kinetic model applied for the reverse water-gas shift reactor is identical to the one used for reforming.

For steam reforming reaction rate, water gas shift reaction rate, methanation reaction rate Equation 3.3, Equation 3.5, Equation 3.6 has been used respectively.

The terms K, K', K1, K2 and K3 have been calculated with Equation 3.4

Reference source not found.

The values of activation energy and frequency factor for every term of each reaction are reported in Table 3.5, Table 3.6, Table 3.7.

3.3. Methanol production section

The third section of the plant is dedicated to methanol synthesis. Figure 3.7 provides an overview of this section.

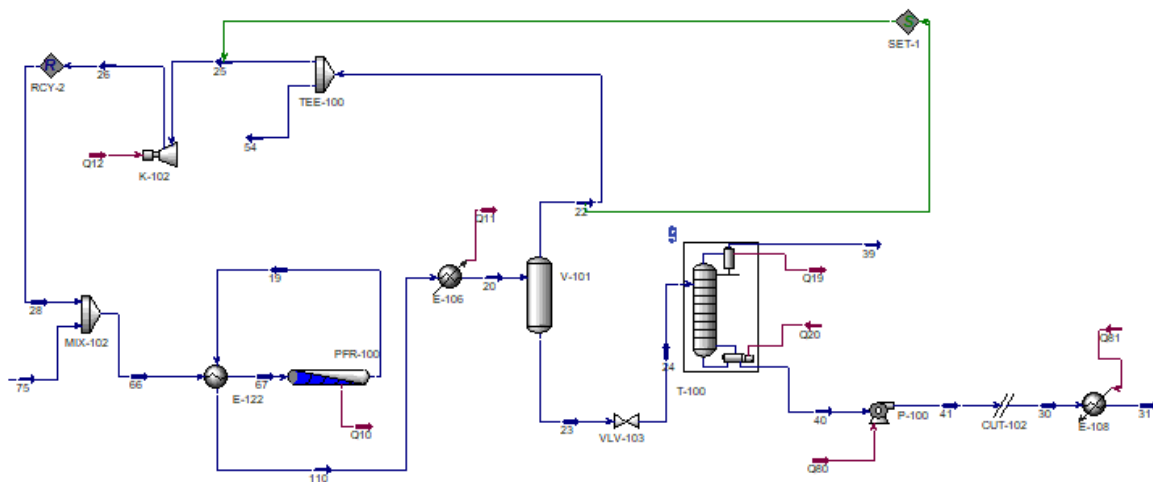


Figure 3.7 Methanol production section

The refined syngas stream exiting from the absorber described in the previous section (stream 75) is mixed with unreacted recycled gas (stream 28). The mixed stream (stream 66) is sent to a process-process heat exchanger (E-122), where it is heated from 36.30°C to 200°C, before entering the methanol synthesis reactor (PFR-100). The reactor has been modeled as a multiple-pipe reactor with external cooling provided by low pressure steam generation (696.7 kg/h). This type of reactor belongs to the family of quasi-isothermal reactors commonly used in methanol production (Lurgi's methanol reactor). The total volume of the reactor is 5 m³. Each tube is 6 m in length, 2 inches in diameter and with wall thickness of 0.5 cm. A total of 411 tubes composes the reactor. A void fraction equal to 0.4 of the total volume has been considered as the reactor is filled with catalyst (catalyst density equal to 2500 kg/m³). The reaction proceeds at 250 °C and 7990 kPa. A total pressure drop of 200 kPa through the reactor has been taken into account. The reactor inlet and outlet composition are reported in Table 3.11.

Chemical species	Stream 67	Stream 19
CH ₄	14.8760	14.8760
CO ₂	7.4150	6.9995
CO	23.4294	6.7175
H ₂ O	0.0639	0.4794
H ₂	69.5190	34.8486
Methanol	0.2727	17.4001

Table 3.11 Methanol synthesis reactor inlet and outlet composition (kmol/h). stream 67 is the inlet stream, stream 19 is the outlet stream

It is important to notice that the reactor inlet stream respects the optimal values of stoichiometric number (SN) and carbon oxide ratio (COR) defined in literature (a value slightly above 2 for SN and below 0.6 for COR). By using **Error! Reference source not found.** and **Error! Reference source not found.** the values of SN and COR for the reactor inlet stream can be calculated. The calculated value for SN is 2.013 and the calculated value for COR is 0.240.

The outlet stream of the reactor is quenched from 250°C to 132.4°C in the process-process heat exchanger used to preheat the reactor inlet stream. A second heat exchanger is used to reduce the stream temperature to 35°C using cooling water. The cooled stream (stream 20) is sent to a flash separator operating at 7770 kPa and 35°C. The liquid stream separated in the flash separator (stream 23) is mainly composed of methanol with traces of water and gases (CO, CO₂, H₂, CH₄). The composition of the liquid stream is reported in Table 3.12.

Chemical species	Stream 23
CH ₄	0.3089
CO ₂	0.9829
CO	0.0273
H ₂ O	0.4761
H ₂	0.0456
Methanol	17.0953

Table 3.12 Flash separator liquid stream composition (kmol/h)

The gaseous stream (stream 22) is rich in unreacted carbon monoxide, carbon dioxide and hydrogen and is therefore recirculated to the reactor. Methane represents a consistent fraction of the gaseous stream exiting the flash separator. Methane is naturally present in low concentrations in syngas, but it is not consumed during methanol synthesis, and it tends to accumulate in the recycled stream. To limit inert accumulation part of the gaseous stream is purged (stream 54). 10% of the gas is purged while the remaining 90% is recirculated. The purged gas can be used to aliment the furnace of the steam reformer. The recirculated stream (stream 25) is compressed to 8000 kPa to balance the pressure drops of the methanol synthesis section before being mixed with fresh syngas (MIX-102). The compressor operating the recycle (K-102) has an adiabatic efficiency of 0.75 and compression ratio of 1.03. The composition of the recirculated stream (stream 28) is reported in Table 3.13.

Chemical species	Stream 28
CH ₄	13.0701
CO ₂	5.3301
CO	5.9703
H ₂ O	0.0029
H ₂	31.1923
Methanol	0.2727

Table 3.13 Recycled stream composition (kmol/h)

Figure 3.8 provides an overview of the subsection described above.

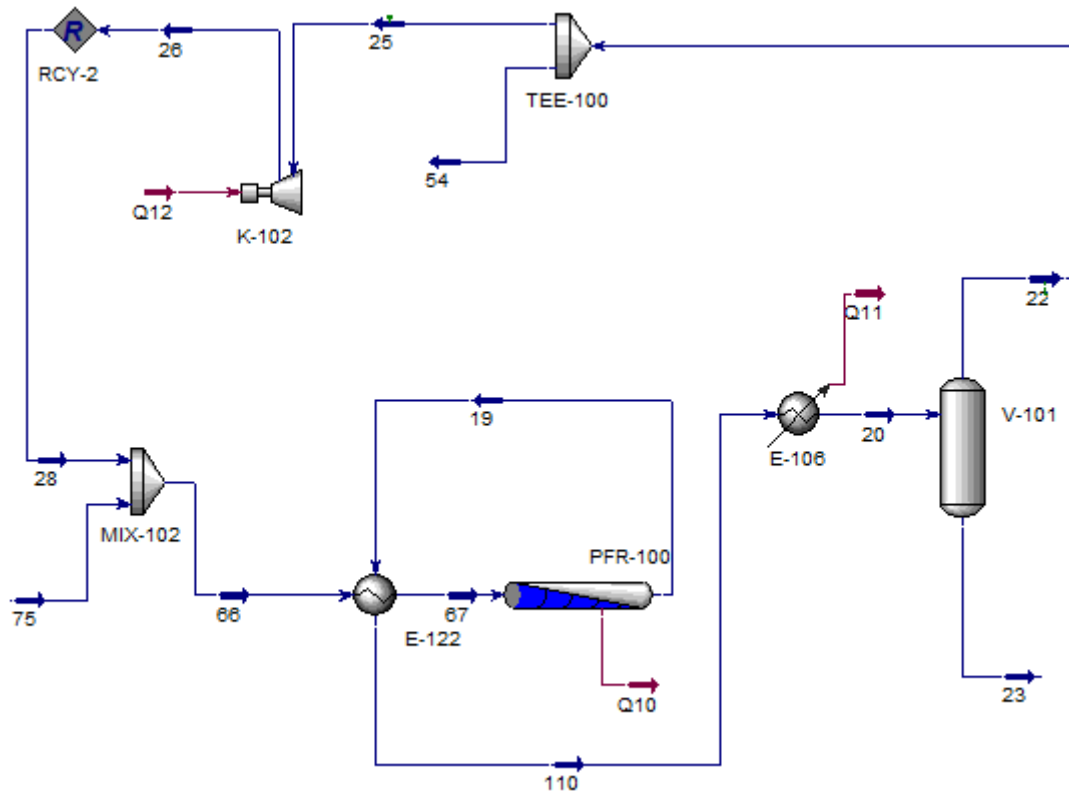


Figure 3.8 Methanol synthesis reactor and recycle subsection

The liquid stream exiting the separator is expanded to atmospheric pressure (VLV-103) and sent to a distillation column (T-100). The column is designed as a full reflux packed column with a number of stages equal to 8. The feed stage is the fourth starting from the top of the column and the feed inlet temperature is 28.77 °C. The column specifications are a reflux ratio equal to 5 and methanol recovery in the bottom stream equal to 99.2% of the methanol entering the column. The column is operated at atmospheric pressure and assuming no pressure drop. The column efficiency has been calculated using O’Connell correlation [52] reported in Equation 3.7.

$$E_{OC} = 0.492(\mu_L \alpha)^{-0.245} \quad \text{Equation 3.7}$$

Where μ_L is the average liquid viscosity between the column top and bottom and α is the average relative volatility of the key components at the column mean temperature. For column T-100 the O’Connell efficiency is 0.4. The column total condenser is operated at 18.22°C by means of glycolated water available at 0°C. The column reboiler is operated at 67.46 °C by means of low-pressure steam. The column temperature profile is provided in Figure 3.9.

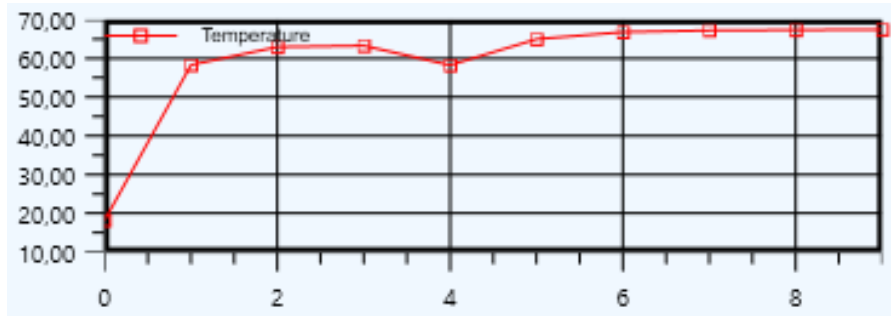


Figure 3.9 Temperature (°C) vs. tray position from top for T-100 column

The composition of the gaseous stream exiting from the column (stream 39) is reported in Table 3.14

Chemical species	Stream 39
CH ₄	0.3089
CO ₂	0.9829
CO	0.0273
H ₂ O	0.0003
H ₂	0.0456
Methanol	0.1368

Table 3.14 Composition of the gaseous stream exiting distillation column T-100 (kmol/h)

The bottom stream of the column (stream 40) is pumped from atmospheric pressure to 4010 kPa (using pump P-100, adiabatic efficiency of the pump is 0.75) and is heated to 180 °C in a heat exchanger (E-108) by means of high-pressure steam. The composition of the liquid stream is reported in Table 3.15.

Chemical species	Stream 31
CH ₄	0
CO ₂	0
CO	0
H ₂ O	0.4758
H ₂	0
Methanol	16.9586

Table 3.15 composition of the bottoms of distillation column T-100 (kmol/h)

Figure 3.10 show the plant subsection described above.

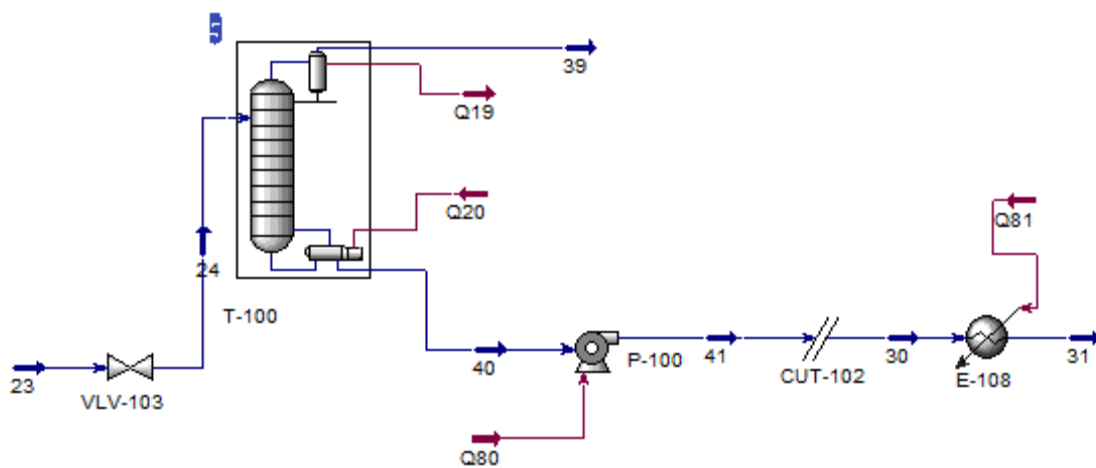
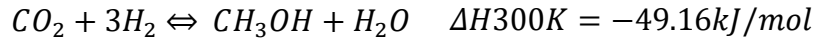


Figure 3.10 Methanol section distillation column

3.3.1. Methanol synthesis thermodynamic and kinetics

Methanol synthesis is based on carbon monoxide and carbon dioxide hydrogenation reactions accompanied by water gas shift.



The thermodynamic equilibrium constant of a reaction (which is related to the equilibrium composition, as it is the product of activities of the products divided by the activities of the reactants all elevated to the respective stoichiometric coefficients) can be calculated from the Gibbs free energy of reaction with Equation 3.8.

$$K_{eq} = \exp\left(-\frac{\Delta G_R^0}{RT}\right) \quad \text{Equation 3.8}$$

Both the exothermic reactions are thermodynamically unfavored at the methanol synthesis temperature (200-250°C) as their Gibbs free energy of reaction is greater than 0, resulting in equilibrium constants smaller than 0. Small equilibrium constants correspond to thermodynamic equilibrium moved towards the reactants. A more favorable condition for methanol synthesis would be provided by reducing the reaction temperature, but under 200°C no known catalyst is active. The only way to maximize conversion is to work at high pressures as methanol synthesis proceeds with a reduction in the number of moles.

The equilibrium composition for methanol synthesis can be calculated using a Gibbs reactor modeled with Hysys if methane is considered as an inert at reaction conditions. Table 3.16 reports the equilibrium composition of methanol synthesis and compares it with the composition at the outlet of the multi-tubular reactor modeled previously. As can be seen the multi-tubular reactor outlet composition approaches the equilibrium one without reaching it.

Chemical species	Gibbs reactor	Multi-tubular reactor
CH ₄	14.8770	14.8770
CO ₂	6.9252	6.9995
CO	4.8294	6.7175
H ₂ O	0.5537	0.4794
H ₂	30.8497	34.8486
Methanol	19.3625	17.4001

Table 3.16 Comparison between equilibrium composition and composition at the outlet of the multi-tubular reactor PFR-100 (kmol/h)

For methanol synthesis kinetic model, the aforementioned reaction set is used.

For carbon monoxide hydrogenation Equation 3.9 has been used

$$R_{CO} = \frac{K P_{CO} P_{H_2}^{1.5} - K' \frac{P_{CH_3OH}}{P_{H_2}}}{1 + K_1 P_{CO} P_{H_2}^{0.5} + K_2 P_{CO_2} P_{H_2}^{0.5} + K_3 P_{H_2O} + K_4 P_{CO} P_{H_2O} + K_5 P_{CO_2} P_{H_2O}} \quad \text{Equation 3.9}$$

Where the rate is expressed in kmol/m³/h and the base unit for the pressure of the components (P_x) is expressed in bar.

The terms K, K', K1, K2 and K3 have been calculated with Equation 3.4.

The values of activation energy and frequency factor for every term are reported in the following table.

K _x	A _x	E _x (kJ/kmol)
K	1.9867e ⁸	91793
K'	8.3011e ²⁰	1.9018e ⁵
K1	1.5401e ⁻³	-14936
K2	8.2062e ⁻⁹	-76595
K3	3.8182e ⁻⁹	-97350
K4	5.8804e ⁻¹²	-1.1229e ⁵
K5	3.1333e ⁻¹⁷	-1.7394e ⁵

Table 3.17 activation energies and frequency factors for carbon monoxide hydrogenation

For carbon dioxide hydrogenation Equation 3.10 has been used

$$R_{CO_2} = \frac{K P_{CO_2} P_{H_2}^{1.5} - K' \frac{P_{CH_3OH} P_{H_2O}}{P_{H_2}^{1.5}}}{1 + K_1 P_{CO} P_{H_2}^{0.5} + K_2 P_{CO_2} P_{H_2}^{0.5} + K_3 P_{H_2O} + K_4 P_{CO} P_{H_2O} + K_5 P_{CO_2} P_{H_2O}} \quad \text{Equation 3.10}$$

Where the rate is expressed in kmol/m³/h and the base unit for the pressure of the components (P_x) is expressed in bar.

The terms K, K', K₁, K₂ and K₃ have been calculated with Equation 3.4.

The values of activation energy and frequency factor for every term are reported in the following table.

K _x	A _x	E _x (kJ/kmol)
K	4.3507e ⁻³	-30706
K'	1.7004e ⁸	27992
K ₁	1.5401e ⁻³	-14936
K ₂	8.2062e ⁻⁹	-76595
K ₃	3.8182e ⁻⁹	-97350
K ₄	5.8804e ⁻¹²	-1.1229e ⁵
K ₅	3.1333e ⁻¹⁷	-1.7394e ⁵

Table 3.18 activation energies and frequency factors for carbon dioxide hydrogenation

For reverse water-gas shift Equation 3.11 has been used

$$R_{RWGS} = \frac{K P_{H_2} P_{CO_2} - K' P_{CO} P_{H_2O}}{1 + K_1 P_{CO} P_{H_2}^{0.5} + K_2 P_{CO_2} P_{H_2}^{0.5} + K_3 P_{H_2O} + K_4 P_{CO} P_{H_2O} + K_5 P_{CO_2} P_{H_2O}} \quad \text{Equation 3.11}$$

Where the rate is expressed in kmol/m³/h and the base unit for the pressure of the components (P_x) is expressed in bar.

The terms K, K', K₁, K₂ and K₃ have been calculated with Equation 3.4.

The values of activation energy and frequency factor for every term are reported in the following table.

K_x	A_x	E_x (kJ/kmol)
K	$2.0048e^9$	73300
K'	$1.8753e^7$	33600
K1	$1.5401e^{-3}$	-14936
K2	$8.2062e^{-9}$	-76595
K3	$3.8182e^{-9}$	-97350
K4	$5.8804e^{-12}$	-1.1229e ⁵
K5	$3.1333e^{-17}$	-1.7394e ⁵

Table 3.19 activation energies and frequency factors for reverse water-gas shift

3.4. Acetic acid production section

The fourth section of the plant is dedicated to acetic acid synthesis. Figure 3.11 provides an overview of this section.

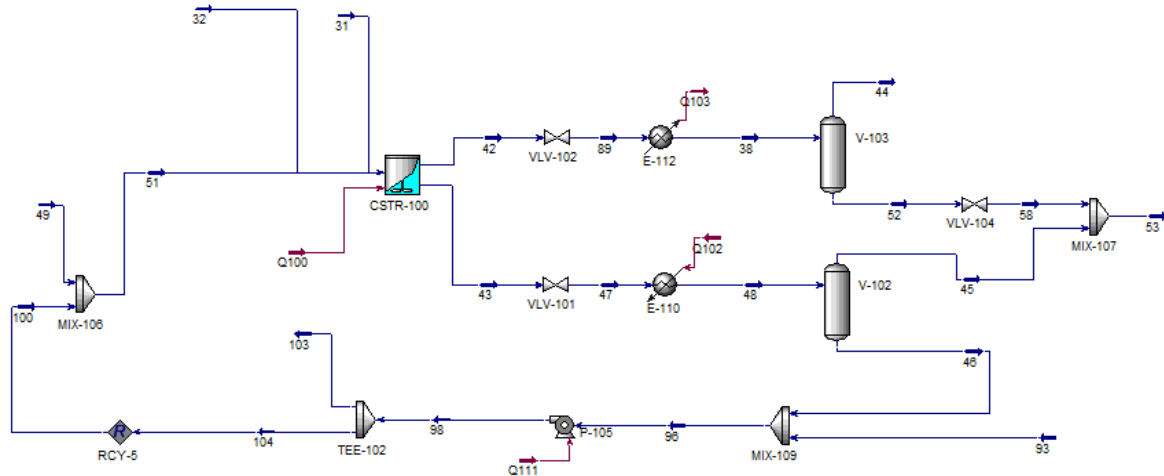


Figure 3.11 Acetic acid synthesis section

This section has been modeled taking as reference the Monsanto methanol carbonylation process (one of the most diffused technologies for acetic acid production). The physical properties of the rhodium catalyst have been computed by Hysys as no data are available in literature. Three input data have been supplied to Hysys: molecular weight of 412, normal boiling point of 600°C and ideal liquid density of 2500 kg/m³.

The methanol stream produced in the methanol synthesis section (stream 31), the carbon monoxide reach stream produced in the syngas refining section (stream 32), and the recycled stream containing the homogeneous catalyst (stream 51) are sent to the acetic acid synthesis reactor (CSTR-100). This reactor has been modeled as a continuously stirred tank reactor (CSTR) working at 4000 kPa and 180°C. The reactor temperature is maintained constant by means of low-pressure steam production in an external cooling jacket (916.4 kg/h). The reactor has a diameter of 1.894 m and a height of 2.840 m. The total volume of the reactor is 8 m³ but only 70% of this volume (equal to 5.6 m³) is occupied by the liquid. The unoccupied volume is necessary to allow vapor disengagement and to guarantee extra space for the bubbling liquid. The residence time inside the reactor can be calculated from Equation 3.12

$$\tau = \frac{V}{Q} \quad \text{Equation 3.12}$$

Where V is the reactor volume occupied by the liquid (5.6 m³) and Q is the outlet liquid stream volumetric flowrate (1.106 m³/h). A residence time of 5.06 h is found.

The composition of the reactor's outlet streams is reported in Table 3.20

Chemical species	Stream 42	Stream 43
CH ₄	1.6091	0.0213
CO ₂	4.1820	0.1192
CO	0.3638	0.0017
H ₂ O	3.4744	5.5628
H ₂	20.1581	0.0681
Methanol	0	0
Acetic acid	3.7949	13.6240
CH ₃ I	0.1307	0.1450
Rhodium catalyst	0	0.0224

Table 3.20 Acetic acid reactor outlet streams composition (kmol/h). Stream 42 is the gaseous outlet stream, stream 43 is the outlet liquid stream

The gaseous stream (stream 42) is expanded at 2000 kPa and sent to a heat exchanger (E-112) where it is cooled down from 175.8 °C to 35 °C by means of cooling water. The cooled stream (stream 38) is sent to a flash separator (V-103) working at 35 °C and 1990 kPa. The separated gaseous stream (stream 44) is rich in hydrogen and can

be used as fuel in the reforming furnace. The liquid stream (stream 52) is recovered as it contains acetic acid and methyl iodide and is expanded from 1990 kPa to 111.3 kPa (in VLV-104) before being mixed in MIX-107. The composition of the two outlet streams of the flash separator is reported in Table 3.21.

Chemical species	Stream 44	Stream 52
CH ₄	1.6062	0.0029
CO ₂	4.1439	0.0380
CO	0.3637	0.0001
H ₂ O	0.0486	3.4257
H ₂	20.1542	0.0039
Methanol	0	0
Acetic acid	0.0325	3.7624
CH ₃ I	0.0154	0.1153
Rhodium catalyst	0	0

Table 3.21 Composition of the outlet streams of flash separator V-103 (kmol/h). Stream 44 is the gaseous stream, stream 52 is the liquid stream

The reactor's outlet liquid stream (stream 43) is expanded from 4000 kPa to 121.3 kPa (in VLV-101) and is heated from 110.7 °C to 140 °C in a heat exchanger (E-110) by means of medium-pressure steam. The heated stream (stream 48) is separated in a flash separator (V-102) working at 140 °C and 111.3 kPa. The separated gaseous stream (stream 45) is mixed with the liquid stream coming from the first flash separator (V-103) in MIX-107. The composition of the gaseous stream of the second flash separator and the composition of the mixed stream (stream 53) is reported in Table 3.22.

The separated liquid stream (stream 46) is mixed with the recycled stream coming from the separation section of the plant (stream 93) in MIX-109. The composition of the separated liquid stream and of the mixed stream is reported in Table 3.23.

Chemical species	Stream 45	Stream 53
CH ₄	0.0213	0.0242
CO ₂	0.1192	0.1572
CO	0.0017	0.0018
H ₂ O	5.5596	8.9853
H ₂	0.0681	0.0719
Methanol	0	0
Acetic acid	13.6069	17.3693
CH ₃ I	0.1450	0.2603
Rhodium catalyst	0	0

Table 3.22 Composition of the outlet gaseous stream of flash separator V-102 and of the mixed stream coming from MIX-107 (kmol/h). Stream 45 is the gaseous stream, stream 53 is the mixed stream

Chemical species	Stream 46	Stream 96
CH ₄	0	0
CO ₂	0	0
CO	0	0
H ₂ O	0.0032	2.3982
H ₂	0	0
Methanol	0	0
Acetic acid	0.0171	0.4692
CH ₃ I	0	0.2445
Rhodium catalyst	0.0224	0.0224

Table 3.23 Composition of the outlet liquid stream of flash separator V-102 and of the mixed stream coming from MIX-109 (kmol/h). Stream 46 is the gaseous stream, stream 96 is the mixed stream

The mixed stream (stream 96) is compressed from 111.3 kPa to 4000 kPa with a pump (P-105, adiabatic efficiency of 0.75). 99% of the stream is then recirculated to the reactor, the remaining 1% is purged (stream 103). A make-up stream of rhodium catalyst and methyl iodide is added to the recirculated stream to counterbalance the loss of catalyst in the separation section. The composition of the recycled stream and of the catalyst make-up is reported in Table 3.24.

Chemical species	Stream 49	Stream 51
CH ₄	0	0
CO ₂	0	0
CO	0	0
H ₂ O	0	2.3528
H ₂	0	0
Methanol	0	0
Acetic acid	0	0.4600
CH ₃ I	5.0	0.2758
Rhodium catalyst	0.0020	0.0224

Table 3.24 Composition of the make-up catalyst stream and of the recycled stream. Stream 49 is the make-up catalyst stream (kg/h), stream 51 is the recycled stream (kmol/h)

3.4.1. Acetic acid synthesis thermodynamic and kinetics

Acetic acid synthesis is based on methanol carbonylation



By using a Hysys modeled Gibbs reactor the equilibrium composition of the product stream at the CSTR reactor conditions can be obtained. To perform this simulation only three chemical species have been considered: methanol, carbon monoxide and acetic acid. The remaining chemical species are not considered as at the reactor conditions they act like inert. The composition at the outlet of the Gibbs reactor is reported in Table 3.25 and compared with the total product composition of the simulated CSTR reactor. As can be seen the reaction is favored by thermodynamic equilibrium and methanol is completely consumed to generate acetic acid.

Chemical species	Gibbs reactor	CSTR reactor
CO	0.3654	0.3655
Methanol	0	0
Acetic acid	17.4216	17.4219

Table 3.25 Composition of the acetic acid Gibbs reactor products and of the acetic acid CSTR reactor (kmol/h).

The kinetic model used for methanol carbonylation is a simplified rate equation of zero order with respect to the reactants and products and of first order with respect to the rhodium catalyst and the methyl iodide promoter [53].

$$R_{\text{carbonylation}} = K C_{\text{Rh}} C_{\text{CH}_3\text{I}} \quad \text{Equation 3.13}$$

Where C_x is the molar concentration of the chemical species (kmol/m^3). The parameter K have been calculated using **Error! Reference source not found..** The activation energy is $61200 \text{ kJ}/\text{kmol}$ and the frequency factor is $4.5e^6 \text{ kmol}/\text{m}^3/\text{s}$.

3.5. Separation section

The last section of the plant is dedicated to products separation. This section has been designed to produce commercial grade glacial acetic acid (acetic acid percentage by mass greater than 99.5%). An overview of this section is provided by Figure 3.12.

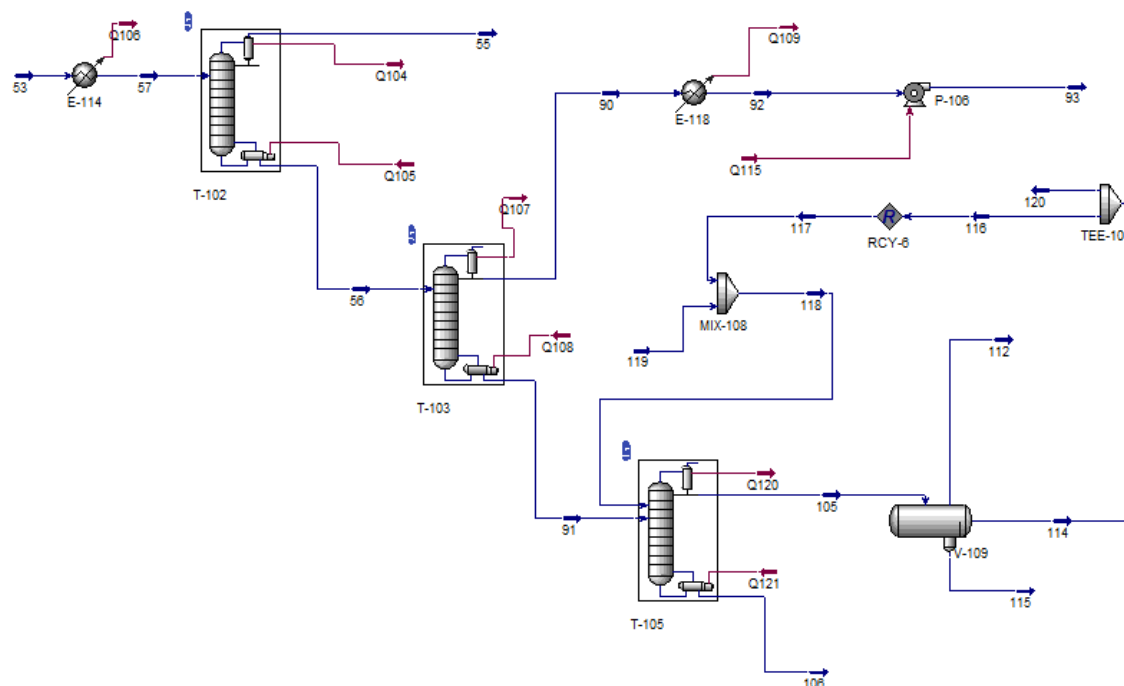


Figure 3.12 Plant separation section

The product stream exiting from the acetic acid production section (stream 53) is cooled from $110.2 \text{ }^\circ\text{C}$ to $90 \text{ }^\circ\text{C}$ in a heat exchanger (E-114) by means of cooling water. The stream is sent to a first distillation column with full reflux (T-102) where the

most volatile species (mainly carbon dioxide, methane and hydrogen) are removed. The column has been modeled as an 8 stages packed column, the feed stage is the second from the top. The column specifications are a reflux ratio equal to 3 and methyl iodide recovery in the bottom stream equal to 94% of the methyl iodide entering the column. The column is operated at atmospheric pressure and assuming no pressure drop. The column efficiency has been calculated using O’Connell correlation reported in Equation 3.7 and is equal to 0.4. The column condenser is operated at 35.88 °C by means of cooling water. The column reboiler is operated at 103.8 °C by means of low-pressure steam. The column temperature profile is provided in Figure 3.13.

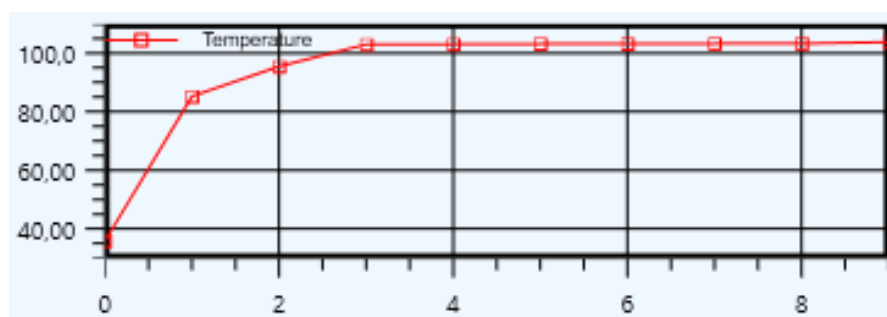


Figure 3.13 Temperature profile inside column T-102

The composition of the gaseous stream exiting from the column (stream 55) is reported in Table 3.26.

Chemical species	Stream 55
CH ₄	0.0242
CO ₂	0.1572
CO	0.0018
H ₂ O	0.0107
H ₂	0.0719
Methanol	0
Acetic acid	0.0051
CH ₃ I	0.0156
Rhodium catalyst	0

Table 3.26 Composition of the gaseous stream exiting column T-102 (kmol/h)

The composition of the bottom stream of the column is reported in Table 3.27.

Chemical species	Stream 55
CH ₄	0
CO ₂	0
CO	0
H ₂ O	8.9746
H ₂	0
Methanol	0
Acetic acid	17.3642
CH ₃ I	0.2447
Rhodium catalyst	0

Table 3.27 Composition of the bottom stream exiting column T-102 (kmol/h)

The bottom stream (stream 55) is sent to a second distillation column (T-103) where methyl iodide is removed. The column has been modeled as a 35 stages packed column, the feed stage is the 17th from the top. The column specifications are a reflux ratio equal to 3.5 and methyl iodide recovery in the top stream equal to 99.9% of the methyl iodide entering the column. The column is operated at atmospheric pressure and assuming no pressure drop. The column efficiency has been calculated using O'Connell correlation reported in Equation 3.7 and is equal to 0.42. The column total condenser is operated at 92.33 °C by means of cooling water. The column reboiler is operated at 106.2 °C by means of low-pressure steam. The column temperature profile is provided in Figure 3.14.

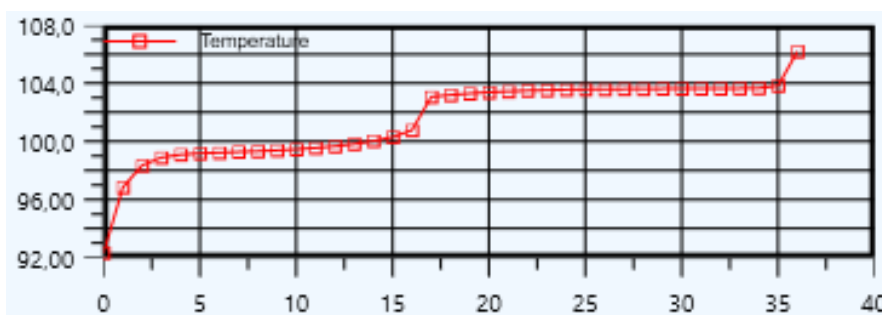


Figure 3.14 Temperature profile inside column T-103

The column top stream (stream 90) is sent to a heat exchanger (E-118) where is cooled from 92.33 °C to 35 °C by means of cooling water. After cooling the stream is compressed with a pump (P-106, adiabatic efficiency 0.75), and recirculated to the acetic acid reactor after mixing in MIX-109 as already described in the previous section. The composition of the column top stream is reported in Table 3.28.

Chemical species	Stream 90
CH ₄	0
CO ₂	0
CO	0
H ₂ O	2.3951
H ₂	0
Methanol	0
Acetic acid	0.4521
CH ₃ I	0.2444
Rhodium catalyst	0

Table 3.28 Composition of the top stream exiting column T-103 (kmol/h)

The composition of the column bottom stream is reported in Table 3.29.

Chemical species	Stream 91
CH ₄	0
CO ₂	0
CO	0
H ₂ O	6.5998
H ₂	0
Methanol	0
Acetic acid	16.9171
CH ₃ I	0
Rhodium catalyst	0

Table 3.29 Composition of the bottom stream exiting column T-103 (kmol/h)

The bottom stream (stream 91) is sent to a third distillation column (T-105). In this column water is removed from the top using propyl-acetate as entrainer [54]. The relative volatility of acetic acid and water tends to one when in concentrated solutions, therefore the use of an entrainer is necessary to achieve high purity without the need of a very tall distillation column (hundreds of plates are necessary for conventional distillation units). The column has been modeled as a 43 stages tray column, the feed stage is the 22nd from the top, the propyl acetate is fed at the 13th stage from the top. The column specifications are a reflux ratio equal to 5 and acetic acid recovery in the bottom stream equal to 99.9% of the acetic acid entering the column. The column is operated at atmospheric pressure and assuming no pressure drop. The column efficiency has been calculated using O'Connell correlation reported in Equation 3.7 and is equal to 0.47. The column condenser is operated at 79.61 °C by means of cooling water. The column reboiler is operated at 117.7 °C by means of medium-pressure steam. The column temperature profile is provided in Figure 3.15.

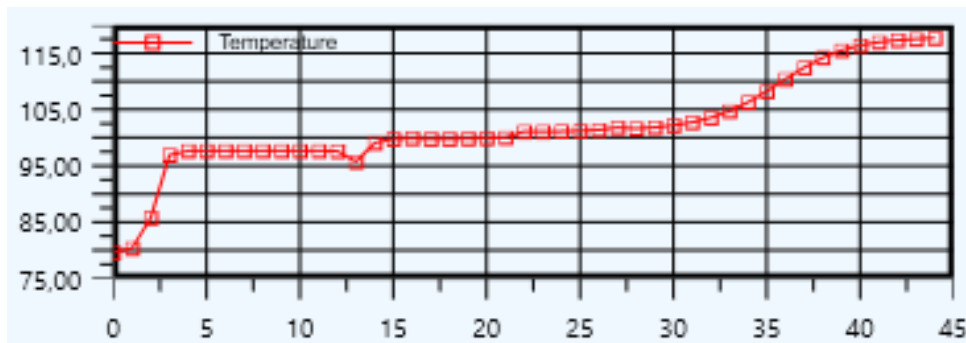


Figure 3.15 Temperature profile inside column T-105

The composition of the column top stream is reported in Table 3.30.

Chemical species	Stream 105
H ₂ O	140.6656
Acetic acid	31.0778
CH ₃ I	0.0810
Rhodium catalyst	0
Propyl acetate	583.3182

Table 3.30 Composition of the top stream exiting column T-105 (kg/h)

The top stream exiting from the column (stream 105) is sent to a phase separator tank (V-109) where two phases are separated. The phase separator has a total volume of 2 m³, a diameter of 1.179 m and a length of 1.768 m. The volume occupied by the liquid is 50% of the total volume. The residence time inside the phase separator can be calculated by dividing the volume occupied by the liquid by the volumetric flowrate of the stream entering the tank (0.8855 m³/h). A residence time of 1.13 h is found.

The bottom stream exiting from the phase separator (stream 115) is the aqueous phase. This stream needs to be treated before being discharged. Its composition is reported in Table 3.31.

Chemical species	Stream 115
H ₂ O	118.0371
Acetic acid	7.6417
CH ₃ I	0.0332
Rhodium catalyst	0
Propyl acetate	4.1287

Table 3.31 Composition of the bottom stream exiting from phase separator V-109 (kg/h)

The top stream exiting from the phase separator (stream 114) is the propyl-acetate rich phase. This stream is recirculated to the column after 1% of it is purged (stream 120 is the purge). A make-up stream of propyl acetate (stream 119) of 10.2134 kg/h is needed to balance the losses of this component. The composition of the propyl-acetate stream entering column T-105 (stream 118) is reported in Table 3.32.

Chemical species	Stream 118
H ₂ O	22.4372
Acetic acid	23.4372
CH ₃ I	0.0463
Rhodium catalyst	0
Propyl acetate	585.3182

Table 3.32 Composition of the propyl acetate stream entering distillation column T-105 (kg/h)

The bottom stream exiting from the distillation column (stream 106) is the final product stream. Its composition is reported in Table 3.33.

Chemical species	Stream 106
H ₂ O	0.3026
Acetic acid	1007.9122
CH ₃ I	0
Rhodium catalyst	0.0015
Propyl acetate	0

Table 3.33 Composition of the bottom stream of distillation column T-105 (kg/h)

As it can be seen from Table 3.33 the product respects the purity for commercial grade glacial acetic acid. The acetic acid percentage by mass is 99.9%, a value greater than 99.5%.

3.6. Plant furnace and utilities

To provide the heat necessary to the reforming reactor and the reverse water-gas shift reactor a furnace is necessary. Figure 3.16 offers an overview of the plant section described below. The furnace has been modeled based on the heat request of the two reactors (7.335×10^6 kJ/h). Stream 44 and stream 54 are mixed with a stream of biogas (291 m³/h) and burned in the furnace with 20% excess of air (4563 m³/h) [55]. The flue gases exit at 1000°C, and the heat of this stream is recovered to generate the high-pressure and medium-pressure steam necessary for the entire plant (215.9 kg/h of high pressure steam and 1847 kg/h of medium pressure steam). In the first heat exchanger (E-102) flue gases are cooled from 1000°C to 573.3°C while high pressure steam is produced at 250°C and 3845 kPa. In the second heat exchanger (E-105) the flue gases are further cooled to 295.8 °C while water at 3865 kPa is heated from 25°C to 250°C. A pump (P-107, with adiabatic efficiency of 0.75) pumps the water recovered from the plant inside the heat exchangers train. A total of 2063 kg/h of steam are produced.

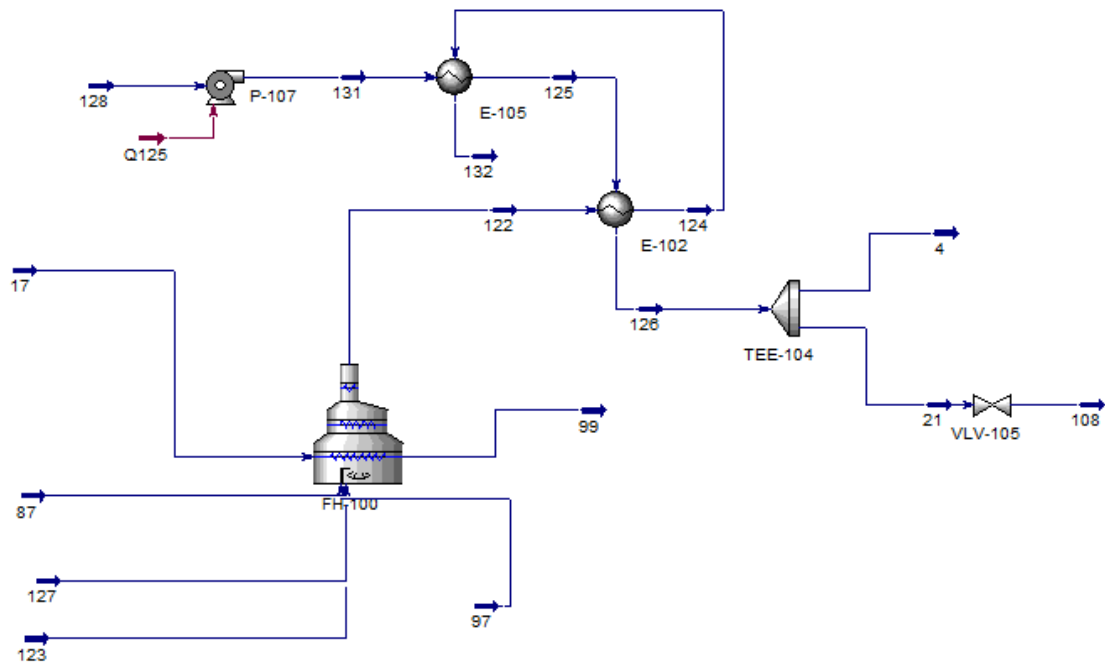


Figure 3.16 Plant furnace and HP and MP Steam generating units

To provide the cooling necessary in the condenser of the methanol distillation column (T-100) a refrigerant is used. The refrigerant chosen is glycolated water (12.4% of ethylene glycol by mass) available at 0°C and heated to 5°C in the condenser. To lower the temperature of the refrigerant after its utilization a heat pump has been modeled. Figure 3.17 provides an overview of the heat pump system. The refrigerant (stream 141) enters the methanol column condenser (E-125) and it is heated from 0 °C to 5 °C, it is then recirculated to a second heat exchanger (E-123) where it is cooled down to 0°C. Shell side of this heat exchanger a stream of trichlorofluoromethane (R11) of 2400 kg/h is evaporated at -15.26 °C. after evaporation, the stream (stream 142) is sent to a compressor (K-109) where it is compressed from 20 kPa to 240 kPa exiting with a temperature of 89.4 °C. The compressed stream is then sent to a condenser (E-119) where it is completely condensed at 49 °C using cooling water. The liquid stream (stream 139) is then expanded back to 20 kPa through a valve decreasing its temperature to -15.26°C.

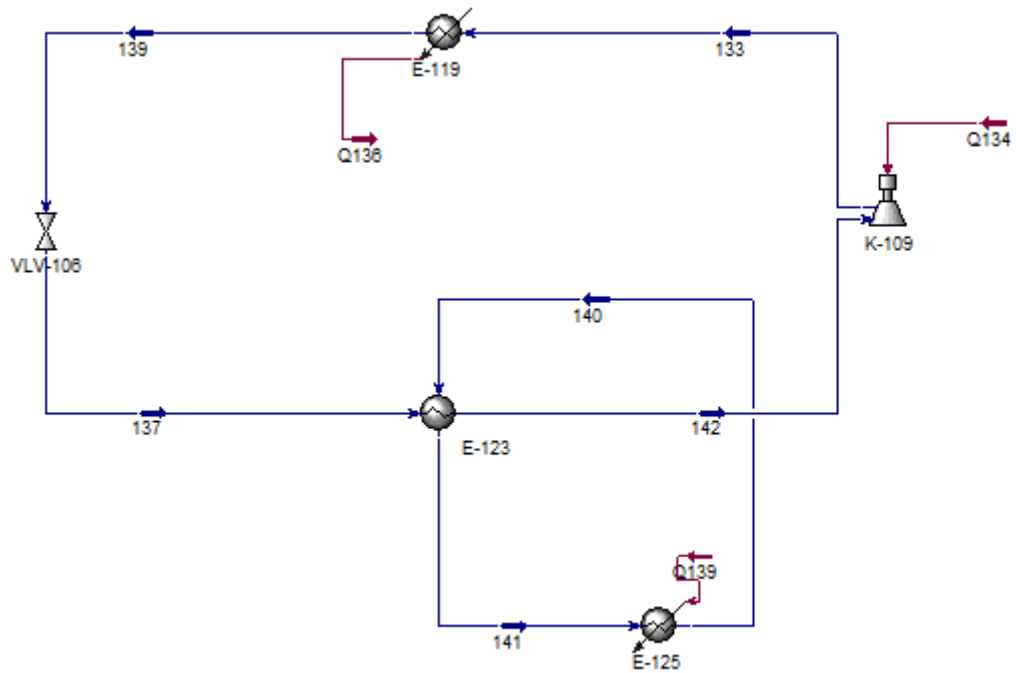


Figure 3.17 Heat pump for refrigerant regeneration

4 Economic analysis

The economic analysis has been carried out using the Turton handbook as a main reference [56]. The economics of the plant consider capital costs and operating costs associated with the construction and operation of a chemical process. To evaluate the economic potential of the plant different profitability criteria using discounted and non-discounted basis have been considered. A cash-flow diagram will be presented at the end of the analysis. Lastly, an analysis using Monte-Carlo method has been carried out in order to assess risk related to the plant investment.

4.1. Capital costs

To estimate the equipment cost Guthrie's equipment module costing technique has been used. This technique relates all costs back to the purchased cost of the equipment at base condition (unit fabricated with common carbon steel, operating at ambient pressure). The deviations from base conditions are taken into account by using multiplying factors that are related to the specific equipment type, the specific pressure of the system and the specific material of construction. Other factors need to be considered when estimating equipment costs. A series of direct and indirect costs are reported in Table 4.1. It is important to note that the costs are expressed in dollars but thanks to a euro dollar change very close to 1 during 2022, the assumption of one dollar equal to one euro has been made.

The bare module cost for the specific equipment (CBM) can be calculated from Equation 4.1

$$C_{BM} = C_P^0 F_{BM} \quad \text{Equation 4.1}$$

Where FBM is the bare module factor, a series of multiplication factors that take into account the items listed in Table 4.1, the specific material of the equipment and its operating pressure. C_P^0 is the purchased cost of the equipment at base conditions (carbon steel and working at atmospheric pressure). C_P^0 can be calculated using Equation 4.2 **Error! Reference source not found.**

$$\log_{10} C_P^0 = K_1 + K_2 \log_{10}(A) + K_3 (\log_{10}(A))^2 \quad \text{Equation 4.2}$$

Where A is the capacity (or size parameter) of the equipment while K1, K2, K3 are specific parameters for the considered equipment.

Direct expenses
Equipment free on-board cost
Materials required for installation
Labor to install equipment
Indirect expenses
Freight, insurance, and taxes
Construction overhead
Contractor engineering expenses
Contingency
Contractor fee
Site development
Auxiliary buildings
Off-site and utilities

Table 4.1 Factors affecting the costs associated with evaluation of capital cost of chemical plants

The effect of pressure on the equipment cost is taken into account inside the bare module factor by the parameter F_P (pressure factor). As the operating pressure increases the cost of the equipment increases. For process vessels the pressure factor is calculated with Equation 4.3.

$$F_P = \frac{\frac{(P + 1)D}{2(850 - 0.6(P + 1))} + 0.00315}{0.0063} \quad \text{Equation 4.3}$$

Where P is the working pressure of the vessel expressed in barg and D is the diameter of the vessel.

For process equipment the pressure factor is expressed with Equation 4.4.

$$\log_{10} F_P = C_1 + C_2 \log_{10}(P) + C_3 (\log_{10}(P))^2 \quad \text{Equation 4.4}$$

Where P is the working pressure of the equipment expressed in barg and C1, C2, C3 are parameters related to the specific equipment.

The effect of the material on the equipment cost is taken into account inside the bare module factor by the parameter F_M (material factor).

By explicitly expressing the factors related to pressure and material in **Error! Reference source not found.** Equation 4.1 the following equation, expressing the bare module cost for the majority of the equipment, is obtained:

$$C_{BM} = C_P^0 F_{BM} = C_P^0 (B_1 + B_2 F_P F_M) \quad \text{Equation 4.5}$$

Where B_1 and B_2 are parameters related to the specific equipment

For other specific equipment different equations are used (the numeric value of F_{BM} is directly given) as reported in Table 4.2.

Equipment	Bare module equation
Compressors	$C_{BM} = C_P^0 F_{BM}$
Furnace	$C_{BM} = C_P^0 F_{BM} F_P$
Trays and Packing	$C_{BM} = C_P^0 F_{BM}$
Fans with drives	$C_{BM} = C_P^0 F_{BM} F_P$

Table 4.2 Equations for bare module cost for different equipment

The calculation of the bare module cost is based on data fitted to match equipment costs in 2001. An important factor to consider is the effect of inflation on the price of equipment. The value of the equipment can be related to the year it was purchased by CEPCI (chemical engineering plant cost index). By dividing the CEPCI index of the current year by the CEPCI index of the year in which the bare module correlation where implemented, the effect of inflation is considered. Equation 4.6 has been used to calculate updated bare module costs.

$$C_{BM}^{2022} = C_{BM}^{2001} \left(\frac{CEPCI_{2022}}{CEPCI_{2001}} \right) \quad \text{Equation 4.6}$$

In Table 4.3 the values of CEPCI indexes for different years are reported.

Year	CEPCI
2001	397
2008	575.4
2015	556.8
2021	708.0
February 2022	801.3

Table 4.3 CEPCI for different years

Once the bare module cost for the equipment is known, other costs need to be considered.

When contingency and fee costs variations are considered the total module cost (C_{TM}) of the equipment is found. Values of 15% and 3% of the bare module cost are considered when accounting for contingency and fee respectively. **Error! Reference source not found.** Equation 4.7 is used to calculate the total module cost of each piece of equipment.

$$C_{TM} = 1.18C_{BM} \quad \text{Equation 4.7}$$

Lastly auxiliary facilities costs can be considered. These costs are related to site development, auxiliary buildings, and off-site utilities. A value equal to 50% of the bare module cost for the base condition (stainless steel and working at atmospheric pressure) is considered. Adding auxiliary costs to the total module cost gives the grassroots cost of the equipment (C_{GR}) as reported by Equation 4.8 **Error! Reference source not found.**

$$C_{GR} = C_{TM} + 0.5C_{BM}^0 \quad \text{Equation 4.8}$$

The total grassroots cost of the entire plant is calculated summing the grassroots costs of each piece of equipment as explicated in Equation 4.9.

$$C_{GR}^{TOT} = \sum_{i=1}^N C_{GRi} \quad \text{Equation 4.9}$$

4.1.1. Compressors capital costs estimation

To estimate the compressors capital costs data from the Hysys simulation were taken. To calculate C_P° Equation 4.2 has been used. Results are reported in Table 4.4.

Compressor	Type	Power (kW)	K1	K2	K3	$C_P^\circ(2001)$ €
K105	Centrifugal	77,96	2,2897	1,3604	-0,1027	31319,9
K106	Centrifugal	69,75	2,2897	1,3604	-0,1027	28094,1
K100	Centrifugal	57,07	2,2897	1,3604	-0,1027	23029,8
K101	Centrifugal	50,95	2,2897	1,3604	-0,1027	20549,3
K107	Centrifugal	6,669	2,2897	1,3604	-0,1027	2192,861
K108	Centrifugal	8,224	2,2897	1,3604	-0,1027	2809,186
K102	Centrifugal	1,599	2,2897	1,3604	-0,1027	365,3826
K104	Centrifugal	28,38	2,2897	1,3604	-0,1027	11208,65
K103	Centrifugal	26,35	2,2897	1,3604	-0,1027	10356,62
K109	Centrifugal	38,65	2,2897	1,3604	-0,1027	15493,6

Table 4.4 Compressors C_P° estimation

To calculate C_{BM} the equation listed in Table 4.2 has been used. Stainless steel is the material of choice for all the compressors in the plant as carbon steel is not suitable in the presence of corrosive chemical species (hydrogen and acetic acid). To calculate $C_{BM(2022)}$, C_{TM} , C_{GR} , Equation 4.6, Equation 4.7, Equation 4.8 have been used respectively. Results are reported in Table 4.5.

Compressor	FBM	CBM	CBM(2022)	CBM $^\circ$ (2022)	CTM	CGR €
K105	6	187919,6	378679,23	63113,2	446841,49	478398,09
K106	6	168564,8	339677,19	56612,86	400819,08	429125,51
K100	6	138179,1	278446,47	46407,75	328566,84	351770,71
K101	6	123295,5	248454,48	41409,08	293176,29	313880,83
K107	6	13157,17	26513,18	4418,86	31285,55	33494,98
K108	6	16855,11	33964,96	5660,83	40078,66	42909,07
K102	6	2192,295	4417,72	736,29	5212,91	5581,06
K104	6	67251,88	135520,17	22586,69	159913,80	171207,14
K103	6	62139,7	125218,55	20869,76	147757,89	158192,76
K109	6	92961,61	187328,19	31221,37	221047,26	236657,95

Table 4.5 Compressors C_{BM} , C_{TM} , C_{GR} estimation

4.1.2. Pumps capital costs estimation

To estimate the pumps capital costs data from the Hysys simulation were taken. To calculate $C_{P^{\circ}}$ Equation 4.2 has been used. For pump P-106 cost estimation the 0.6 rule of thumb has been used as reported in the following equation:

$$C_{P1}^{\circ} = C_{P2}^{\circ} \left(\frac{A_1}{A_2} \right)^{0.6} \quad \text{Equation 4.10}$$

Where C_{P1}° is the cost of the investigated equipment, C_{P2}° is the cost of a similar piece of equipment but with different size (or capacity), A_1 is the size parameter of the investigated equipment and A_2 is the size parameter of the different size equipment. Results are reported in Table 4.6.

Pump	Type	Power (kW)	K1	K2	K3	$C_{P^{\circ}}(2001) \text{ €}$
P101	Reciprocating	0,228	3,8696	0,3161	0,122	5211,196
P102	Reciprocating	0,05447	3,8696	0,3161	0,122	4623,488
P104	Reciprocating	132,1	3,8696	0,3161	0,122	122687,8
P100	Reciprocating	1,076	3,8696	0,3161	0,122	7581,922
P105	Reciprocating	0,1289	3,8696	0,3161	0,122	4840,968
P106	Reciprocating	0,0006256	3,8696	0,3161	0,122	197,9514
P107	Reciprocating	2,855	3,8696	0,3161	0,122	10938,09

Table 4.6 Pumps $C_{P^{\circ}}$ estimation

To calculate F_P Equation 4.4 has been used. Stainless steel is the material of choice for all the pumps in the plant. Results are reported in Table 4.7.

Pump	P(barG)	C1	C2	C3	FP	FM
P101	19,3	-0,245382	0,259016	-0,01363	1,35	2,4
P102	19,3	-0,245382	0,259016	-0,01363	1,35	2,4
P104	79	-0,245382	0,259016	-0,01363	1,35	2,4
P100	59	-0,245382	0,259016	-0,01363	1,35	2,4
P105	59	-0,245382	0,259016	-0,01363	1,35	2,4
P106	0,1	-0,245382	0,259016	-0,01363	1,35	2,4
P107	40	-0,245382	0,259016	-0,01363	1,35	2,4

Table 4.7 Pumps F_P and F_M estimation

To calculate C_{BM} , $C_{BM(2022)}$, C_{TM} , C_{GR} , Equation 4.5, Equation 4.6, Equation 4.7, Equation 4.8 have been used respectively. Results are reported in Table 4.8.

Pump	B1	B2	CBM	CBM(2022)	CBM°(2022)	CTM	CGR €
P101	1,89	1,35	29462,64	59370,56	34023,73	70057,26	87069,12
P102	1,89	1,35	26139,90	52674,86	30186,6	62156,34	77249,64
P104	1,89	1,35	857626,65	1728214,9	801024,5	2039293,59	2439805,82
P100	1,89	1,35	50711,18	102188,78	49502,12	120582,76	145333,82
P105	1,89	1,35	32378,49	65246,33	31606,52	76990,67	92793,94
P106	1,89	1,35	1015,49	2046,33	1292,42	2414,67	3060,88
P107	1,89	1,35	68987,87	139018,39	71414,43	164041,70	199748,91

Table 4.8 Pumps C_{BM} , $C_{BM(2022)}$, C_{TM} , C_{GR} estimation

4.1.3. Heat exchangers capital costs estimation

To estimate the capital cost of heat exchangers the fundamental parameter to know is the total area of heat exchange. To determine this parameter Equation 4.11 **Error! Reference source not found.** can be used.

$$A = \frac{Q}{U\Delta T_{lm}} \quad \text{Equation 4.11}$$

Where A is the area of heat exchange, Q is the heat exchanged, U is the global coefficient of heat exchange and ΔT_{lm} is the mean logarithmic temperature difference inside the heat exchanger and it can be calculated with Equation 4.12.

$$\Delta T_{lm} = \frac{\Delta T_1 - \Delta T_2}{\ln\left(\frac{\Delta T_1}{\Delta T_2}\right)} \quad \text{Equation 4.12}$$

Where ΔT_1 and ΔT_2 are the temperature differences at the inlet and outlet of the heat exchanger respectively. All the parameters have been taken from the Hysys simulation. The global heat exchange coefficients have been chosen according to data found in literature [57]. The results are reported in Table 4.9 and Table 4.10.

exchangers	utility	ΔT_1	ΔT_2	ΔT_{lm}	Q [W]	U [W/m ² /k]	A [m ²]
E100	cooling water	152,9	10	52,40	7,44E+04	120	11,84
E107	HP steam	72,1	20	40,63	2,93E+04	250	2,88
E115	process-process	314,2	250	280,88		164,33	11,31
E120	process-process	318,4	25,9	116,58		160,75	20,73
E117	process-process	25,9	95,07	53,19		159,31	33,93
E103	cooling water	96,5	10	38,16	3,45E+05	230	39,35
E104	cooling water	108,3	25	56,82	4,81E+04	340	2,49
E116	cooling water	8,4	10	9,18	1,51E+05	1400	11,71
E101	cooling water	170,9	45	94,35	5,78E+03	120	0,51
E109	cooling water	249,9	105	167,11	6,24E+04	230	1,62
E122	process-process	96,1	50	70,56		225,61	11,31
E106	cooling water	102,4	10	39,72	2,08E+05	340	15,40
E113	cooling water	165,7	110	135,95	2,66E+04	230	0,85
E111	cooling water	165,9	155	160,39	7,13E+03	340	0,13
E121	process-process	221,05	210	215,48		123,47	11,31
E108	HP steam	181,69	70	117,10	7,16E+04	770	0,79
E112	cooling water	145,8	10	50,68	1,15E+05	230	9,89
E110	MP steam	64,3	35	48,17	1,24E+05	770	3,34
E114	cooling water	80,2	65	72,33	1,58E+05	770	2,83
E118	cooling water	62,33	10	28,60	3,93E+03	700	0,20

Table 4.9 Estimation of the heat exchange area for the plant heat exchangers

exchangers	utility	ΔT_1	ΔT_2	ΔT_{lm}	Q [W]	U [W/m ² /k]	A [m ²]
T102 condenser	cooling water	5,88	10,88	8,13	9,02E+03	1100	1,01
T102 reboiler	LP steam	21,2	21,2	21,2	1,49E+04	1100	0,64
T103 condenser	cooling water	62,33	67,33	64,80	1,42E+05	1100	1,99
T103 reboiler	LP steam	18,8	18,8	18,8	1,43E+05	1100	6,91
T105 condenser	cooling water	49,61	54,61	52,07	8,89E+05	1100	15,52
T105 reboiler	MP steam	57,3	57,3	57,3	8,91E+05	1100	14,14
T100 condenser	refrigerant	13,22	18,22	15,59	1,33E+05	1100	7,76
T100 reboiler	LP steam	57,54	57,54	57,54	1,56E+05	1100	2,46
E102	process-process	750	323,3	507,08		64,33	30,16
E105	process-process	323,3	270,57	296,15		67,94	30,16
E123	process-process	15,26	20,26	17,64		1002,78	7,54
E119	cooling water	20,57	24	22,24	168200	700	10,80

Table 4.10 Estimation of the heat exchange area for the plant heat exchangers

Once the heat of exchange area is known C_P° can be calculated using Equation 4.2 **Error! Reference source not found.** The results are reported in Table 4.11.

Exchanger	Type	Area (m ²)	K1	K2	K3	C _P ^o (2001) €
E100	S&T	11,84	2,7652	0,7282	0,0783	4333,918
E107	S&T	2,88	2,7652	0,7282	0,0783	1307,894
E115	S&T	11,31	2,7652	0,7282	0,0783	4161,286
E120	S&T	20,73	2,7652	0,7282	0,0783	7238,948
E117	S&T	33,93	2,7652	0,7282	0,0783	11566,54
E103	S&T	39,35	2,7652	0,7282	0,0783	13359,02
E104	S&T	2,49	2,7652	0,7282	0,0783	1163,869
E116	S&T	11,71	2,7652	0,7282	0,0783	4294,101
E101	S&T	0,51	2,7652	0,7282	0,0783	362,366
E109	S&T	1,62	2,7652	0,7282	0,0783	835,252
E122	S&T	11,31	2,7652	0,7282	0,0783	4161,286
E106	S&T	15,40	2,7652	0,7282	0,0783	5500,782
E113	S&T	0,85	2,7652	0,7282	0,0783	517,4325
E111	S&T	0,13	2,7652	0,7282	0,0783	152,3385
E121	S&T	11,31	2,7652	0,7282	0,0783	4161,286
E108	S&T	0,79	2,7652	0,7282	0,0783	493,1051
E112	S&T	9,89	2,7652	0,7282	0,0783	3694,242
E110	S&T	3,34	2,7652	0,7282	0,0783	1471,647
E114	S&T	2,83	2,7652	0,7282	0,0783	1289,265
E118	S&T	0,20	2,7652	0,7282	0,0783	194,6885
T102 condenser	S&T	1,01	2,7652	0,7282	0,0783	586,1775
T102 reboiler	Kettle	0,64	2,7652	0,7282	0,0783	423,5495
T103 condenser	S&T	1,99	2,7652	0,7282	0,0783	978,202
T103 reboiler	Kettle	6,91	2,7652	0,7282	0,0783	2703,66
T105 condenser	S&T	15,52	2,7652	0,7282	0,0783	5540,779
T105 reboiler	Kettle	14,14	2,7652	0,7282	0,0783	5087,754
T100 condenser	S&T	7,76	2,7652	0,7282	0,0783	2985,84
T100 reboiler	Kettle	2,46	2,7652	0,7282	0,0783	1154,193
E102	S&T	30,16	2,7652	0,7282	0,0783	10325,2
E105	S&T	30,16	2,7652	0,7282	0,0783	10325,2
E123	S&T	7,54	2,7652	0,7282	0,0783	2913,236
E119	S&T	10,80	2,7652	0,7282	0,0783	3994,803

Table 4.11 Heat exchangers C_P^o estimation

To calculate F_p **Error! Reference source not found.** has been used. Stainless steel is the material of choice for all the heat exchangers in the plant. Results are reported in Table 4.12.

Exchanger	P(barG)	C1	C2	C3	FP	FM
E100	4	0	0	0	1	2,8
E107	37	0	0	0	1	2,8
E115	20	0	0	0	1	2,8
E120	20	0	0	0	1	2,8
E117	20	0	0	0	1	2,8
E103	20	0	0	0	1	2,8
E104	39	0	0	0	1	2,8
E116	79	0,6072	-0,912	0,3327	1,187	2,8
E101	4	0	0	0	1	2,8
E109	17	0	0	0	1	2,8
E122	79	0,6072	-0,912	0,3327	1,187	2,8
E106	76,8	0,6072	-0,912	0,3327	1,176	2,8
E113	26	0	0	0	1	2,8
E111	39	0	0	0	1	2,8
E121	17	0	0	0	1	2,8
E108	39	0	0	0	1	2,8
E112	19	0	0	0	1	2,8
E110	4	0	0	0	1	2,8
E114	0,1	0	0	0	1	2,8
E118	0,1	0	0	0	1	2,8
T102 condenser	0,1	0	0	0	1	2,8
T102 reboiler	2	0	0	0	1	2,8
T103 condenser	0,1	0	0	0	1	2,8
T103 reboiler	2	0	0	0	1	2,8
T105 condenser	0,1	0	0	0	1	2,8
T105 reboiler	8	-0,00164	-0,00627	0,0123	1,006	2,8
T100 condenser	0,1	0	0	0	1	2,8
T100 reboiler	2	0	0	0	1	2,8
E102	20	0	0	0	1	2,8
E105	20	0	0	0	1	2,8
E123	20	0	0	0	1	2,8
E119	20	0	0	0	1	2,8

Table 4.12 Heat exchangers FP and FM estimation

To calculate C_{BM} , $C_{BM(2022)}$, C_{TM} , C_{GR} , Equation 4.5, Equation 4.6, Equation 4.7, Equation 4.8 have been used respectively. Results are reported in Table 4.13.

Exchanger	B1	B2	CBM	CBM(2022)	CBM°(2022)	CTM	CGR €
E100	1,74	1,55	26350,22	53098,68	28732,67	62656,44	77022,78
E107	1,74	1,55	7951,99	16024,17	8670,97	18908,52	23244,01
E115	1,74	1,55	25300,62	50983,61	27588,17	60160,66	73954,74
E120	1,74	1,55	44012,81	88690,79	47992,22	104655,1 3	128651,24
E117	1,74	1,55	70324,58	141712,0	76682,97	167220,1 6	205561,64
E103	1,74	1,55	81222,83	163673,21	88566,59	193134,3 9	237417,68
E104	1,74	1,55	7076,32	14259,59	7716,13	16826,32	20684,380
E116	1,74	1,55	29601,40	59650,19	28468,7	70387,22	84621,57
E101	1,74	1,55	2203,19	4439,67	2402,39	5238,81	6440,00
E109	1,74	1,55	5078,33	10233,41	5537,49	12075,43	14844,17
E122	1,74	1,55	28685,84	57805,23	27588,17	68210,17	82004,25
E106	1,74	1,55	37643,52	75855,96	36468,66	89510,04	107744,37
E113	1,74	1,55	3145,99	6339,53	3430,43	7480,64	9195,86
E111	1,74	1,55	926,22	1866,43	1009,96	2202,39	2707,37
E121	1,74	1,55	25300,62	50983,61	27588,17	60160,66	73954,74
E108	1,74	1,55	2998,08	6041,47	3269,15	7128,93	8763,51
E112	1,74	1,55	22460,99	45261,45	24491,8	53408,51	65654,41
E110	1,74	1,55	8947,62	18030,46	9756,61	21275,94	26154,25
E114	1,74	1,55	7838,73	15795,93	8547,47	18639,19	22912,93
E118	1,74	1,55	1183,71	2385,30	1290,73	2814,66	3460,02
T102 condenser	1,74	1,55	3563,96	7181,78	3886,19	8474,50	10417,60
T102 reboiler	1,63	1,66	2659,04	5358,27	2808,02	6322,76	7726,77
T103 condenser	1,74	1,55	5947,47	11984,82	6485,21	14142,09	17384,69
T103 reboiler	1,63	1,66	16973,58	67885,01	17924,52	40360,35	49322,60
T105 condenser	1,74	1,55	33687,94	64664,98	36733,83	80104,32	98471,23
T105 reboiler	1,63	1,66	32090,00	36582,18	33730,4	76304,67	93169,87
T100 condenser	1,74	1,55	18153,91	14601,56	19795,29	43166,97	53064,62
T100 reboiler	1,63	1,66	7246,03	130622,88	7651,98	17229,84	21055,83
E102	1,74	1,55	64821,60	130622,88	68453,21	154134,9 9	188361,60
E105	1,74	1,55	64821,60	36855,00	68453,21	154134,9 9	188361,60
E123	1,74	1,55	18289,29	50537,77	19313,95	43488,90	53145,87
E119	1,74	1,55	25079,37	67885,01	26484,43	59634,57	72876,79

Table 4.13 Heat exchangers C_{BM} , $C_{BM(2022)}$, C_{TM} , C_{GR} estimation

4.1.4. Reactors and furnace capital cost estimation

To estimate the reactors capital costs data from the Hysys simulation were taken. The methanol multiple-pipes reactor (PFR-100) has been treated as a shell and tube heat exchanger for the economic evaluation. To calculate C_P° Equation 4.2 has been used. Results are reported in Table 4.14.

Reactor	Type	Volume (m ³)	K1	K2	K3	$C_P^\circ(2001)$ €
PFR100	PFR	5	2,7652	0,7282	0,0783	2053,261
CSTR100	CSTR	8	4,1052	0,532	-0,0005	59185,74

Table 4.14 Reactors C_P° estimation

To calculate F_P Equation 4.4 has been used for PFR-100 while Equation 4.3 has been used for CSTR-100 (the reactor diameter is 1.894 m). Stainless steel is the material of choice for the two reactors. Results are reported in Table 4.15.

Reactor	P(barG)	C1	C2	C3	FP	FM
PFR100	79	0,6072	-0,912	0,3327	1,187	2,8
CSTR100	40	/	/	/	7,967	3,2

Table 4.15 Reactors F_P and F_M estimation

To calculate C_{BM} , $C_{BM(2022)}$, C_{TM} , C_{GR} , Equation 4.5, Equation 4.6 **Error! Reference source not found.**, Equation 4.7, Equation 4.8 have been used respectively. Results are reported in Table 4.16.

Reactor	B1	B2	CBM	CBM(2022)	CBM ^o (2022)	CTM	CGR €
PFR100	1,74	1,55	14154,16	28522,24	13612,55	33656,25	40462,53
CSTR100	2,25	1,82	187198,25	3772256,43	315594,9	4451262,59	4609060,0

Table 4.16 Reactors C_{BM} , $C_{BM(2022)}$, C_{TM} , C_{GR} estimation

To estimate the cost of the furnace the data for the reformer reactor and the reverse water gas shift reactor have been taken from the Hysys simulation. To calculate C_P° Equation 4.2 has been used. Results are reported in Table 4.17.

Furnace	Type	Heat (kW)	K1	K2	K3	C _P [°] (2001) €
PFR101+PFR103	Furnace	2036,7	3,068	0,6597	0,0194	290609,5

Table 4.17 Furnace C_P[°] estimation

To calculate F_P Equation 4.4 has been used. Special alloy steel is the material of choice for the furnace. Results are reported in Table 4.18.

Furnace	P(barG)	C1	C2	C3	FP	FBM
PFR101+PFR103	19	0,1405	-0,2629	0,1293	1,036928	3

Table 4.18 Furnace F_P and F_{BM} estimation

To calculate C_{BM} the related equation in Table 4.2 has been used. To calculate C_{BM(2022)}, C_{TM}, C_{GR}, Equation 4.6, Equation 4.7, Equation 4.8 have been used respectively. Results are reported in Table 4.19.

Furnace	CBM	CBM(2022)	CBM [°] (2022)	CTM	CGR €
PFR101+PFR103	904022,91	1821708,64	585611	2149616,19	3297076,65

Table 4.19 Furnace C_{BM}, C_{BM(2022)}, C_{TM}, C_{GR} estimation

4.1.5. Flash separators capital cost estimation

To estimate the flash separators capital costs data from the Hysys simulation were taken. To calculate C_P[°] Equation 4.2 has been used. Results are reported in Table 4.20.

Separator	Type	Volume (m ³)	K1	K2	K3	C _P [°] (2001) €
V100	Flash	0,4128	3,4974	0,4485	0,1074	2192,388
V106	Flash	5,244	3,4974	0,4485	0,1074	7512,642
V101	Flash	0,4128	3,4974	0,4485	0,1074	2192,388
V103	Flash	0,1223	3,4974	0,4485	0,1074	1505,055
V102	Flash	1,2116	3,4974	0,4485	0,1074	3431,887

Table 4.20 Flash separators C_P[°] estimation

To calculate F_P Equation 4.3 has been used. Stainless steel is the material of choice for the flash separators. Results are reported in Table 4.21.

Separator	P(barG)	FP	FM
V100	17	1,278292	3
V106	0	1	3
V101	77	4,023762	3
V103	19	1,077338	3
V102	0	1	3

Table 4.21 Flash separators F_P and F_M estimation

To calculate C_{BM} , $C_{BM(2022)}$, C_{TM} , C_{GR} , Equation 4.5, Equation 4.6, Equation 4.7, Equation 4.8 have been used respectively. Results are reported in Table 4.22.

Separator	B1	B2	CBM	CBM(2022)	CBM°(2022)	CTM	CGR €
V100	2,25	1,82	20234,596	40775,00	17980,9	48114,5	49210,7
V106	2,25	1,82	57922,473	116720,35	61615,02	137730	141486,3
V101	2,25	1,82	53099,080	107000,67	17980,9	126260,8	127357
V103	2,25	1,82	12239,5122	24664,00	12343,73	29103,53	29856,05
V102	2,25	1,82	26459,846	53319,59	28146,66	62917,11	64633,06

Table 4.22 Flash separators C_{BM} , $C_{BM(2022)}$, C_{TM} , C_{GR} estimation

4.1.6. Columns capital cost estimation

To size the columns diameters and tray spacing or packed height, Hysys automatic internal sizing has been used. To calculate the total volume of the column the following equation has been used:

$$V = \frac{\pi D^2}{4} (h + 3) \tag{Equation 4.13}$$

Where D is the column diameter, h is the packed height for packed columns and the tray spacing multiplied by the number of trays for trays columns. 3 additional meters are considered for liquid height in the bottom of the column and vapor disengagement in the top. Results are reported in Table 4.23.

Column	Diameter (m)	Height (m)	Volume (m ³)
T101	0,45	0,4	0,540746635
T100	0,2435	0,3	0,209929568
T102	0,13	0,4	0,045128978
T103	0,3	1,5	0,318086256
T105	0,9	26,21	18,58438037

Table 4.23 Column sizing

Once the volume of each column is known C_P° can be calculated with Equation 4.2. Results are reported in Table 4.24.

Column	Type	Volume (m ³)	K1	K2	K3	$C_P^\circ(2001)$ €
T101	Packed	0,540746635	3,4974	0,4485	0,1074	2428,312
T100	Packed	0,209929568	3,4974	0,4485	0,1074	1748,676
T102	Packed	0,045128978	3,4974	0,4485	0,1074	1225,66
T103	Packed	0,318086256	3,4974	0,4485	0,1074	1999,258
T105	Plated	18,58438037	3,4974	0,4485	0,1074	17362,25

Table 4.24 Columns C_P° estimation

To calculate F_P Equation 4.3 has been used. Stainless steel is the material of choice for the columns. Results are reported in Table 4.25.

Column	P(barG)	FP	FM
T101	79	3,666686	3
T100	0	1	3
T102	0	1	3
T103	0	1	3
T105	0	1	3

Table 4.25 Columns F_P and F_M estimation

To calculate C_{BM} , $C_{BM(2022)}$, C_{TM} , C_{GR} , Equation 4.5, Equation 4.6, Equation 4.7, Equation 4.8 have been used respectively. Results are reported in Table 4.26.

Column	B1	B2	CBM	CBM(2022)	CBM°(2022)	CTM	CGR €
T101	2,25	1,82	54078,7753	108974,862	19915,83	128590,3	138548,25
T100	2,25	1,82	13482,2922	27168,3469	14341,79	32058,65	39229,542
T102	2,25	1,82	9449,83654	19042,4917	10052,26	22470,14	27496,271
T103	2,25	1,82	15414,2763	31061,5140	16396,93	36652,59	44851,053
T105	2,25	1,82	133862,963	269749,043	142396,7	318303,9	389502,22

Table 4.26 Columns C_{BM} , $C_{BM(2022)}$, C_{TM} , C_{GR} estimation

To estimate the internals packing and tray capital costs data from the Hysys simulation were taken. To calculate C_{P° Equation 4.2 has been used. Results are reported in Table 4.27.

Column	Type	Volume (m ³) or Area (m ²)	K1	K2	K3	$C_{P^\circ}(2001)$ €
T101	Packed	0,063617251	2,4493	0,9744	0,0055	19,56033
T100	Packed	0,019084506	2,4493	0,9744	0,0055	6,169555
T102	Packed	0,005309292	2,4493	0,9744	0,0055	1,824066
T103	Packed	0,106028752	2,4493	0,9744	0,0055	31,98134
T105	Sieve Tray	0,636172512	2,9949	0,4465	0,3961	836,5249

Table 4.27 Trays and packing C_{P° estimation

Stainless steel is the material of choice for the columns' internals. Pressure has little effect on columns internals (FP=1). To calculate C_{BM} the corresponding equation from Table 4.2 has been used. To calculate $C_{BM(2022)}$, C_{TM} , C_{GR} , Equation 4.6, Equation 4.7, Equation 4.8 have been used respectively. Results are reported in Table 4.28.

Column	FP	FM	CBM	CBM(2022)	CBM°(2022)	CTM	CGR €
T101	1	7	136,92	275,91	39,41	325,57	345,29
T100	1	7	43,19	87,03	12,43	102,69	108,9074
T102	1	7	12,76	25,73	3,68	30,36	32,19
T103	1	7	223,86	451,12	64,44	532,32	564,54
T105	1	1,8	64747,02	130472,59	1685,69	153957,65	154800,50

Table 4.28 Columns internals C_{BM} , $C_{BM(2022)}$, C_{TM} , C_{GR} estimation. To estimate the values for column T105 the values for a single tray have been multiplied by the total number of trays

4.1.7. Tank separator capital cost estimation

To estimate the tank separator capital costs data from the Hysys simulation were taken. To calculate $C_{P^{\circ}}$ Equation 4.2 has been used. Results are reported in Table 4.29.

Tank	Type	Volume (m ³)	K1	K2	K3	$C_{P^{\circ}}(2001)$ €
V109	separator	2	3,5565	0,3776	0,0905	4768,37

Table 4.29 Tank separator $C_{P^{\circ}}$ estimation

Stainless steel is the material of choice for the tank separator. To calculate C_{BM} , $C_{BM(2022)}$, C_{TM} , C_{GR} , Equation 4.5, Equation 4.6, Equation 4.7, Equation 4.8 have been used respectively. Results are reported in Table 4.30 and Table 4.31.

Tank	FP	FM	B1	B2	CBM	CBM(2022)
V109	1	3	1,49	1,52	28848,63	58133,27

Table 4.30 Tank separator C_{BM} , $C_{BM(2022)}$ estimation

Tank	$CBM^{\circ}(2022)$	CTM	CGR €
V109	28922,51	68597,26	83058,52

Table 4.31 Tank separator C_{TM} , C_{GR} estimation

4.1.8. Cooling towers capital cost estimation

To restore the temperature of the utility cooling water used in the plant, cooling towers are modeled (based on the approach exposed in the Turton handbook). A total of 5 identical cooling towers are needed to decrease the temperature of the cooling water of the plant (416.3 m³ of water per hour) from 30°C to 25°C. A total volume per column of 1 m³ has been considered with packing inside the column occupying 0,5 m³.

To calculate $C_{P^{\circ}}$ for the tower vessel Equation 4.2 **Error! Reference source not found.** has been used. Results are reported in Table 4.32.

Cooling T	Type	Volume (m ³)	K1	K2	K3	C _P [°] (2001) €
1	Packed	1	3,4974	0,4485	0,1074	3143,403
2	Packed	1	3,4974	0,4485	0,1074	3143,403
3	Packed	1	3,4974	0,4485	0,1074	3143,403
4	Packed	1	3,4974	0,4485	0,1074	3143,403
5	Packed	1	3,4974	0,4485	0,1074	3143,403

Table 4.32 Cooling tower vessels C_P[°] estimation

The cooling towers work at ambient pressure and are made of carbon steel (base case condition FP=1, FM=1). To calculate C_{BM}, C_{BM(2022)}, C_{TM}, C_{GR}, Equation 4.5, Equation 4.6, Equation 4.7 **Error! Reference source not found.**, Equation 4.8 have been used respectively. Results are reported in Table 4.33.

Cooling T	B1	B2	CBM	CBM(2022)	CBM [°] (2022)	CTM	CGR €
1	2,25	1,82	12793,648	25780,651	25780,65	30421,16	43311,49
2	2,25	1,82	12793,648	25780,651	25780,65	30421,16	43311,49
3	2,25	1,82	12793,648	25780,651	25780,65	30421,16	43311,49
4	2,25	1,82	12793,648	25780,651	25780,65	30421,16	43311,49
5	2,25	1,82	12793,648	25780,651	25780,65	30421,16	43311,49

Table 4.33 Cooling tower vessels C_{BM}, C_{BM(2022)}, C_{TM}, C_{GR} estimation

To calculate C_P[°] for the tower internals Equation 4.2 has been used. Results are reported in Table 4.34.

Cooling T	Type	Volume (m ^{^3})	K1	K2	K3	C _P [°] (2001) €
1	Packed	0,5	2,4493	0,9744	0,0055	143,3754
2	Packed	0,5	2,4493	0,9744	0,0055	143,3754
3	Packed	0,5	2,4493	0,9744	0,0055	143,3754
4	Packed	0,5	2,4493	0,9744	0,0055	143,3754
5	Packed	0,5	2,4493	0,9744	0,0055	143,3754

Table 4.34 Cooling tower internals C_P[°] estimation

The tower packing material is plastic (FBM=1) and the working pressure is 1 atm (FP=1). To calculate C_{BM} the corresponding equation from Table 4.2 has been used.

To calculate $C_{BM(2022)}$, C_{TM} , C_{GR} , Equation 4.6, Equation 4.7, Equation 4.8 have been used respectively. Results are reported in Table 4.35.

Cooling T	FP	FBM	CBM	CBM(2022)	CBM°(2022)	CTM	CGR €
1	1	1	143,38	288,92	288,92	340,92	485,38
2	1	1	143,38	288,92	288,92	340,92	485,38
3	1	1	143,38	288,92	288,92	340,92	485,38
4	1	1	143,38	288,92	288,92	340,92	485,38
5	1	1	143,38	288,92	288,92	340,92	485,38

Table 4.35 Cooling tower internals C_{BM} , $C_{BM(2022)}$, C_{TM} , C_{GR} estimation

To calculate C_P° for the tower fans Equation 4.2 has been used. Results are reported in Table 4.36. To evaluate the fans flowrate the following equation has been used:

$$Q_{AIR} = \frac{\frac{m_w}{h_r^1 - h_r^2}}{\frac{3600 * \rho_{AIR}}{5}} \quad \text{Equation 4.14}$$

Where Q_{AIR} is the volumetric flowrate for each fan (in m^3/s), m_w is the mass of water evaporated in the cooling towers (in kg/h), h_{r1} is the humid ratio of the air exiting the cooling tower (100% relative humidity, 20.96 °C), h_{r2} is the humid ratio of the air entering the cooling tower (70% relative humidity, 25.00 °C). ρ_{AIR} is the density of air (1.225 kg/m^3).

The mass of water evaporated in the cooling towers can be found with the following equation:

$$m_w = (m_w^{TOT} c_{p_w} \Delta T) / \lambda_w^{30^\circ C} \quad \text{Equation 4.13}$$

Where m_w^{TOT} is the total mass of cooling water used in the plant (416.3e³ kg of water per hour), c_{p_w} is the specific heat of water (4.186 kJ/kg/K), ΔT is the temperature difference between the water at the inlet and at outlet of the cooling tower (5°C), and λ_w is the latent heat of evaporation for water at 30°C (2441.7 kJ/kg).

The total water evaporated is 3568.92 kg/h and the corresponding air flowrate to achieve such evaporation is 95.234 m^3/s of air per cooling tower.

Cooling T	Type	flowrate (m ³ /s)	K1	K2	K3	C _P [°] (2001) €
1	Centrifugal/radial	95,23	3,5391	-0,3533	0,4477	39175,64
2	Centrifugal/radial	95,23	3,5391	-0,3533	0,4477	39175,64
3	Centrifugal/radial	95,23	3,5391	-0,3533	0,4477	39175,64
4	Centrifugal/radial	95,23	3,5391	-0,3533	0,4477	39175,64
5	Centrifugal/radial	95,23	3,5391	-0,3533	0,4477	39175,64

Table 4.36 Cooling tower fans C_P[°] estimation

The fans work at ambient pressure conditions (FP=1). Carbon steel is the material of choice for the fans. To calculate C_{BM} the corresponding equation from Table 4.2 has been used. To calculate C_{BM(2022)}, C_{TM}, C_{GR}, Equation 4.6, Equation 4.7, Equation 4.8 **Error! Reference source not found.** have been used respectively. Results are reported in Table 4.37.

Cooling T	FP	FBM	CBM	CBM(2022)	CBM [°] (2022)	CTM	CGR €
1	1	3	117526,92	236830,07	78943,36	279459,488	318931,17
2	1	3	117526,92	236830,07	78943,36	279459,488	318931,17
3	1	3	117526,92	236830,07	78943,36	279459,488	318931,17
4	1	3	117526,92	236830,07	78943,36	279459,488	318931,17
5	1	3	117526,92	236830,07	78943,36	279459,488	318931,17

Table 4.37 Cooling tower fans C_{BM}, C_{BM(2022)}, C_{TM}, C_{GR} estimation

Lastly the cooling tower pump needed to circulate the utility cooling water through the plant needs to be considered. The power needed to operate the pump is given by:

$$Power = \frac{1}{\xi} V \Delta P \tag{Equation 4.14}$$

Where ξ is the pump efficiency (equal to 0.75), V is the volumetric flowrate (0.1157 m³/s) and ΔP is the pressure drop around the cooling loop plus the static head needed to pump the water to the top of the cooling tower (266.7 kPa have been considered).

To calculate C_P[°] for the tower pump Equation 4.2 has been used. Results are reported in Table 4.38.

Pump	Type	Power (kW)	K1	K2	K3	C _P [°] (2001) €
1	reciprocating	41,13	3,8696	0,3161	0,122	49851,63

Table 4.38 Cooling tower pump C_P[°] estimation

To calculate F_P Equation 4.4 has been used. Stainless steel is the material of choice for all the pumps in the plant. Results are reported in Table 4.39.

Pump	P(barG)	C1	C2	C3	FP	FM
1	2,6	0	0	0	1	2,4

Table 4.39 Cooling tower pump F_P and F_M estimation

To calculate C_{BM}, C_{BM(2022)}, C_{TM}, C_{GR}, Equation 4.5, Equation 4.6, Equation 4.7, Equation 4.8 have been used respectively. Results are reported in Table 4.40.

Pump	B1	B2	CBM	CBM(2022)	CBM [°] (2022)	CTM	CGR €
1	1,89	1,35	255738,87	515342,80	325479,7	608104,51	770844,34

Table 4.40 Cooling tower pump C_{BM}, C_{BM(2022)}, C_{TM}, C_{GR} estimation

4.2. Operating costs

Operating costs (or manufacturing costs) are the costs related to the day-to-day operation of a chemical plant. They can be divided into three categories: direct manufacturing costs, fixed manufacturing costs, general expenses.

Direct manufacturing costs are the principal expenses in a chemical plant. They change with production rate and are related to raw materials, waste treatments, utilities, operating labor, supervision, maintenance, operating supplies and patents and royalties.

Fixed manufacturing costs are independent with respect to the production rate. They include taxes, insurance and depreciation, all of which are charged even when the plant is not operating.

General expenses are related to business functions. They include management, sales (distribution and selling costs), financing and research. They may or may not vary in function of the production levels depending on the expense.

The sum of all these operating costs generates the cost of manufacture (COM). The cost of manufacture can be calculated with empirical formulas once five parameters are known: fixed capital investment (grassroot cost), cost of operating labor, cost of utilities, cost of waste treatment and cost of raw material.

4.2.1. Cost of operating labor

The cost of operating labor is directly correlated to the number of operators needed to operate the chemical plant. Equation 4.15 provides the number of operators per shift needed to run the plant.

$$N_{OL} = (6.29 + 31.7P^2 + 0.23N_{np})^{0.5} \quad \text{Equation 4.15}$$

Where P is the number of processing steps involving the handling of particulate solids, N_{np} is the number of processing steps that do not include particulate (compression, heating and cooling, mixing, reactions, separations). In the case of the acetic acid plant designed in this thesis work P is equal to 0 and N_{np} is given by the sum of compressors, towers, reactors, exchangers and it is equal to 38. Each operator can work 245 shifts per year (8-hour shifts, 5 time a week). The total number of shifts needed to operate the plant 24 hours a day for 365 days is 1095 shifts per year. This means that 4.5 operators are needed for each operator needed in the plant at any time. For the acetic acid plant, a total of 18 operators are hired. The wage for each operator is assumed to be 40000€. The cost of operating labor for the plant (C_{OL}) is given by multiplying the total number of operator times the wage. The result is 720000€/year.

4.2.2. Utility costs

Fuels (gas, oil, coal), electric power, steam, cooling water, process water, boiler feed water, inert gases, refrigeration are some of the most common utilities. The cost of utilities is governed by the market and is subject to fluctuations. For the acetic acid plant, the following utilities are needed:

- Electric power, needed for pumps and compressors
- Cooling water (25°C), needed in the heat exchangers and condensers of the plant
- Steam, needed in the process' heaters and reboilers. Steam is directly generated inside the plant and the costs of its production have already been taken into account in the capital costs and operating costs of the steam generating units.
- Biogas, needed to fuel the furnace of the reformer
- Refrigerant (glycolated water) used in the condenser of the methanol column, is produced inside the plant and the costs of its production have already been considered in the capital costs and operating costs of the heat pump.

The price per year has been calculated assuming 8000 working hours per year.

For electric power the cost of 0.165 €/kW/h has been considered (based on the average Italian price in 2021) [58]. Table 4.41 reports the costs generated by electric power consumption. To calculate the power consumed by the cooling tower fans the following equation has been used:

$$Power = \left(\frac{Q * \Delta P}{\xi} \right) 5 \quad \text{Equation 4.16}$$

Where Q is the volumetric flowrate for each fan (95.23 m³/s), ΔP is the pressure difference across the fan (assumed to be 250 Pa) and ξ is the fan efficiency (assumed to be 0.75).

Equipment	Power (kW)	€/year
K105	77,96	102907,2
K106	69,75	92070
K100	57,07	75332,4
K101	50,95	67254
K107	6,669	8803,08
K108	8,224	10855,68
K104	28,38	37461,6
K103	26,35	34782
K102	1,599	2110,68
K109	38,65	51018
P101	0,228	300,96
P102	0,05447	71,9004
P104	132,1	174372
P100	1,076	1420,32
P105	0,1327	175,164
P106	0,0006434	0,849288
P107	2,855	3768,6
COOLING TOWER PUMP	41,12623643	54286,63209
COOLING TOWER FANS	158,7236461	209515,2128

Table 4.41 Electric power costs estimation

For determining cooling water expenses, it is necessary to calculate the amount of water makeup needed to supply the cooling water loop. The makeup is calculated with the following equation:

$$W_{MU} = W_{tower} + W_{wind} + W_{BD} \quad \text{Equation 4.17}$$

Where W_{tower} is the water lost in the tower through evaporation (3568.92 kg/h), W_{wind} is the water lost through windage losses (assumed to be 0.3% of the water circulating) and W_{BD} is the water lost in the blowdown to avoid salt accumulation (assumed to be equal to the water lost through evaporation). The total makeup of water is equal to 8386,89 kg/h. the cost of water is assumed to be 2.5 €/m³ based on the average price of water in Italy for industrial operations [59]–[61]. The total cost of cooling water is 167737,81 €/year.

The cost related to the biogas used in the furnace is calculated taking into account the price of 0.162 €/m³ for biogas produced in Italy from maize [62]. A total of 291 m³/h of biogas are needed to fire the furnace. The total cost for biogas used in the furnace is 377265,6 €/year.

4.2.3. Raw material costs

The cost of raw materials can be easily computed once their price is known. In the acetic acid plant, the raw materials used are biogas, water, reforming catalyst, water-gas shift catalyst, methanol synthesis catalyst, acetic acid synthesis catalyst and propyl acetate.

For biogas price, it has been considered Italian biogas produced from maize [62].

For the reforming, water-gas shift, and methanol catalysts the assumption of replacing the catalytic bed each year has been made. The amount of catalyst needed has been calculated by multiplying the reactor volume occupied by catalyst times the catalyst density (3000 kg/m³ for reforming and WGS, 1500 kg/m³ for methanol copper zeolite catalyst) [21], [63], [64], [65].

The price for acetic acid synthesis catalyst has been calculated based on rhodium price. For the Monsanto process the rhodium species formed is RhCO₂I₂, its total molecular weight is 179 kg/kmol while pure rhodium molecular weight is 45 kg/kmol. Rhodium therefore accounts for 25.14 % of the total molecule weight. In the plant simulation the addition of 2 g/h of RhCO₂I₂ and 5 kg/h of CH₃I is needed resulting in 201.12 €/h of rhodium or 40.20 € per kg of total catalyst. A more conservative catalyst price of 50 €/kg has been selected.

Results for raw material costs estimation are reported in Table 4.42.

Raw material	m ³ /h or kg/year	€/nm ³ or €/kg	€/year
biogas	1052	0,162	1363392
reforming Cat.	4500	50	225000
WGS cat.	4500	50	225000
methanol Cat.	4500	120	540000
acetic acid cat.	40016	50	2000800
water	0,3192	2,5	6384
propyl acetate	81707,2	1,52	124292,9926

Table 4.42 Raw materials costs estimation. Biogas and water are expressed in m³/h and their price is expressed in €/nm³.

4.2.4. Waste treatment costs

Table 4.43 reports the costs for waste treatment

Type	m ³ /h or kg/h	€/nm ³ or €/kg	€/year
Wastewater	0,1306	0,056	58,5088
Waste liquid disposal	6,274	0,036	1806,912
Waste liquid disposal	1,156	0,036	332,928

Table 4.43 Waste treatment cost estimation. Wastewater is expressed in m³/h and its price is in €/nm³, waste liquid disposal is expressed in kg/h and its price is in €/kg

4.2.5. Cost of manufacture estimation

In order to estimate the cost of manufacture the following costs need to be taken into account (following “Chemical Engineering Cost Estimation” book [66]):

- Supervision costs. They are related to administration, engineering and support personnel and are assumed to be equal to 10% of the cost of operating labor
- Maintenance costs. They are associated with the cost of materials and labor associated with maintenance and repair and are assumed to be equal to 6% of the fixed capital investment
- Supplies costs. They are associated to supplies not considered raw materials and are assumed to be equal to 1% of the fixed capital investment
- Depreciation costs. They are operating expenses for tax purposes and are assumed to be equal to 10% of the fixed capital investment
- Local taxes. They are costs related to property taxes and are assumed to be equal to 1% of the fixed capital investment
- Insurance costs are assumed to be equal to 1% of the fixed capital investment
- Plant overhead costs. They are related to auxiliary facilities supporting the manufacturing process (like medical service, cafeteria, recreation facilities, accounting services and others) and are assumed to be equal to 60% of the operating labor
- Sales expenses. They are cost related to the product distribution and marketing and are assumed to be equal to 10% of the manufacturing cost
- Administration expenses. They are related to management and are assumed to be equal to 1% of the fixed capital investment

4.3. Cash flow diagram and economic assessment

In Table 4.44 are reported the values for the fixed capital investment (FCI), the cost of operating labor (C_{OL}), the cost of utilities (C_{UT}), the cost for waste treatment (C_{WT}), the cost of raw materials (C_{RM}), the total cost of manufacture (COM) and the total cost of manufacture without depreciation (COM_d).

Where FCI has been computed with Equation 4.9, C_{UT} has been computed summing each term of the last column of Table 4.41 with the cost of cooling water and the cost of biogas needed for the furnace, C_{WT} has been computed summing each term of the last column of Table 4.43 and C_{RM} has been computed summing each term of the last column of of Table 4.42.

Costs	€/year
FCI	19277413,89
C_{OL}	720000
C_{UT}	1471509,69
C_{WT}	2198,35
C_{RM}	4484868,99
COM	12139510,78
COM_d	10018995,26

Table 4.44 Plant estimated costs

The revenue provided by the plant is related to the market price of glacial acetic acid. The price of acetic acid in the time period between 2021-2022 has seen a lot of fluctuation and therefore a mean value of 1800 €/ton has been taken into account for the European market [67]. The plant can produce 1008 kg/h of acetic acid. Table 4.45 reports the plant revenues.

Acetic acid price (€/ton)	Acetic acid production (kg/h)	Revenues (€/year)
1800	1008	14515200

Table 4.45 Plant revenues

With the data provided the cash-flow diagram of the acetic acid plant can be produced. The following assumptions have been made:

- Two years are needed to build the plant
- In the first year 70% of FCI is spent
- In the second year the remaining 30% of FCI is spent
- A working capital (WC) equal to the 20% of FCI is needed to start the plant operations and it is recovered at the end of the plant operations
- The plant works for 10 years after the two years of building
- A discount rate of 5% is taken into account
- Depreciation is calculated for three different cases that are straight line depreciation (SL), double declining balance depreciation (ddb) and sum of the years digit depreciation (soyd)
- A taxation equal to 50% of the net profit is taken into account
- The plant salvage value and the value of the land are not taken into consideration

4.3.1. Straight line depreciation

To calculate depreciation with the straight-line approach the following equation has been used:

$$d_k^{SL} = \frac{FCI - S}{n} \quad \text{Equation 4.18}$$

Where FCI is the fixed capital investment, S is the salvage value (equal to zero in this evaluation) and n are the number of years in which depreciation is allowed (10 years for the acetic acid plant).

The cash flow for the first year is equal to 70% of FCI. For the second year it is equal to 30% of FCI plus the value of the working capital (WC is equal to 20% of FCI).

For the following 10 years the cash flow is calculated through Equation 4.19.

$$CF_i = (R - COM_d - d_k^{SL})(1 - T) + d_k^{SL} \quad \text{Equation 4.19}$$

Where CF_i is the cash flow at the i^{th} year, R are the revenues, COM_d is the cost of manufacture without depreciation, d_k^{SL} is the straight-line depreciation, T is the taxation rate (equal to 0.5). At the end of the last year the working capital is recovered. The cumulative cash flow is calculated through the following equation:

$$CCF_n = \sum_{i=1}^n CF_i \quad \text{Equation 4.20}$$

The discounted cash flow takes into account the value of the money invested related to time (for each year the cash flow value is discounted back to time zero) and is calculate through Equation 4.21 **Error! Reference source not found.:**

$$DCF_i = \frac{CF_i}{(1 + \text{discount rate})^i} \quad \text{Equation 4.21}$$

Where DCF_i is the discounted cash flow at i^{th} year CF_i is the non-discounted cash flow at i^{th} year. The discount rate is assumed to be 5%.

The results obtained are reported in Table 4.466.

year	Cash Flow (€)	Cumulative cash flow (€)	discounted cash flow (€)	cumulative discounted cash flow (€)
0	0	0	0	0
1	-13494189,73	-13494189,73	-12851609,26	-12851609,26
2	-5783224,168	-19277413,89	-5245554,801	-18097164,06
2	-3855482,779	-23132896,67	-3497036,534	-21594200,6
3	3211973,067	-19920923,61	2774623,101	-18819577,5
4	3211973,067	-16708950,54	2642498,191	-16177079,31
5	3211973,067	-13496977,47	2516664,944	-13660414,36
6	3211973,067	-10285004,4	2396823,756	-11263590,61
7	3211973,067	-7073031,338	2282689,291	-8980901,314
8	3211973,067	-3861058,271	2173989,801	-6806911,513
9	3211973,067	-649085,2041	2070466,478	-4736445,035
10	3211973,067	2562887,863	1971872,836	-2764572,199
11	3211973,067	5774860,93	1877974,129	-886598,07
12	3211973,067	8986833,996	1788546,79	901948,7198
12	3855482,779	12842316,78	2146877,076	3048825,796

Table 4.46 Cash flow and discounted cash flow for the straight-line depreciation case

A list of indicators are calculated to determine the profitability of the plant:

- Payback period (PBP). It is the time needed after the startup to recover the fixed capital investment. Shorter PBP are related to more profitable projects.
- Cumulative cash position (CCP). CCP is the worth of the project at the end of its life (equal to the cumulative cash flow at the end of operations). The higher CCP is, the more profitable the project is.

- Cumulative cash ratio (CCR). It is equal to the sum of all the positive cash flows divided by the absolute value of the sum of all the negative cash flows. Projects with CCR greater than 1 are potentially profitable.
- Rate of return on investment (ROROI). It represents the non-discounted rate at which money is made from a fixed capital investment and is calculated dividing the average annual net profit times the fixed capital investment. Higher ROROI are related to more profitable projects.
- Discounted payback period (DPBP). It is the time needed after the startup to recover the fixed capital investment considering the value time of money.
- Net present value (NPV). It is the equivalent of cumulative cash position when the value time of money is considered.
- Present value ratio (PVR). It is the ratio between the sum of the positive discounted cash flows and the absolute value of the negative discounted cash flows. A value of 1 represents a break-even situation, value greater than 1 represents profitable situations.
- Discounted cash flow rate of return (DCFROR). It is the interest rate at which all the cash flows must be discounted in order for the net present value of the project to be equal to zero.

The values for all the listed indicators are reported in Table 4.477.

PBP (years)	CCP (€)	CCR	ROROI	DPBP (years)	NPV (€)	PVR	DCFROR
6,0017	12842316,78	1,555	0,1866	8,238	3.048.825,80	1,141	0,073

Table 4.47 Profitability indicators for the straight-line depreciation case

The cash flow diagram of the plant is reported in Figure 4.1.

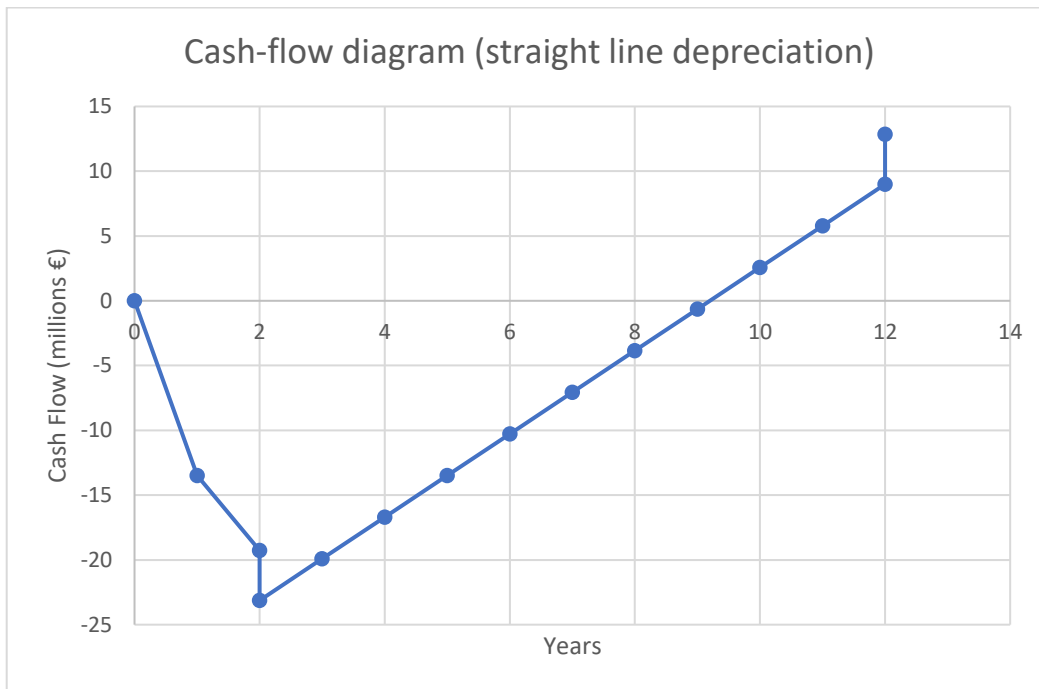


Figure 4.1 Plant cash flow diagram for straight-line depreciation

4.3.2. Sum of the years digit depreciation

To calculate depreciation with the sum of the years digit approach the following equation has been used:

$$d_k^{SOYD} = \frac{(n + 1 - k)(FCI - S)}{\frac{n}{2}(n + 1)} \quad \text{Equation 4.22}$$

Where FCI is the fixed capital investment, S is the salvage value (equal to zero in this evaluation), n is the number of years in which the depreciation is allowed (10 years for the acetic acid plant) and k is the year considered.

The cash flow for the first year is equal to 70% of FCI. For the second year it is equal to 30% of FCI plus the value of the working capital (WC is equal to 20% of FCI).

For the following 10 years the cash flow is calculated through Equation 4.23.

$$CF_i = (R - COM_d - d_k^{SOYD})(1 - T) + d_k^{SOYD} \quad \text{Equation 4.23}$$

Where CF_i is the cash flow at the i^{th} year, R are the revenues, COM_d is the cost of manufacture without depreciation, d_k^{SOYD} is the sum of the years digit depreciation, T is the taxation rate (equal to 0.5).

At the end of the last year the working capital is recovered. The cumulative cash flow is calculated through Equation 4.20 **Error! Reference source not found..**

The results obtained are reported in Table 4.488.

year	Cash Flow (€)	Cumulative cash flow (€)	discounted cash flow (€)	cumulative discounted cash flow (€)
0	0	0	0	0
1	-13494189,73	-13494189,73	-12851609,26	-12851609,26
2	-5783224,168	-19277413,89	-5245554,801	-18097164,06
2	-3855482,779	-23132896,67	-3497036,534	-21594200,6
3	4000594,544	-19132302,13	3455863,984	-18138336,61
4	3825345,327	-15306956,8	3147121,068	-14991215,55
5	3650096,11	-11656860,69	2859945,812	-12131269,73
6	3474846,893	-8182013,798	2592984,252	-9538285,481
7	3299597,675	-4882416,123	2344962,465	-7193323,016
8	3124348,458	-1758067,664	2114682,017	-5078640,999
9	2949099,241	1191031,577	1901015,666	-3177625,334
10	2773850,024	3964881,6	1702903,293	-1474722,041
11	2598600,807	6563482,407	1519348,072	44626,03165
12	2423351,589	8986833,996	1349412,842	1394038,874
12	4168721,303	13155555,3	2321300,007	3715338,882

Table 4.48 Cash flow and discounted cash flow for the sum of the years digit depreciation case

As in the previous case the profitability indicators are calculated and reported in Table 4.49.

PBP (years)	CCP (€)	CCR	ROROI	DPBP (years)	NPV (€)	PVR	DCFROR
5,3287	13155555,3	1,56869	0,1882	7,50551	3.715.338,88	1,1721	0,08008

Table 4.49 Profitability indicators for the sum of the years digit depreciation case

The cash flow diagram of the plant is reported in Figure 4.2.

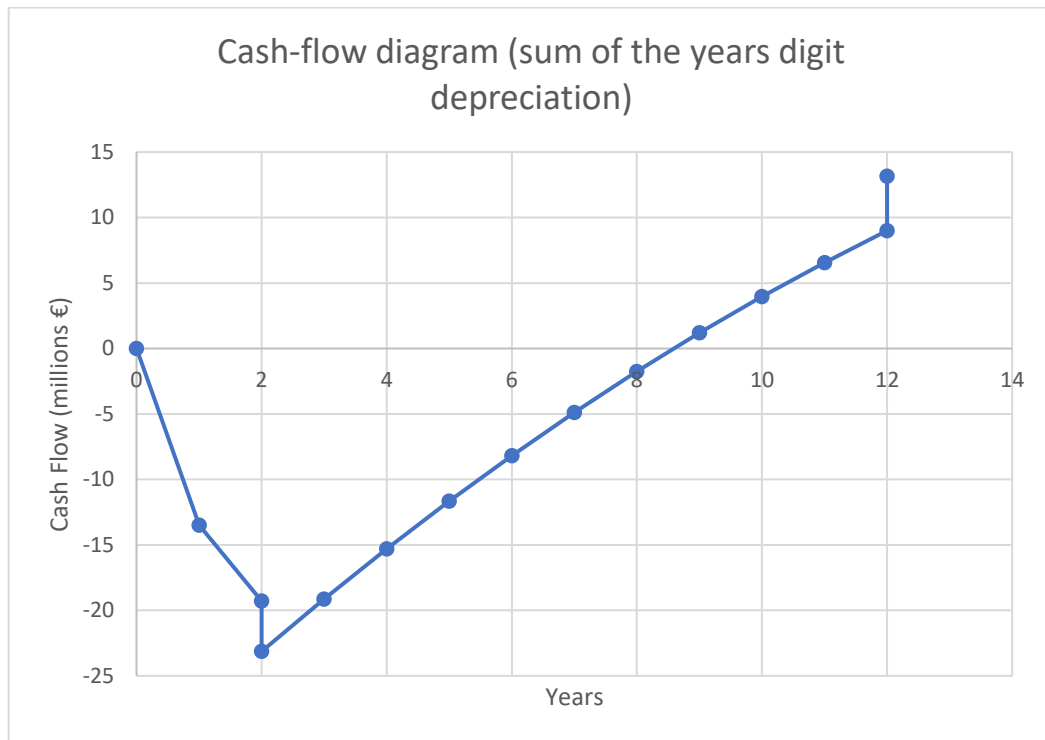


Figure 4.2 Plant cash flow diagram for sum of the years digit depreciation

4.3.3. Double declining balance depreciation

To calculate depreciation with the double declining balance approach the following equation has been used:

$$d_k^{DDB} = \frac{2}{n} \left(FCI - \sum_{j=0}^{j=k-1} d_j \right) \quad \text{Equation 4.24}$$

Where FCI is the fixed capital investment, n is the number of years in which the depreciation is allowed (10 years for the acetic acid plant), d_j is the depreciation of the year before the considered one and k is the year considered.

The cash flow for the first year is equal to 70% of FCI. For the second year it is equal to 30% of FCI plus the value of the working capital (WC is equal to 20% of FCI).

For the following 10 years the cash flow is calculated through Equation 4.25.

$$CF_i = (R - COM_d - d_k^{DDB})(1 - T) + d_k^{DDB} \quad \text{Equation 4.25}$$

Where CF_i is the cash flow at the i^{th} year, R are the revenues, COM_d is the cost of manufacture without depreciation, d_kDDB is the double declining balance depreciation, T is the taxation rate (equal to 0.5).

At the end of the last year the working capital is recovered. The cumulative cash flow is calculated through Equation 4.20 **Error! Reference source not found..**

The results obtained are reported in Table 4.50.

year	Cash Flow (€)	Cumulative cash flow (€)	discounted cash flow (€)	cumulative discounted cash flow (€)
0	0	0	0	0
1	-13494189,73	-13494189,73	-12851609,26	-12851609,26
2	-5783224,168	-19277413,89	-5245554,801	-18097164,06
2	-3855482,779	-23132896,67	-3497036,534	-21594200,6
3	4175843,762	-18957052,91	3607250,847	-17986949,75
4	3790295,484	-15166757,43	3118285,475	-14868664,28
5	3481856,861	-11684900,57	2728125,959	-12140538,32
6	3235105,964	-8449794,602	2414085,88	-9726452,437
7	3037705,245	-5412089,357	2158840,404	-7567612,033
8	2879784,671	-2532304,686	1949151,619	-5618460,414
9	2753448,211	221143,5249	1774897,267	-3843563,147
10	2652379,043	2873522,568	1628330,648	-2215232,499
11	2571523,709	5445046,277	1503516,654	-711715,8445
12	2506839,442	7951885,719	1395902,002	684186,1579
12	4168721,303	12120607,02	2321300,007	3005486,165

Table 4.50 Cash flow and discounted cash flow for the double declining line depreciation case

As in the previous case the profitability indicators are calculated and reported in Table 4.51.

PBP (years)	CCP (€)	CCR	ROROI	DPBP (years)	NPV (€)	PVR	DCFRROR
5,5405	12120607,02	1,52396	0,1829	7,93763	3.005.486,17	1,1392	0,07462

Table 4.51 Profitability indicators for the double declining line depreciation case

The cash flow diagram of the plant is reported in Figure 4.3.

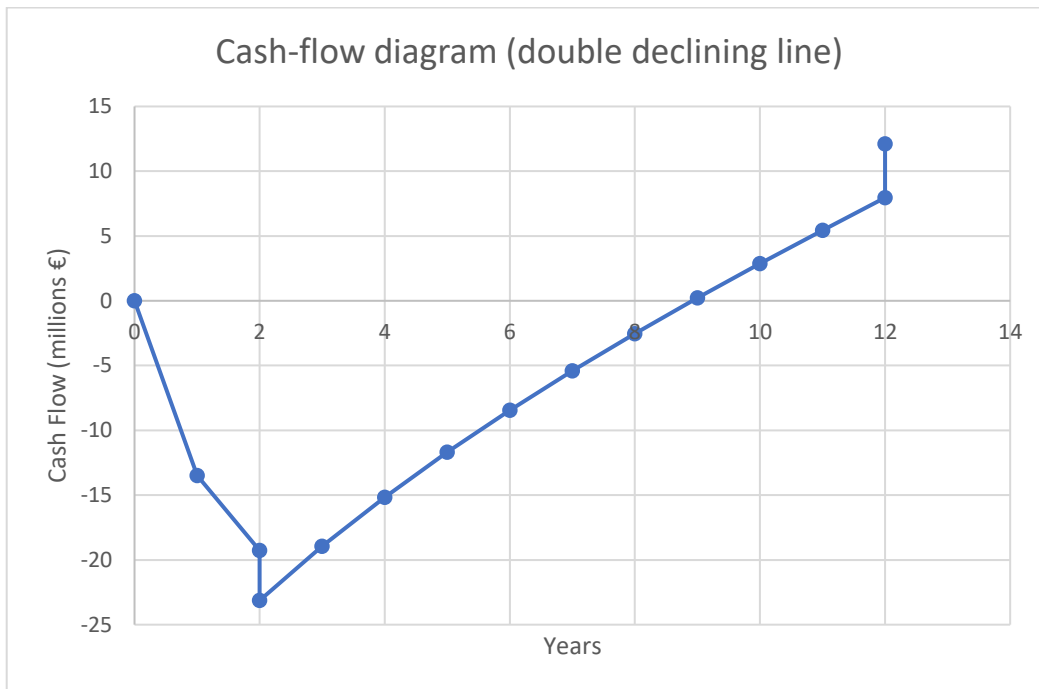


Figure 4.3 Plant cash flow diagram for sum of the double declining line depreciation

4.3.4. Case comparison

The three cases analyzed are all profitable as can be seen from their profitability indicators. The payback period (discounted and non-discounted) is shorter than the estimated plant lifespan. Cumulative cash position and net present values are positive, indicating that the project is profitable. Both cumulative cash ratio and present value ratio are greater than 1.

The profitability indicators are compared in Table 4.52. As can be seen, the sum of the years digit depreciation case seems to be the more profitable one.

case	PBP (years)	CCP (€)	CCR	ROROI	DPBP (years)	NPV (€)	PVR	DCFRO R
SL	6,0017	12842316,78	1,555	0,1866	8,238	3.048.825,80	1,141	0,073
SOYD	5,3287	13155555,3	1,569	0,1882	7,506	3.715.338,88	1,172	0,0801
DDL	5,5405	12120607,02	1,524	0,1829	7,938	3.005.486,17	1,139	0,0746

Table 4.52 Profitability indicators comparison

The sum of the years digit depreciation case has overall better profitability indicators. It is the case with the lowest payback period (both discounted and non-discounted) and the highest end-life value (highest CCP and NPV). The straight-

line depreciation case and double declining line depreciation case are similar with the former having longer payback periods but higher CCP and NPV than the latter.

The cash flow diagrams for the three cases are reported and compared in Figure 4.4

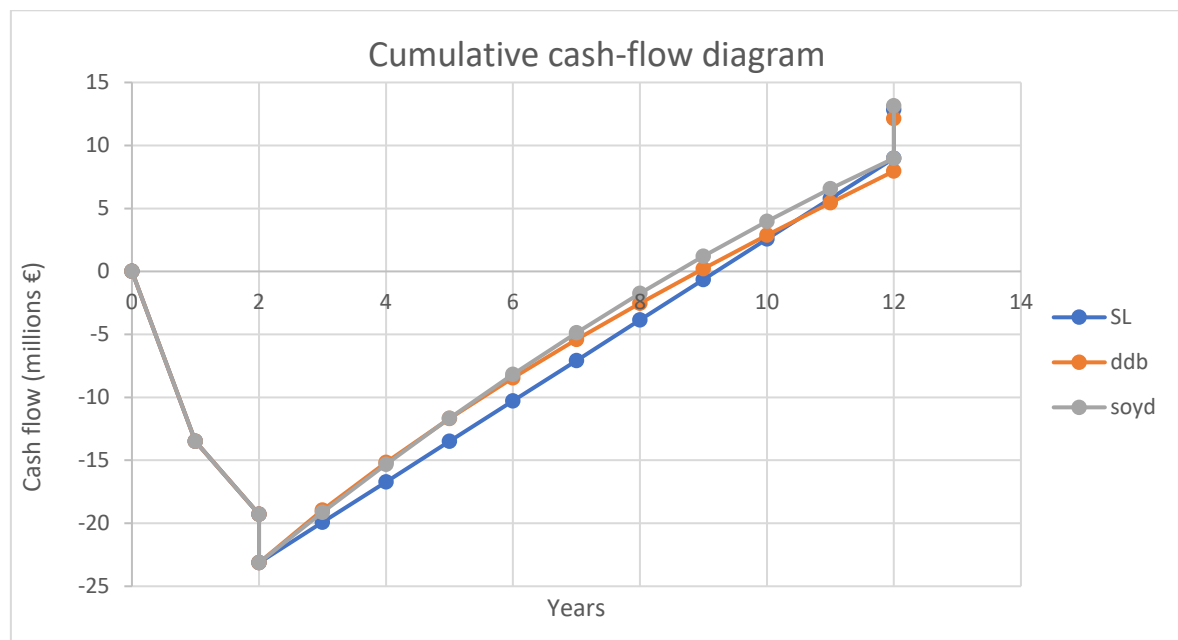


Figure 4.4 Cash flow diagrams comparison

4.3.5. Risk analysis

In order to better assess the profitability of the project, a risk analysis based on Monte Carlo method has been performed. The Monte Carlo method relies on random sampling based on a probability distribution and it is used to obtain numerical results. Through Monte Carlo risk analysis several future scenarios can be randomly generated. A cumulative probability distribution of a chosen profitability indicator can then be generated.

Two parameters have been chosen as random variables in this risk analysis: the price of the produced good (acetic acid) and the operating costs of the plant.

For the price of acetic acid a variation from -50% to +20% on the initial price has been considered over the 10 years of plant operations. Each year starting from the plant startup the price of acetic acid is randomly changed from -5% to +2% compared with the price of acetic acid of the previous year. The probability distribution chosen is the uniform distribution (each value from -5% to +2% has the same probability to be drawn).

For the operating costs a variation from -25% to +50% on the initial value of operating costs has been considered over the 10 years of plant operations. Each year starting from the plant startup the value of operating costs randomly changed from -2.5% to +5% compared with the value of operating costs of the previous year. The probability distribution chosen is the uniform distribution.

The chosen profitability indicators are the cumulative cash position (CCP) and the net present value of the plant (NPV).

The following algorithm developed with Matlab® has been used to calculate the random values of revenues and operating costs and to compute the cumulative cash position and the net present values of each of the 1000 scenarios generated. The base case scenario chosen is the straight-line depreciation case. The utilization of straight-line depreciation greatly simplifies the algorithm still offering valuable results.

Algorithm 1 Monte Carlo risk analysis

```

1:
2:   for z=1:1000
3:     R0=14515200; %revenues in base case scenario
4:     M0=10018995.26; %operating costs in base case scenario
5:     FCI=19277413.89; %fixed capital investment
6:     DEP=FCI/10; %straight-line depreciation
7:     CDCF1=-21594200.6; %cumulative discounted cash flow at the year in
      which the plant starts operating
8:     DCFWC=2146877.076; %discounted cash flow of working capital in the 10th
      year
9:     %randomized revenues for each year
10:    R1(z)=R0*(rand*(-0.05-0.02)+0.02)+R0;
11:    R2(z)=R0*(rand*(-0.05-0.02)+0.02)+R1(z);
12:    R3(z)=R0*(rand*(-0.05-0.02)+0.02)+R2(z);
13:    R4(z)=R0*(rand*(-0.05-0.02)+0.02)+R3(z);
14:    R5(z)=R0*(rand*(-0.05-0.02)+0.02)+R4(z);
15:    R6(z)=R0*(rand*(-0.05-0.02)+0.02)+R5(z);
16:    R7(z)=R0*(rand*(-0.05-0.02)+0.02)+R6(z);
17:    R8(z)=R0*(rand*(-0.05-0.02)+0.02)+R7(z);
18:    R9(z)=R0*(rand*(-0.05-0.02)+0.02)+R8(z);
19:    R10(z)=R0*(rand*(-0.05-0.02)+0.02)+R9(z);
20:    % randomized operating costs for each year
21:    M1(z)=M0*(rand*(-0.025-0.05)+0.05)+M0;
22:    M2(z)=M0*(rand*(-0.025-0.05)+0.05)+M1(z);
23:    M3(z)=M0*(rand*(-0.025-0.05)+0.05)+M2(z);

```

```

24: M4(z)=M0*(rand*(-0.025-0.05)+0.05)+M3(z);
25: M5(z)=M0*(rand*(-0.025-0.05)+0.05)+M4(z);
26: M6(z)=M0*(rand*(-0.025-0.05)+0.05)+M5(z);
27: M7(z)=M0*(rand*(-0.025-0.05)+0.05)+M6(z);
28: M8(z)=M0*(rand*(-0.025-0.05)+0.05)+M7(z);
29: M9(z)=M0*(rand*(-0.025-0.05)+0.05)+M8(z);
30: M10(z)=M0*(rand*(-0.025-0.05)+0.05)+M9(z);
31: %cash flow for each year
32: CF1(z)=(R1(z)-M1(z)-DEP)*0.5+DEP;
33: CF2(z)=(R2(z)-M2(z)-DEP)*0.5+DEP;
34: CF3(z)=(R3(z)-M3(z)-DEP)*0.5+DEP;
35: CF4(z)=(R4(z)-M4(z)-DEP)*0.5+DEP;
36: CF5(z)=(R5(z)-M5(z)-DEP)*0.5+DEP;
37: CF6(z)=(R6(z)-M6(z)-DEP)*0.5+DEP;
38: CF7(z)=(R7(z)-M7(z)-DEP)*0.5+DEP;
39: CF8(z)=(R8(z)-M8(z)-DEP)*0.5+DEP;
40: CF9(z)=(R9(z)-M9(z)-DEP)*0.5+DEP;
41: CF10(z)=(R10(z)-M10(z)-DEP)*0.5+DEP;
42: %discounted cash flow for each year
43: DCF1(z)=CF1(z)/(1.05^3);
44: DCF2(z)=CF2(z)/(1.05^4);
45: DCF3(z)=CF3(z)/(1.05^5);
46: DCF4(z)=CF4(z)/(1.05^6);
47: DCF5(z)=CF5(z)/(1.05^7);
48: DCF6(z)=CF6(z)/(1.05^8);
49: DCF7(z)=CF7(z)/(1.05^9);
50: DCF8(z)=CF8(z)/(1.05^10);
51: DCF9(z)=CF9(z)/(1.05^11);
52: DCF10(z)=CF10(z)/(1.05^12);
53: %cumulative cash position and net present value
54: CCF(z)= -
    FCI+CF1(z)+CF2(z)+CF3(z)+CF4(z)+CF5(z)+CF6(z)+CF7(z)+CF8(z)+CF9(z)
    +CF10(z);
55: NPV(z)=CDCF1+DCF1(z)+DCF2(z)+DCF3(z)+DCF4(z)+DCF5(z)+DCF6(z)+
    DCF7(z)+DCF8(z)+DCF9(z)+DCF10(z)+DCFWC;
56: end

```

Figure 4.5 shows the cumulative probability of the cumulative cash flow position. As already mentioned, CCP is an indicator of the worth of the project at the end of its life. The graph shows that in 17% of the generated scenarios the plant does not reach the break-even point. Only 31.3% of the scenarios present CCP higher than 5 millions € (almost $\frac{1}{4}$ of the fixed capital investment). Only 0.1% of the scenarios generated presents CCP higher than the base case.

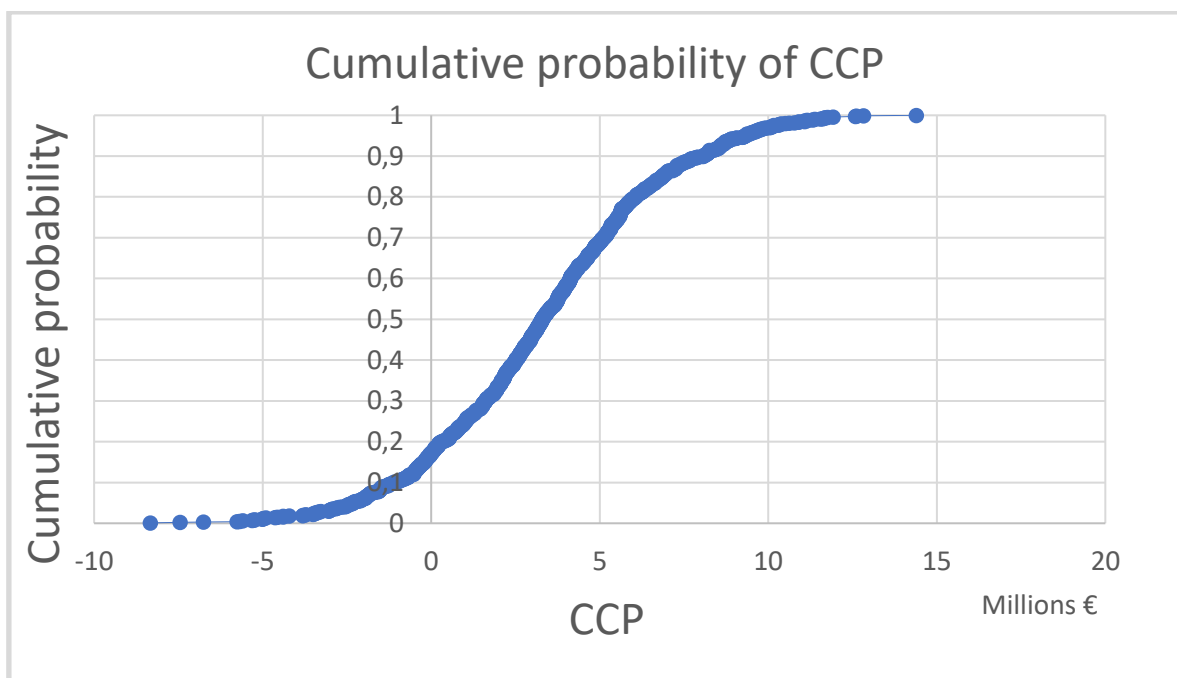


Figure 4.5 Cumulative cash position cumulative probability distribution

Figure 4.6 shows the cumulative probability distribution for the net present values calculated in the 1000 scenarios. As can be seen 90.1% of the scenarios generated have negative net present values at the end of the plant operations. Only 9.9% of the scenarios generated have positive net present values after 10 years and only 0.2% of the generated scenarios have net present values greater than the base case.

The risk analysis carried out suggests that the project risk is high and therefore its realization should be considered carefully. This is especially clear when the discounted profitability indicator is considered (only 9.9% of the scenarios present a positive NPV).

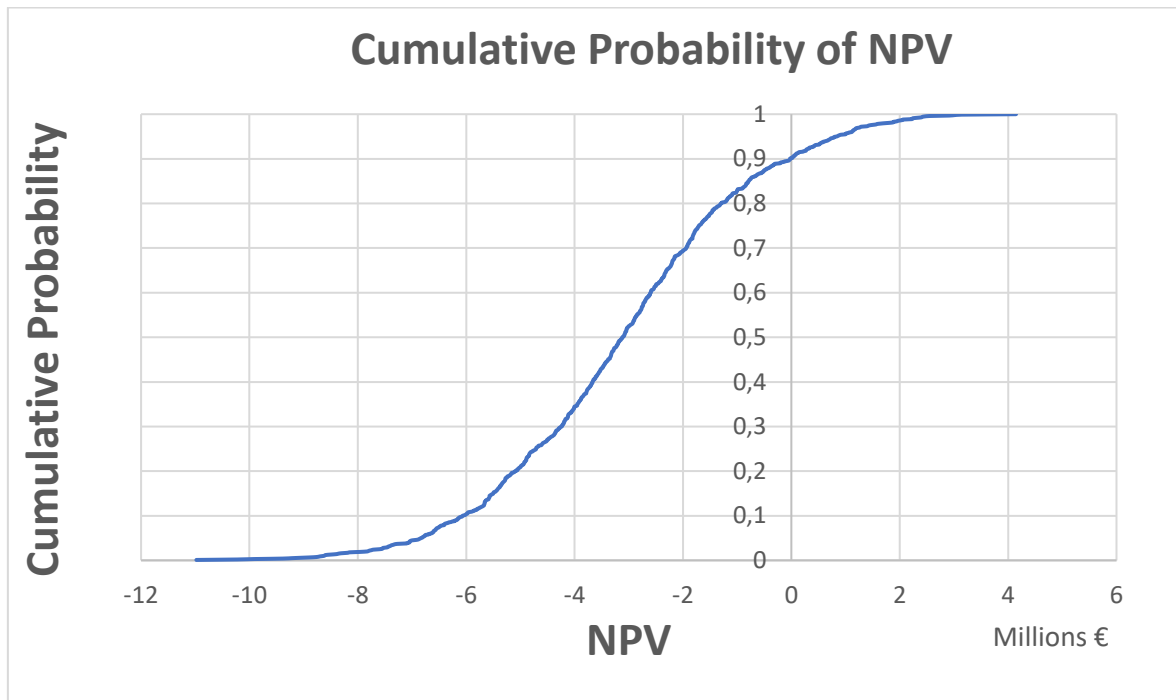


Figure 4.6 net present value cumulative probability distribution

5 Conclusions

This thesis work has provided a possible design for a biogas based acetic acid synthesis plant. The main advantage related to the realization of aforementioned plant is the possibility to convert a renewable and easily available raw material like biogas into a valuable chemical product, integrating the production of acetic acid in the circular economy. The economic evaluation that has been carried out suggests that the project is economically viable according to the evaluated indicators (payback period, cumulative cash flow position, net present value and others). A deeper analysis using the Monte Carlo method, however, shows that the risks correlated to the project are high as the probability of a negative net present value is much greater than that of a positive one. Variations in the price of the produced good, sales volume, raw material availability and price, and inflation are the main factors contributing to risk. In the case of the designed plant the main risk factors considered have been the price of acetic acid and the manufacturing costs (mainly related to raw materials price and costs of utilities like biogas and electric power). The two factors considered are characterized by high variations in short periods of time. An example of this variations is given by the rise in price of gas and electrical power occurred after the outbreak of the Ukrainian war, leading to a general crisis in the manufacturing sector. It is also important to notice that the performed economic analysis is strongly influenced by socio-economical and geopolitical factors (covid-19 pandemic and Ukrainian war outbreak), and therefore is subjected to a certain degree of uncertainty.

Two main possibilities exist in order to reduce the plant's economic risks.

The first one is to implement new and cheaper production processes. In the acetic acid production section of the plant, for example, a costly rhodium catalyst is utilized. Implementing a better recovery system for the catalyst or using a different catalyst (like the iridium catalyst of the Cativa process) could reduce the manufacturing costs. Reduced manufacturing costs has a direct positive impact on the project profitability, reducing the overall risks related to the plant investment.

A second possibility is represented by government incentives. As for the case of biogas production, government incentives (like reduced taxation) could in principle

make the production of acetic acid from biogas more profitable, reducing the plant payback period and increasing its net present value.

In conclusion, the production of acetic acid from biogas is a promising technology for the future, especially in the perspective of a green circular economy, but its implementation seems economically non-convenient when compared with traditional hydrocarbon-based production.

Bibliography

- [1] *Ullmann's Encyclopedia of Industrial Chemistry*, 6th ed. Weinheim, Germany: Wiley-VCH, 2005.
- [2] "Vinegar." <https://en.wikipedia.org/wiki/Vinegar> (accessed Oct. 07, 2022).
- [3] "acetic acid." <https://www.encyclopedia.com/science-and-technology/chemistry/organic-chemistry/acetic-acid#:~:text=The%20first%20person%20to%20extract,vinegar%20in%201700%20by%20distillation.> (accessed Oct. 07, 2022).
- [4] "Acetic Acid Market: Global Industry Trends, Share, Size, Growth, Opportunity and Forecast 2022-202." <https://www.imarcgroup.com/acetic-acid-technical-material-market-report> (accessed Oct. 06, 2022).
- [5] "Acetic Acid Market Size, Share & COVID-19 Impact Analysys, By Applications (Vinyl Acetate Monomer (VAM), Purified Terephthalic Acid (PTA), Ester Solvents, Acetic Anhydride, Others), and Regional Forecast, 2021-2028." <https://www.fortunebusinessinsights.com/acetic-acid-market-103386> (accessed Oct. 06, 2022).
- [6] Khevna Shah, "Acetic Acid: Overview & Market Outlook," 2014.
- [7] "Acetic Acid Market size worth \$ 8.48 Billion, Globally, by 2028 at 2.62% CAGR: Verified Market Research®." <https://www.bloomberg.com/press-releases/2022-05-30/acetic-acid-market-size-worth-8-48-billion-globally-by-2028-at-2-62-cagr-verified-market-research> (accessed Oct. 06, 2022).
- [8] Zhe Lyu, Nana Shao, Taiwo Akinyemi, and William B. Whitman, "Methanogenesis," 2018.
- [9] P. G. Kougiyas and I. Angelidaki, "Biogas and its opportunities—A review," *Front Environ Sci Eng*, vol. 12, no. 3, Jun. 2018, doi: 10.1007/s11783-018-1037-8.
- [10] P. Weiland, "Biogas production: Current state and perspectives," *Applied Microbiology and Biotechnology*, vol. 85, no. 4. Springer Verlag, pp. 849–860, 2010. doi: 10.1007/s00253-009-2246-7.
- [11] R. Borja, "2.55 Biogas Production," 2011.

- [12] S. Achinas, V. Achinas, and G. J. W. Euverink, "A Technological Overview of Biogas Production from Biowaste," *Engineering*, vol. 3, no. 3, pp. 299–307, Jun. 2017, doi: 10.1016/J.ENG.2017.03.002.
- [13] "Outlook for biogas and Prospects for organic growth World Energy Outlook Special Report biomethane." Accessed: Nov. 18, 2022. [Online]. Available: <https://www.iea.org/reports/outlook-for-biogas-and-biomethane-prospects-for-organic-growth>
- [14] S. Achinas, V. Achinas, and G. J. W. Euverink, "A Technological Overview of Biogas Production from Biowaste," *Engineering*, vol. 3, no. 3, pp. 299–307, Jun. 2017, doi: 10.1016/J.ENG.2017.03.002.
- [15] M. Torrijos, "State of Development of Biogas Production in Europe," *Procedia Environ Sci*, vol. 35, pp. 881–889, 2016, doi: 10.1016/j.proenv.2016.07.043.
- [16] C. Tricase and M. Lombardi, "State of the art and prospects of Italian biogas production from animal sewage: Technical-economic considerations," *Renewable Energy*, vol. 34, no. 3, pp. 477–485, Mar. 2009. doi: 10.1016/j.renene.2008.06.013.
- [17] D. J. Wilhelm, D. R. Simbeck, A. D. Karp, and R. L. Dickenson, "Syngas production for gas-to-liquids applications: technologies, issues and outlook q," 2001. [Online]. Available: www.elsevier.com/locate/fuproc
- [18] J. R. Rostrup-Nielsen, "New aspects of syngas production and use," 2000.
- [19] I. Dybkjx, "Tubular reforming and autothermal reforming of natural gas-an overview of available processes," ELSEVIER, 1995.
- [20] S. A. Ghoneim, R. A. El-Salamony, and S. A. El-Temtamy, "Review on Innovative Catalytic Reforming of Natural Gas to Syngas," *World Journal of Engineering and Technology*, vol. 04, no. 01, pp. 116–139, 2016, doi: 10.4236/wjet.2016.41011.
- [21] R. M. Swanson, A. Platon, J. A. Satrio, and R. C. Brown, "Techno-economic analysis of biomass-to-liquids production based on gasification," *Fuel*, vol. 89, no. SUPPL. 1, Nov. 2010, doi: 10.1016/j.fuel.2010.07.027.
- [22] S. A. Al-Sayari, "Recent Developments in the Partial Oxidation of Methane to Syngas," 2013.
- [23] S. S. Bharadwaj and L. D. Schmidt, "Catalytic partial oxidation of natural gas to syngas*," ELSEVIER, 1995.
- [24] C. Wang *et al.*, "Recent advances during CH₄ dry reforming for syngas production: A mini review," *International Journal of Hydrogen Energy*, vol. 46,

- no. 7. Elsevier Ltd, pp. 5852–5874, Jan. 27, 2021. doi: 10.1016/j.ijhydene.2020.10.240.
- [25] F. M. Baena-Moreno, D. Sebastia-Saez, L. Pastor-Pérez, and T. R. Reina, “Analysis of the potential for biogas upgrading to syngas via catalytic reforming in the United Kingdom,” *Renewable and Sustainable Energy Reviews*, vol. 144, Jul. 2021, doi: 10.1016/j.rser.2021.110939.
- [26] X. Zhao, B. Joseph, J. Kuhn, and S. Ozcan, “iScience Review Biogas Reforming to Syngas: A Review”, doi: 10.1016/j.isci.
- [27] B. Hernández and M. Martín, “Optimal Process Operation for Biogas Reforming to Methanol: Effects of Dry Reforming and Biogas Composition,” *Ind Eng Chem Res*, vol. 55, no. 23, pp. 6677–6685, Jun. 2016, doi: 10.1021/acs.iecr.6b01044.
- [28] U. S. Mohanty, M. Ali, M. R. Azhar, A. Al-Yaseri, A. Keshavarz, and S. Iglauer, “Current advances in syngas (CO + H₂) production through bi-reforming of methane using various catalysts: A review,” *International Journal of Hydrogen Energy*, vol. 46, no. 65. Elsevier Ltd, pp. 32809–32845, Sep. 21, 2021. doi: 10.1016/j.ijhydene.2021.07.097.
- [29] G. Bozzano and F. Manenti, “Efficient methanol synthesis: Perspectives, technologies and optimization strategies,” *Progress in Energy and Combustion Science*, vol. 56. Elsevier Ltd, pp. 71–105, Sep. 01, 2016. doi: 10.1016/j.pecs.2016.06.001.
- [30] “THE METHANOL INDUSTRY.” <https://www.methanol.org/the-methanol-industry/> (accessed Nov. 02, 2022).
- [31] F. Bisotti *et al.*, “Century of Technology Trends in Methanol Synthesis: Any Need for Kinetics Refitting?,” *Ind Eng Chem Res*, vol. 60, no. 44, pp. 16032–16053, Nov. 2021, doi: 10.1021/acs.iecr.1c02877.
- [32] F. Nestler *et al.*, “Kinetic modelling of methanol synthesis over commercial catalysts: A critical assessment,” *Chemical Engineering Journal*, vol. 394, Aug. 2020, doi: 10.1016/j.cej.2020.124881.
- [33] G. H. Graaf and J. G. M. Winkelman, “Chemical Equilibria in Methanol Synthesis Including the Water-Gas Shift Reaction: A Critical Reassessment,” *Ind Eng Chem Res*, vol. 55, no. 20, pp. 5854–5864, May 2016, doi: 10.1021/acs.iecr.6b00815.
- [34] J.-P. Lange, “Methanol synthesis: a short review of technology improvements,” 2001.

- [35] K. M. vanden Bussche and G. F. Froment, "A Steady-State Kinetic Model for Methanol Synthesis and the Water Gas Shift Reaction on a Commercial Cu/ZnO/Al₂O₃ Catalyst," 1996.
- [36] S. Ledakowicz, L. Nowicki, J. Petera, J. Nizioł, P. Kowalik, and A. Gołębiowski, "Kinetic characterisation of catalysts for methanol synthesis," *Chemical and Process Engineering - Inżynieria Chemiczna i Procesowa*, vol. 34, no. 4, pp. 497–506, Dec. 2013, doi: 10.2478/cpe-2013-0040.
- [37] C. Jia, J. Gao, Y. Dai, J. Zhang, and Y. Yang, "The thermodynamics analysis and experimental validation for complicated systems in CO₂ hydrogenation process," *Journal of Energy Chemistry*, vol. 25, no. 6, pp. 1027–1037, Nov. 2016, doi: 10.1016/j.jechem.2016.10.003.
- [38] T. Inui, M. Anpo, K. Izui, S. Yanagida, and T. Yamaguchi, "Advances in Chemical Conversions for Mitigating Carbon Dioxide Studies in."
- [39] *Selected topics on energy and development - environment - biomedicine : proceedings of the 3rd International Conference on Energy and development - environment - biomedicine (EDEB '09), Athens, Greece, December 29-31, 2009*. WSEAS Press, 2009.
- [40] R. O. dos Santos, L. de S. Santos, and D. M. Prata, "Simulation and optimization of a methanol synthesis process from different biogas sources," *J Clean Prod*, vol. 186, pp. 821–830, Jun. 2018, doi: 10.1016/j.jclepro.2018.03.108.
- [41] A. Vita *et al.*, "Methanol synthesis from biogas: A thermodynamic analysis," *Renew Energy*, vol. 118, pp. 673–684, Apr. 2018, doi: 10.1016/j.renene.2017.11.029.
- [42] R. Y. Chein, W. H. Chen, H. Chyuan Ong, P. Loke Show, and Y. Singh, "Analysis of methanol synthesis using CO₂ hydrogenation and syngas produced from biogas-based reforming processes," *Chemical Engineering Journal*, vol. 426, Dec. 2021, doi: 10.1016/j.cej.2021.130835.
- [43] Anita Kovac Kralj and Davorin Kralj, "Methanol production from biogas," WSEAS Press, 2009.
- [44] R. Tamnitra, R. Jitwung, T. Puangpetch, W. Patthaveekongka, and K. Leeheng, "Kinetic modeling and simulation of bio-methanol process from biogas by using aspen plus," in *MATEC Web of Conferences*, Aug. 2018, vol. 192. doi: 10.1051/mateconf/201819203030.
- [45] "Carbon Recycling International." <https://www.carbonrecycling.is/projects> (accessed Nov. 03, 2022).

- [46] J. H. Jones, "The Cativa™ Process for the Manufacture Plant of Acetic Acid Location Year Debottlenecking or increased throughput achieved, % Iridium Catalyst Improves Productivity in an Established Industrial Process."
- [47] G. J. Sunley and D. J. Watson, "High productivity methanol carbonylation catalysis using iridium The Cativa™ process for the manufacture of acetic acid," 2000.
- [48] P. Kalck, C. le Berre, and P. Serp, "Recent advances in the methanol carbonylation reaction into acetic acid," *Coordination Chemistry Reviews*, vol. 402. Elsevier B.V., Jan. 01, 2020. doi: 10.1016/j.ccr.2019.213078.
- [49] N. Yoneda, S. Kusano, M. Yasui, P. Pujado, and S. Wilcher, "Recent advances in processes and catalysts for the production of acetic acid," 2001.
- [50] K.-I. Sano, H. Uchida, and S. Wakabayashi, "A new process for acetic acid production by direct oxidation of ethylene," 1999.
- [51] A. Vidra and Á. Németh, "Bio-produced acetic acid: A review," *Periodica Polytechnica Chemical Engineering*, vol. 62, no. 3. Budapest University of Technology and Economics, pp. 245–256, May 16, 2018. doi: 10.3311/PPch.11004.
- [52] M. Correia, "Livro. Kisper. Distillation Design."
- [53] S. L. * and R. Z. Lech Nowicki, "Kinetics of Rhodium-Catalyzed Methanol Carbonylation," Łódź, Poland, 1992.
- [54] F. Galli, D. Previtali, S. Casagrande, C. Pirola, F. Manenti, and D. C. Boffito, "Simulation of the water-acetic acid separation via distillation using different entrainers: An economic comparison," *Chem Eng Trans*, vol. 57, pp. 1159–1164, 2017, doi: 10.3303/CET1757194.
- [55] E. Khodabandeh, M. Pourramezan, and M. H. Pakravan, "Effects of excess air and preheating on the flow pattern and efficiency of the radiative section of a fired heater," *Appl Therm Eng*, vol. 105, pp. 537–548, Jul. 2016, doi: 10.1016/j.applthermaleng.2016.03.038.
- [56] R. Turton, *Analysis, synthesis, and design of chemical processes*. Prentice Hall, 2012.
- [57] K.J. BELL, "Estimate S&T exchanger design fast," *The Oil and Gas Journal*, Dec. 1978.
- [58] "Prezzi finali dell'energia elettrica per i consumatori industriali - Ue a Area euro." <https://www.arera.it/it/dati/eepcfr2.htm> (accessed Nov. 18, 2022).

- [59] *ACQUEDOTTO-FOGNATURA-DEPURAZIONE*. Accessed: Nov. 18, 2022. [Online]. Available: https://www.publiacqua.it/sites/publiacqua/files/tariffe_2021.pdf
- [60] *Tariffe_SII_Brianzacque_Anno_2021_x_Sito_Definitive*.
- [61] VIACQUA S.p.A, *ALLEGATO B-Articolazioni tariffarie per tutte le utenze anno 2021*. Accessed: Nov. 18, 2022. [Online]. Available: <https://www.viacqua.it/it/clienti/patto-con-gli-utenti/tariffe-in-vigore/>
- [62] A. Schievano, G. D'Imporzano, V. Orzi, G. Colombo, T. Maggiore, and F. Adani, "Biogas from dedicated energy crops in Northern Italy: Electric energy generation costs," *GCB Bioenergy*, vol. 7, no. 4, pp. 899–908, Jul. 2015, doi: 10.1111/gcbb.12186.
- [63] H. Song and U. S. Ozkan, "Economic analysis of hydrogen production through a bio-ethanol steam reforming process: Sensitivity analyses and cost estimations," *Int J Hydrogen Energy*, vol. 35, no. 1, pp. 127–134, Jan. 2010, doi: 10.1016/j.ijhydene.2009.10.043.
- [64] V. Stenberg, V. Spallina, T. Mattisson, and M. Rydén, "Techno-economic analysis of H₂ production processes using fluidized bed heat exchangers with steam reforming – Part 1: Oxygen carrier aided combustion," *Int J Hydrogen Energy*, vol. 45, no. 11, pp. 6059–6081, Feb. 2020, doi: 10.1016/j.ijhydene.2019.10.202.
- [65] J. Reeve, O. Grasham, T. Mahmud, and V. Dupont, "Advanced Steam Reforming of Bio-Oil with Carbon Capture: A Techno-Economic and CO₂ Emissions Analysis," *Clean Technologies*, vol. 4, no. 2, pp. 309–328, Jun. 2022, doi: 10.3390/cleantechnol4020018.
- [66] ROBERT D. NEWTON and ROBERT S. ARIES, "INDUSTRIAL AND ENGINEERING CHEMISTRY Preliminary Estimation of Operating Costs T." [Online]. Available: <https://pubs.acs.org/sharingguidelines>
- [67] "Acetic acid price trend and forecast." <https://www.chemanalyst.com/Pricing-data/acetic-acid-9#:~:text=The%20prices%20of%20Acetic%20Acid%20in%20US%20market%20observed%20to,and%20%241476%2Fton%20FOB%20Louisiana.> (accessed Nov. 18, 2022).

List of tables

Table 1.1: Methane yields of various substrates [9]	12
Table 3.1 Composition and Physical properties of stream 6	50
Table 3.2 Composition of stream 60	51
Table 3.3 Composition and physical properties of stream 10	51
Table 3.4 Gibbs reactor outlet stream composition and multiple pipe reformer outlet stream composition (molar fractions).....	54
Table 3.5 activation energies and frequency factors for steam reforming reaction	55
Table 3.6 activation energies and frequency factors for water-gas shift.....	55
Table 3.7 activation energies and frequency factors for methanation	56
Table 3.8 Absorber inlet and outlet streams composition comparison (molar fractions)	58
Table 3.9 water-gas shift reactor inlet and outlet streams compositions (kmol/h) .	59
Table 3.10 Comparison between Gibbs reactor outlet composition and multi-tubular reverse water-gas shift reactor outlet composition (kmol/h)	61
Table 3.11 Methanol synthesis reactor inlet and outlet composition (kmol/h). stream 67 is the inlet stream, stream 19 is the outlet stream	63
Table 3.12 Flash separator liquid stream composition (kmol/h)	63
Table 3.13 Recycled stream composition (kmol/h)	64
Table 3.14 Composition of the gaseous stream exiting distillation column T-100 (kmol/h).....	66
Table 3.15 composition of the bottoms of distillation column T-100 (kmol/h).....	67
Table 3.16 Comparison between equilibrium composition and composition at the outlet of the multi-tubular reactor PFR-100 (kmol/h)	69
Table 3.17 activation energies and frequency factors for carbon monoxide hydrogenation.....	69
Table 3.18 activation energies and frequency factors for carbon dioxide hydrogenation.....	70

Table 3.19 activation energies and frequency factors for reverse water-gas shift...	71
Table 3.20 Acetic acid reactor outlet streams composition (kmol/h). Stream 42 is the gaseous outlet stream, stream 43 is the outlet liquid stream	72
Table 3.21 Composition of the outlet streams of flash separator V-103 (kmol/h). Stream 44 is the gaseous stream, stream 52 is the liquid stream	73
Table 3.22 Composition of the outlet gaseous stream of flash separator V-102 and of the mixed stream coming from MIX-107 (kmol/h). Stream 45 is the gaseous stream, stream 53 is the mixed stream.....	74
Table 3.23 Composition of the outlet liquid stream of flash separator V-102 and of the mixed stream coming from MIX-109 (kmol/h). Stream 46 is the gaseous stream, stream 96 is the mixed stream.....	74
Table 3.24 Composition of the make-up catalyst stream and of the recycled stream. Stream 49 is the make-up catalyst stream (kg/h), stream 51 is the recycled stream (kmol/h).....	75
Table 3.25 Composition of the acetic acid Gibbs reactor products and of the acetic acid CSTR reactor (kmol/h).	75
Table 3.26 Composition of the gaseous stream exiting column T-102 (kmol/h).....	77
Table 3.27 Composition of the bottom stream exiting column T-102 (kmol/h).....	78
Table 3.28 Composition of the top stream exiting column T-103 (kmol/h).....	79
Table 3.29 Composition of the bottom stream exiting column T-103 (kmol/h).....	79
Table 3.30 Composition of the top stream exiting column T-105 (kg/h)	80
Table 3.31 Composition of the bottom stream exiting from phase separator V-109 (kg/h)	81
Table 3.32 Composition of the propyl acetate stream entering distillation column T-105 (kg/h)	81
Table 3.33 Composition of the bottom stream of distillation column T-105 (kg/h)	82
Table 4.1 Factors affecting the costs associated with evaluation of capital cost of chemical plants.....	86
Table 4.2 Equations for bare module cost for different equipment.....	87
Table 4.3 CEPCI for different years.....	88
Table 4.4 Compressors $C_{P^{\circ}}$ estimation.....	89
Table 4.5 Compressors C_{BM} , C_{TM} , C_{GR} estimation	89
Table 4.6 Pumps $C_{P^{\circ}}$ estimation	90

Table 4.7 Pumps F_P and F_M estimation.....	90
Table 4.8 Pumps C_{BM} , $C_{BM(2022)}$, C_{TM} , C_{GR} estimation.....	91
Table 4.9 Estimation of the heat exchange area for the plant heat exchangers	92
Table 4.10 Estimation of the heat exchange area for the plant heat exchangers	93
Table 4.11 Heat exchangers C_{P° estimation.....	94
Table 4.12 Heat exchangers F_P and F_M estimation.....	95
Table 4.13 Heat exchangers C_{BM} , $C_{BM(2022)}$, C_{TM} , C_{GR} estimation.....	96
Table 4.14 Reactors C_{P° estimation.....	97
Table 4.15 Reactors F_P and F_M estimation.....	97
Table 4.16 Reactors C_{BM} , $C_{BM(2022)}$, C_{TM} , C_{GR} estimation.....	97
Table 4.17 Furnace C_{P° estimation.....	98
Table 4.18 Furnace F_P and F_{BM} estimation	98
Table 4.19 Furnace C_{BM} , $C_{BM(2022)}$, C_{TM} , C_{GR} estimation.....	98
Table 4.20 Flash separators C_{P° estimation	98
Table 4.21 Flash separators F_P and F_M estimation	99
Table 4.22 Flash separators C_{BM} , $C_{BM(2022)}$, C_{TM} , C_{GR} estimation	99
Table 4.23 Column sizing	100
Table 4.24 Columns C_{P° estimation.....	100
Table 4.25 Columns F_P and F_M estimation.....	100
Table 4.26 Columns C_{BM} , $C_{BM(2022)}$, C_{TM} , C_{GR} estimation.....	101
Table 4.27 Trays and packing C_{P° estimation	101
Table 4.28 Columns internals C_{BM} , $C_{BM(2022)}$, C_{TM} , C_{GR} estimation. To estimate the values for column T105 the values for a single tray have been multiplied by the total number of trays.....	101
Table 4.29 Tank separator C_{P° estimation	102
Table 4.30 Tank separator C_{BM} , $C_{BM(2022)}$ estimation.....	102
Table 4.31 Tank separator C_{TM} , C_{GR} estimation	102
Table 4.32 Cooling tower vessels C_{P° estimation	103
Table 4.33 Cooling tower vessels C_{BM} , $C_{BM(2022)}$, C_{TM} , C_{GR} estimation	103
Table 4.34 Cooling tower internals C_{P° estimation	103

Table 4.35 Cooling tower internals C_{BM} , $C_{BM(2022)}$, C_{TM} , C_{GR} estimation	104
Table 4.36 Cooling tower fans $C_{P^{\circ}}$ estimation	105
Table 4.37 Cooling tower fans C_{BM} , $C_{BM(2022)}$, C_{TM} , C_{GR} estimation	105
Table 4.38 Cooling tower pump $C_{P^{\circ}}$ estimation.....	106
Table 4.39 Cooling tower pump F_P and F_M estimation.....	106
Table 4.40 Cooling tower pump C_{BM} , $C_{BM(2022)}$, C_{TM} , C_{GR} estimation.....	106
Table 4.41 Electric power costs estimation.....	109
Table 4.42 Raw materials costs estimation. Biogas and water are expressed in m^3/h and their price is expressed in $\text{€}/nm^3$	110
Table 4.43 Waste treatment cost estimation. Wastewater is expressed in m^3/h and its price is in $\text{€}/nm^3$, waste liquid disposal is expressed in kg/h and its price is in $\text{€}/kg$	111
Table 4.44 Plant estimated costs	112
Table 4.45 Plant revenues	112
Table 4.46 Cash flow and discounted cash flow for the straight-line depreciation case.....	114
Table 4.47 Profitability indicators for the straight-line depreciation case.....	115
Table 4.48 Cash flow and discounted cash flow for the sum of the years digit depreciation case.....	117
Table 4.49 Profitability indicators for the sum of the years digit depreciation case	117
Table 4.50 Cash flow and discounted cash flow for the double declining line depreciation case.....	119
Table 4.51 Profitability indicators for the double declining line depreciation case	119
Table 4.52 Profitability indicators comparison.....	120

List of figures

Figure 0.1 Acetic acid different applications	2
Figure 0.2 Global acetic acid market share, by application (2020) [5].....	2
Figure 1.1 The stages of the methane fermentation process [10].....	6
Figure 1.2 Representation of the functional roles of the microbial species involved in biogas production [9].....	7
Figure 1.3 Different reactor configurations for anaerobic digestion [1]	9
Figure 1.4 Typical two-stage agricultural biogas plant [10]	9
Figure 1.5 Biogas consumption by end use (2018) [13]	13
Figure 1.6 Biogas and biomethane production in 2018 against the sustainable potential today [13].....	14
Figure 1.7 Equilibrium composition for methane reforming at 500 – 1000 °C and pressures (in the direction of the arrows) of 0.1, 0.5, 1, 1.5, 2, 2.5, 3, 3.5, 4 MPa. Molar steam/methane ratio 3.333 corresponding to 5 kg H ₂ O per kilogram of carbon [1] 19	19
Figure 1.8 Reformer types [1].....	20
Figure 1.9 Autothermal reformer [1].....	22
Figure 1.10 Reforming section for production of ammonia synthesis gas [19]	23
Figure 1.11 Texaco gasification process [1]	24
Figure 1.12 Methanol synthesis [1].....	31
Figure 1.13 Different methanol synthesis reactors. (a) isothermal reactor with external cooling bath; (b) adiabatic reactor with intermediate coolers; (c) adiabatic reactor with cold feed cooling; (d) adiabatic reactor with intermediate feed gas quench; (e) feed–effluent heat exchange by periodic flow reversal; (f) radial flow reactor; (g) fluidized bed reactor [34].	33
Figure 1.14 ICI low-pressure methanol process [1]	34
Figure 1.15 Lurgi low-pressure methanol process [1]	34
Figure 1.16 Oxidation of acetaldehyde to acetic acid [1]	38

Figure 1.17 Reaction cycle proposed for the cobalt-catalyzed methanol carbonylation reaction (BASF process) [1]	39
Figure 1.18 BASF acetic acid production process [1]	40
Figure 1.19 Monsanto rhodium catalyzed carbonylation of methanol reaction cycle [46]	41
Figure 1.20 Monsanto acetic acid production process [1]	41
Figure 1.21 Reaction cycle proposed for the iridium-catalyzed methanol carbonylation reaction (Cativa process) [1]	42
Figure 1.22 Oxidation of <i>n</i> -butane in the liquid phase (Chemische Werke Hüls process) [1]	43
Figure 1.23 Process flowsheet of direct oxidation to ethylene into acetic acid [50]	44
Figure 3.1 Biogas compression train	50
Figure 3.2 Reforming reactor, water separation and steam generation subsection	52
Figure 3.3 Syngas synthesis section	52
Figure 3.4 syngas refining section	57
Figure 3.5 Carbon dioxide removal subsection	58
Figure 3.6 Carbon dioxide recovery and reverse water-gas shift reactor section ...	60
Figure 3.7 Methanol production section	62
Figure 3.8 Methanol synthesis reactor and recycle subsection	65
Figure 3.9 Temperature (°C) vs. tray position from top for T-100 column	66
Figure 3.10 Methanol section distillation column	67
Figure 3.11 Acetic acid synthesis section	71
Figure 3.12 Plant separation section	76
Figure 3.13 Temperature profile inside column T-102	77
Figure 3.14 Temperature profile inside column T-103	78
Figure 3.15 Temperature profile inside column T-105	80
Figure 3.16 Plant furnace and HP and MP Steam generating units	83
Figure 3.17 Heat pump for refrigerant regeneration	84
Figure 4.1 Plant cash flow diagram for straight-line depreciation	116
Figure 4.2 Plant cash flow diagram for sum of the years digit depreciation	118

Figure 4.3 Plant cash flow diagram for sum of the double declining line depreciation	120
Figure 4.4 Cash flow diagrams comparison	121
Figure 4.5 Cumulative cash position cumulative probability distribution.....	124
Figure 4.6 net present value cumulative probability distribution.....	125

List of acronyms

Acronym	Description
CAGR	Compound annual growth rate
CBM	Bare module cost
CCF	Cumulative cash flow
CCP	Cumulative cash position
CCR	Cumulative cash ratio
CEPCI	Chemical engineering plant cost index
CF	Cash flow
CGR	Grassroot cost
CHP	Combined heat and power
COG	Coke oven gas
COL	Cost of operating labor
COM	Cost of manufacture
COMD	Cost of manufacture without depreciation
COR	Carbon oxides ratio
CPO	Catalytic partial oxidation
CRM	Cost of raw materials
CSTR	Continuously stirred tank reactor
CTM	Total module cost
CUT	Cost of utilities

CWT	Cost of waste treatment
DCF	Discounted cash flow
DCFROR	Discounted cash flow rate of return
DDDB	Double declining line depreciation
DMFC	Direct methanol fuel cell
DPBP	Discounted payback period
DSL	Straight line depreciation
DSOYD	Sum of the years digit depreciation
EU	European union
FCI	Fixed capital investment
LCFA	Long chain fatty acids
LPG	Liquefied petroleum gas
LPO	Liquid phase oxidation
MTBE	Methyl tert-butyl ether
NPV	Net present value
PBP	Payback period
PFR	Plug flow reactor
PTA	Polyethylene terephthalate
PVR	Present value ratio
ROROI	Rate of return on investment
SN	Stoichiometric number
UASB	Upflow anaerobic sludge blanket
VFA	Volatile fatty acids
WC	Working capital